Dissertation

submitted to the

Combined Faculty of Natural Sciences and Mathematics
of the Ruperto Carola University Heidelberg, Germany

for the degree of

Doctor of Natural Sciences

Presented by:
Anna Montebaur (M.Sc.)
Born in: Kaluga, Russia
Oral examination: 18th May 2020

Identification of myeloid cell targets for cancer immunotherapy using CRISPR screening

Referees:

Prof. Dr. Michael Platten

Prof. Dr. Frank Lyko

Non-disclosure notice

for Dissertation

“Identification of myeloid cell targets for cancer immunotherapy using CRISPR screening”

by Anna Montebaur

This work contains internal information and confidential data of the Bayer AG and the DKFZ (Deutsches Krebsforschungszentrum). Therefore, this work is not permitted to be published neither in whole nor in part till 18th May 2021. During this period, publication and copying neither in whole nor in part without explicit written consent of the Bayer AG and DKFZ is prohibited.

Bayer AG and DKFZ reserve all rights to acquire and register commercial property rights.

Regardless of this, the work can be handed over to the executive examiners from the university, as these are also members of the DKFZ, who themselves are bound to secrecy.

Berlin, 12th March 2020

Statutory declaration

Declarations according to § 8 of the Doctoral Degree Regulations of the Combined Faculty of Natural Sciences and Mathematics at the Heidelberg University

I hereby declare that I have written the submitted dissertation myself and that I have used no other sources or materials than those expressly indicated.

I hereby declare that I have not applied to be examined at any other institution, nor have I used the dissertation in this or any other form at any other institution as an examination paper, nor submitted it to any other faculty as a dissertation.

I hereby consent to the verification of the dissertation by means of electronic data processing programs against standing scientific standards.

Berlin, 12th March 2020 Anna Montebaur

Acknowledgement

The last three years have been an intense, instructive and joyful time, during which I have had the opportunity to work on a challenging project and the progress of which has been placed under my responsibility which I am very grateful for. The project and the scientific background have inspired and motivated me from the very beginning to do justice to the project.

But this great time and the result of this work would not have been possible without many people who were directly or indirectly involved in this process. I would like to thank all those who supported me and from whom I could learn, not only from a scientific point of view but also in terms of the development of my personality.

I am incredible grateful to my doctoral supervisor Dr. Barbara Nicke. I have always looked up to you, not only because of your broad scientific knowledge, but also because of your enjoyment of working in science and your talent for handling and successfully accomplishing vast amounts of work, where I have tried to learn from. You showed me how science is working in an industrial environment and I enjoyed from the start working in a very target-driven group with many smart scientists and demanding scientific milestones. You supported me in different ways without putting me under negative pressure and gave me freedom to operate but also brought me back on track when I needed it. Thank you for your time and effort that you have invested in me, which is by no means a matter of course. You and your whole laboratory, especially Katja Mann, Tanja Schiller, Mario Mann and Birgit Jahnke, have welcomed me lovingly and supported me wherever you could. Thank you all so much for that.

Thanks also to the postdocs in our laboratory Dr. Jan Naujoks, Dr. Anne Buttgereit and Dr. Zuzanna Makowska, who not only shared the office with me but always had an open ear and could give useful tips from their time as PhD students.

My gratitude also goes to our collaboration partners at the DKFZ in Heidelberg. Even though we all had our own areas of responsibility it was a pleasure for me to feel the sense of community because we all had a common goal in mind that strengthened us. Thank you, Dr. Rafael Carretero, for your productive discussions, your input and support not only during our TDMC meetings but also during the time of my lab rotation at your site. Many thanks also to Frederik Cichon for welcoming me to Heidelberg and introducing me to the scientific life at the DKFZ. I appreciate this very much.

Special thanks go to Dr. Ralf Lesche and Martina Runge who helped me with the next generation sequencing and to Dr. Atanas Kamburov and Dr. Andreas Steffen for the data

analysis. Thank you very much Dr. Helge Roider for the RNA-seq analysis and the platform you developed, which helped me a lot with data analysis and visualization. I highly appreciate your helpful manner and your curiosity for science.

I would like to thank Prof. Dr. Michael Platten for initiating this exciting project and taking the responsibility of evaluating this thesis as the first reviewer. I would like also to thank Prof. Dr. Frank Lyko for taking over the chair of the disputation and for his time and effort in his role as the second reviewer. Thank you also to my other committee members apl. Prof. Dr. Umansky and Dr. Guoliang Cui for their time in evaluating this work.

After all, family and friends are the ones who also share your experience as a PhD student with all its ups and down, who never complain when not seeing you for a longer period of time due to extensive experimental workload or writing processes when finishing the PhD.

My dear Lara, you have accompanied me on this way without being permanently at my side. Whether you are in Munich or Zurich, or elsewhere you have experienced this path and all the happy but also exhausting moments with me. You shared my joy and the numerous moments of happiness, but you also stood by me in difficult and stressful times and motivated me. Thank you so much!

My beloved family, I feel incredible gratitude to you Мама, Ваня, Kati and especially you Pati for your unconditional love, constant support and encouragement. You never doubted me, you built me up and I know I can always rely on you, no matter what happens. Because of you I know what counts in life. Thank you so much!

Table of contents

List of figures

List of tables

Summary

Over the recent years, immunotherapeutic approaches, especially immune checkpoint blockade-based therapies, have been found to be very effective to treat specific cancer types. However, many cancer patients do not respond to these currently available immune-system stimulating therapies or become resistant. Previously, this has been linked to tumor infiltrating immunosuppressive myeloid cells such as tumor-associated macrophages of the M2-like polarized phenotype and myeloid-derived suppressor cells. In the search for new approaches to treat cancer, this thesis was therefore aiming to gain a better understanding of the biology of the myeloid cell compartment in the tumor microenvironment and find novel modifiers of macrophage polarization.

This work presents a new methodology using CRISPR/Cas9-based screening to identify druggable targets promoting the immunosuppressive (M2) or preventing the proinflammatory (M1) macrophage phenotype. Inhibiting these targets will reinstruct tumor-infiltrating myeloid cells to stimulate the antitumor immune response in the tumor microenvironment.

As genetic perturbation of primary monocytes is very challenging, human monocytic THP-1 cells were used as surrogates to study macrophage biology. A THP-1 cell clone was engineered to stably express Cas9 that enables the performance of CRISPR/Cas9-based functional genomics studies. Myeloid cell transcriptome and whole genome targeting pooled CRISPR/Cas9 screens were performed detecting the effects of sgRNA-mediated knockout on CD80 expression in differentiated and polarized THP-1 cells. Thereby, 170 genes potentially involved in M2 polarization were identified. Some of the hits, such as OGT and TNFAIP3 have been described before to have a role in macrophage biology and polarization, supporting the validity of the screening approach. To confirm the screening results an RNP/gRNA-based CRISPR/Cas9 validation approach was developed, which will allow further characterization of the identified targets both in THP-1 cells but most importantly in human primary monocytes/macrophages. As readouts, the effects of gene knockouts on the expression of M1 macrophage markers and on secretion of various proinflammatory cytokines and chemokines are measured. Investigating a first selection of 20 hits using this approach, the screening data of knockout of the transcriptional regulators GFI1 and OTX1, the histone deacetylase KDM1A, as well as TNFAIP3 could be verified. More extensive experimental work has been performed to better understand the function of TNFAIP3 in macrophage polarization. Knockout of TNFAIP3 in primary myeloid cells promoted the M1 polarization of the cells under both M1 and M2 polarizing conditions. Furthermore, in coculture-experiments it was shown that the knockout cells are able to activate T cells better than the control cells. To evaluate the role of

the potentially druggable deubiquitinase function in macrophage polarization, Jurkat cells were genetically engineered to only express TNFAIP3 with a function-inhibiting C103A mutation in the de-ubiquitinase domain. RNA-seq experiments however implicate that the deubiquitinase function of TNFAIP3 does not seem to be essential for mediating the therapeutically relevant effect on macrophage polarization seen in TNFAIP3 knockout cells. Other options of targeting TNFAIP3 are now being investigated.

Based on the results generated in this thesis, projects have been started to further study the role of the screening hits in macrophage polarization to evaluate their potential as starting points for a pharmaceutical development program. Also, an extended target identification project is planned in mouse models.

Zusammenfassung

In den letzten Jahren haben sich immuntherapeutische Ansätze, insbesondere auf der Blockade von Immunkontrollpunkten basierende Therapien, als sehr wirksam für die Behandlung bestimmter Krebsarten erwiesen. Viele Krebspatienten sprechen jedoch auf diese derzeit verfügbaren immunsystemstimulierenden Therapien nicht an oder werden resistent. Mehrere in der letzten Zeit veröffentliche Studien zeigen, dass tumorinfiltrierende immunsuppressive myeloische Zellen, wie tumorassoziierte Makrophagen des M2-polarisierten Phänotyps und myeloische Suppressor-Zellen, dafür ursächlich verantwortlich sind. Auf der Suche nach neuen Ansätzen zur Krebsbehandlung zielte diese Arbeit daher darauf ab, die Biologie des myeloischen Zellkompartiments in der Mikroumgebung des Tumors besser zu verstehen und neue Modifikatoren der Makrophagenpolarisation zu finden.

In dieser Arbeit wird eine neue Methode vorgestellt, bei der CRISPR/Cas9-basiertes Screening eingesetzt wird, um pharmakologisch adressierbare Moleküle zu identifizieren, die den immunsuppressiven (M2) Phänotyp fördern oder den proinflammatorischen (M1) Phänotyp von Makrophagen verhindern. Durch die Inhibierung dieser Targets werden die tumorinfiltrierenden myeloischen Zellen repolarisiert und damit die Antitumor-Immunantwort in der Mikroumgebung des Tumors stimuliert.

Da primäre Monozyten nur sehr schwer genetisch manipulierbar sind, wurden humane monozytäre THP-1-Zellen als Surrogate zur Untersuchung der Makrophagenbiologie etabliert. Ein stabil Cas9 exprimierender THP-1-Zellklon wurde hergestellt, um die Durchführung von funktionellen CRISPR/Cas9-basierten genetischen Studien zu ermöglichen. Damit wurden gepoolte CRISPR/Cas9-Screens durchgeführt, die entweder das Transkriptom von myeloischen Zellen oder das ganze Genom adressieren. Dabei wurden die Auswirkungen des sgRNA-vermittelten Knockouts auf die CD80-Expression in differenzierten und polarisierten THP-1-Zellen nachgewiesen. Insgesamt wurden 170 Gene identifiziert, die möglicherweise an der M2-Polarisierung beteiligt sind. Für einige der gefundenen Targets, wie OGT und TNFAIP3, war es bereits bekannt, dass sie eine Rolle in der Makrophagenbiologie und -polarisation spielen. Dies bestätigt die Relevanz des Screening-Ansatzes. Zur Verifizierung der Screening-Ergebnisse wurde ein RNP/gRNA-basierter CRISPR/Cas9-Validierungsansatz entwickelt, der eine weitere Charakterisierung der identifizierten Targets sowohl in THP-1-Zellen als auch, besonders wichtig, in humanen primären Monozyten/Makrophagen ermöglicht. Dabei wurden die Effekte von Gen-Knockouts auf die Expression von M1-Makrophagen-Markern und auf die Sekretion verschiedener proinflammatorischer Zytokine und Chemokine gemessen. Bei der so erfolgten Untersuchung einer ersten Auswahl von 20

Targets konnten die Screening-Daten vom Knockout der Transkriptionsregulatoren GFI1 und OTX1, der Histondeacetylase KDM1A, sowie von TNFAIP3 verifiziert werden. Es wurden weitere umfangreiche experimentelle Arbeiten durchgeführt, um die Funktion von TNFAIP3 in der Makrophagenpolarisation besser zu verstehen. Der Knockout von TNFAIP3 in primären myeloischen Zellen förderte die M1-Polarisation der Zellen sowohl unter M1- als auch unter M2-Polarisationsbedingungen. Darüber hinaus wurde in Kokulturexperimenten gezeigt, dass Knockout-Zellen T-Zellen besser aktivieren konnten als Kontrollzellen. Um die Rolle der potenziell chemisch adressierbaren Deubiquitinase-Funktion bei der Makrophagen-Polarisierung zu untersuchen, wurden Jurkat-Zellen genetisch so verändert, dass sie nur TNFAIP3 mit einer funktions-hemmenden C103A-Mutation in der De-Ubiquitinase-Domäne exprimieren. RNA-Seq-Experimente implizieren jedoch, dass die Deubiquitinase-Funktion von TNFAIP3 nicht wesentlich für die Vermittlung der therapeutisch relevanten Wirkung auf die Makrophagen-Polarisation, die in TNFAIP3-Knockout-Zellen beobachtet wird, zu sein scheint. Andere Möglichkeiten, TNFAIP3 zu adressieren, werden jetzt untersucht.

Auf der Grundlage der in dieser Arbeit erzielten Ergebnisse wurden Projekte zur weiteren Untersuchung der Rolle der Screening-Hits bei der Makrophagenpolarisation gestartet, um ihr Potenzial als Ausgangspunkt für ein pharmazeutisches Entwicklungsprogramm zu bewerten. Außerdem ist ein erweitertes Target-Identifizierungsprojekt in Mausmodellen geplant.

1 Introduction

1.1 The role of the immune system in cancer

The immune system is a remarkable, complex, and multifunctional system that can not only defend the organism against infections, eliminate pathogens and maintain homeostasis but is also able to differentiate between healthy and cancerous cells in the body and attack tumor cells (Murphy et al., 2012; Schreiber et al., 2011).

However, cancer cells, like pathogens, develop mechanisms to breach the barriers of the immune system and its recognition so that the immune response fails, causing immune suppression and tumor growth (Pollard, 2004). To overcome this tumor-associated immunosuppression and to reactivate the intrinsic immune response is the main goal of cancer immunotherapy (June et al., 2018; Wolchok et al., 2017).

1.1.1 Immunosurveillance

In the process known as immunosurveillance first described by Frank MacFarlane Burnet and Lewis Thomas (1950s), a variety of different immune cells recognize and eliminate tumor cells (elimination phase) (Burnet, 1957; Thomas, 1982). Tumor cells that survive this phase change or mutate in the subsequent equilibrium phase. This process is fostered by the cells' genetic instability allowing certain clones to evade the selection pressure imposed by the immune system. The equilibrium phase can last years, until tumor cell variants might arise which are more resistant to immunogenic clearance (Dunn et al., 2002). The tumor cells can now proliferate in an uncontrolled manner and form a tumor (escape phase).

One way how tumors can avoid the recognition of the immune system is by creating an immunosuppressive tumor-microenvironment (TME) consisting of malignant and stromal cells, as well as infiltrating cells of the innate and adaptive immune system (Guerriero, 2018). Especially myeloid cells in the TME have a critical role in suppressing the antitumor immune response and are the most abundant immunosuppressive cell type found in cancer (Gabrilovich et al., 2012).

1.1.2 Tumor-associated myeloid cells

Myeloid cells are a compartment of the innate immune system with various subtypes of cells and diverse functions. They are not only important for initiating and dissolving the inflammatory response but also essential for tissue repair (Mantovani et al., 2008). In response to cytokines, chemokines, and growth factors produced in the tumor, the myeloid cells migrate into the TME. Most of these myeloid cells endorse tumor growth, but some also have antitumor activity (Gabrilovich et al., 2012).

The myeloid cell compartment comprises monocytes, macrophages, dendritic cells and granulocytes as basophils, eosinophils and neutrophils (Figure 1.1). In tumor-bearing hosts, other subtypes of myeloid cells develop such as myeloid derived suppressor cells (MDSCs), tumor-associated macrophages (TAMs) and suppressive dendritic cells. The majority of them suppresses the immune system to attack the tumor (Wynn, 2013).

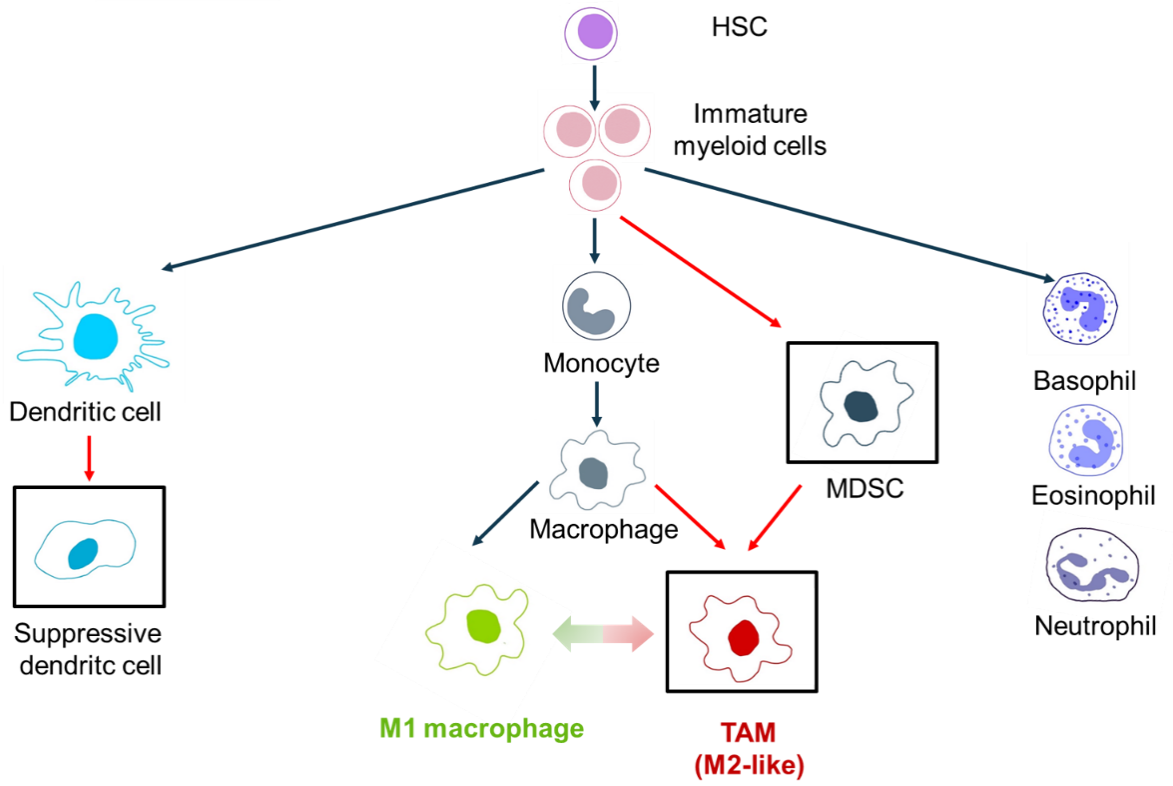

Figure 1.1. The development of immature myeloid cells to immunosuppressive tumor promoting myeloid cells
The tumor microenvironment (TME) promotes the development of the pro-tumorigenic suppressive dendritic cells, the tumor-associated macrophages (TAMs), which have an M2-like macrophage phenotype, and the myeloid derived suppressor cells (MDSCs) (HSC, hematopoietic stem cell) (depicted in boxes), black arrows indicate the myeloid cell differentiation under normal physiological conditions, red arrows indicate differentiation of immature myeloid cells in the TME, modified from (Wynn, 2013).

1.1.3 Macrophages

Macrophages arise from three different sources: the embryonic yolk sac, the fetal liver and the bone marrow and subsequently infiltrate every tissue of the body (van de Laar et al., 2016). Tissue-resident macrophages that derive from the yolk sac and fetal liver are tissue-specific from embryonic development to adulthood (Ginhoux & Guilliams, 2016; Gomez Perdiguero et al., 2015). The bone marrow-derived macrophages are differentiated from blood monocytes and belong to the mononuclear phagocyte system (Hume, 2006). In case of tissue damage or infection these monocytes are recruited to the affected tissue and differentiate into macrophages. They recognize, phagocytize and degrade pathogens and damaged, dying or dead cells. Recognition of these is based on conserved pathogen-associated molecular patterns (PAMPs) or damage-associated molecular patterns (DAMPs), respectively, through pattern-recognition receptors (PRRs) which is essential for host defense and tissue remodeling (Cao, 2016). The toll-like receptors (TLR), retinoic acid inducible gene I-like receptors (RLR) and nucleotide-binding oligomerization domain-like receptors (NLR) recognize a variety of PAMPs, such as proteins, nucleic acids, lipids or carbohydrates originating from the foreign microorganism (Iwasaki & Medzhitov, 2015). TLRs (TLR1-TLR13) are specialized to recognize components of conserved molecules derived from these foreign microorganisms, such as bacterial lipopeptides, flagellin, glycolipids and viral nucleic acids. The TLR4 for instance is well-known to recognize lipopolysaccharides (LPS) (O'Neill et al., 2013). When such PAMPs ligate to the TLRs a signaling cascade is initiated leading to Nuclear Factor kappa-light-chain-enhancer of activated B cells (NF-κB) dependent proinflammatory cytokine secretion or interferon regulated factor (IRF) dependent type I interferon (IFN) expression. RLRs are in charge of recognizing viruses and controlling viral replication and dissemination through production of type I IFNs, and NLRs are crucial for host defense against bacterial infections (Kato et al., 2006). NLR signaling also leads to activation of NF-κB and Mitogen-activated protein kinases (MAPK) resulting in proinflammatory cytokine production (Philpott et al., 2014).

Through PRR signaling macrophages get activated to initiate an inflammatory response. Activated macrophages produce stimulatory molecules, such as chemokines and cytokines (e.g. Tumor necrosis factor alpha (TNF-α), Interleukin 1 (IL-1), Interleukin 6 (IL-6) and Interleukin 12 (IL-12)), to attract and activate other immune cells, such as monocytes, neutrophils, eosinophils and lymphocytes. This leads to the initiation of an adaptive immune response (Mantovani & Sica, 2010). Furthermore, macrophages can directly kill pathogens or cells by phagocytosis and the production of reactive oxygen species (ROS) and nitric oxide (NO) (Murray et al., 2014).

Macrophages have also a very important role in resolving the immune response and supporting the tissue recovery. In the resolution phase of the inflammatory response, macrophages produce anti-inflammatory cytokines like IL-10 and IL-1Ra (Interleukin-1 receptors antagonist). Macrophages producing growth factors, such as the vascular-endothelial growth factor (VEGF) or transforming growth factor beta (TGF-β), support the repair of tissue damage caused during inflammation (Mantovani et al., 2013).

Besides pathogen recognition and clearance, and the initiation and resolution of inflammation, macrophages can present antigens to T cells. They express the co-stimulatory molecules Cluster of differentiation 80 (CD80) and Cluster of differentiation 86 (CD86) as well as Major histocompatibility complex class II (MHC-II) on their surface, through which the latter presents processed antigen peptides to T cells (Gordon & Taylor, 2005).

Thus, macrophages perform various functions in the human body, are very heterogeneous, dynamic and are present at different sites. They play a complex role as described before in inflammation and tissue homeostasis but also in development and disease. Macrophages adapt their phenotype and function in response to localized environmental stimuli. In contrast to T cells which have clear markers for activation and exhaustion, it is difficult to classify macrophages because of their heterogeneous and dynamic nature. One commonly used classification refers to the inflammatory states and uses the M1-M2 macrophage paradigm (Figure 1.2), which defines *ex vivo* stimulated macrophages generated without environmental stimuli. The classically activated proinflammatory M1 macrophages and alternatively activated immunosuppressive M2 macrophages are characterized by their response to IFN-γ and activation of TLRs and IL-4/IL-13, respectively (Mantovani et al., 2017). General expression for M1 macrophages are: CD80, CD86, HLA-DR, CCL2, CCL5, CXCL9, CXCL10, IL-1β, IL-6, IL-12 IFN-γ, TNF-α, ROS, NO and for M2 macrophages: CD163, CD206, CD209, CCL18, CCL22, CXCL12, TGF-β and IL-10 (Mantovani et al., 2002; Murray et al., 2014). Although this characterization is useful to study cells *in vitro,* these expression profiles do not comprehensively reflect the complexity of macrophage biology and their regulation *in vivo*.

1.1.4 Tumor associated macrophages

Most macrophages found in the TME show an M2-like phenotype and contribute to tumor development and poor prognosis in breast, lung, colon cancer, melanoma and brain tumor (Belgiovine et al., 2016). These TAMs can constitute up to 50 % of the tumor mass (Kelly et al., 1988; Tu et al., 2014) and inhibit the antitumor immune response through various mechanisms, such as the release of immunosuppressive cytokines or the expression of inhibitory membrane proteins like Programmed-death ligand 1 (PD-L1). They also increase

tumor motility, invasion and metastasis and inhibit the activation of T cells (Mantovani et al., 2017).

A minority of myeloid cells in the TME are M1 macrophages. These have been shown to scavenge and destroy phagocytized tumor cells and are believed to promote T helper 1 (T_H1) cell activation by releasing proinflammatory cytokines and presenting antigens to T cells (Y. Chen et al., 2019).

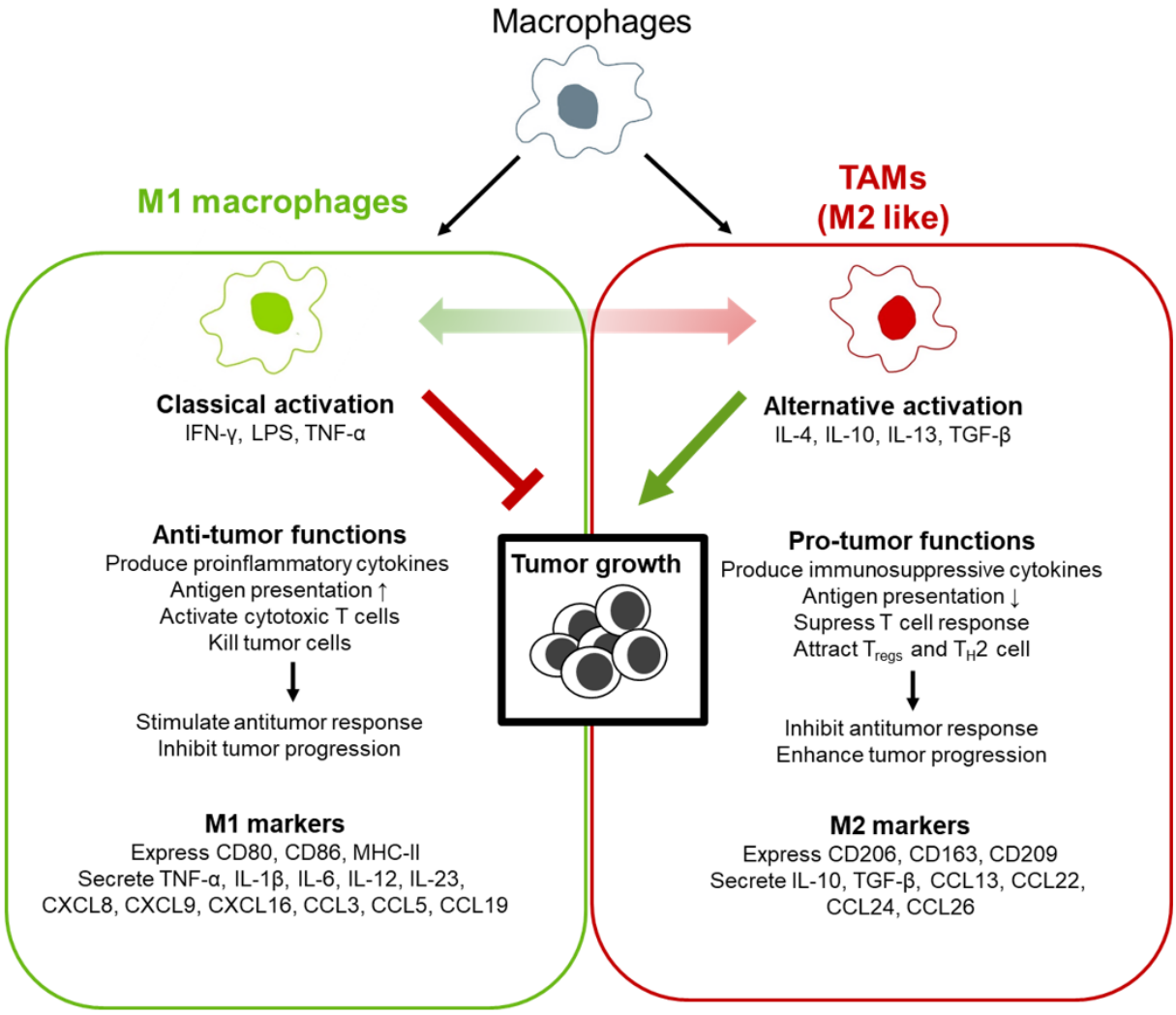

Figure 1.2. Macrophage plasticity and macrophage function in the tumor
Through innate recognition or signals from lymphocyte subsets macrophages get activated and polarized. Classically activated M1 macrophages are proinflammatory and anti-tumoral. Alternatively activated M2 macrophages, such as tumor-associated macrophages (TAMs), are immunosuppressive and pro-tumoral.

Re-polarizing the tumor infiltrating myeloid cells of the immunosuppressive M2 like state into the inflammatory M1 state is believed to inhibit tumor progression and activate the immune response to cancer (Guerriero, 2018; Mantovani et al., 2017). So called “cold” tumors, like prostate cancer, which are poorly infiltrated by immune cells could be “heated”. For instance, melanomas are classified as hot tumors per se. This degree of immune infiltration, especially considering T cell infiltration, reflects how well the immune system recognizes and fights the

tumor (Wargo et al., 2016). Many cold tumors contain myeloid cells but also others have neither myeloid cell - nor T cell populations (“immune desert”) (Kather et al., 2018). It could be shown that combination of anti-CD40 and anti-Colony stimulating factor 1 receptor (CSF-1R) antibodies was able to turn “cold” tumors “hot” by increased infiltration of T cells and decreasing the presence of immunosuppressive cells in preclinical tumor models that where not responsive to immune checkpoint blockade (Wiehagen et al., 2017). Furthermore, re-polarization also can decrease tumor angiogenesis, invasion and metastasis, decrease MDSC activity, activate dendritic cells (DCs) and all in all creates a more favorable environment for T cell antitumor activity (Mantovani et al., 2017). It has already been shown by Ino and colleagues that the proportion of proinflammatory M1 macrophages in the TME is as important for the survival of pancreatic cancer patients as the infiltration of CD8+ T cells (Ino et al., 2013).

1.1.5 Therapeutic approaches to address tumor associated macrophages

In general, activating the body’s own immune system with immunotherapies has revolutionized the treatment of cancer and displayed great success for many human cancers. Tumor-promoting immune cells from the innate and adaptive immune system in the tumor microenvironment are key drivers of the response to cancer and thus targeting these cells is of great clinical interest (Schreiber et al., 2011).

Over the past fifteen years therapeutics have been developed to specifically block immunosuppressive proteins secreted or presented by the tumor cells. Despite the overall success of PD1/PD-L1 and Cytotoxic T-lymphocyte-associated antigen-4 (CTLA-4) checkpoint inhibitors and Chimeric antigen receptor T cell (CAR-T cell) therapies in stimulating the adaptive immune response, many patients are still resistant to this type of immunotherapy treatment (Sharma et al., 2017).

Other available anti-cancer therapies attempt to increase the immunogenicity of the cancer via the myeloid cell compartment (Jahchan et al., 2019). There are several strategies targeting TAMs for anticancer therapy: by inhibition, depletion or reprogramming (Figure 1.3). Since macrophages are recruited in response to CCL2 (C-C motif chemokine ligand 2) and CSF1 (colony stimulating factor 1), secreted by immune and tumor cells, inhibitors against these ligands and their receptors have been developed in both mono- and combination therapy to suppress TAMs. So far they have shown limited clinical efficacy (Bingle et al., 2002; Bonapace et al., 2014; Scholl et al., 1994). Depletion of TAMs is another potential strategy and several compounds, such as trabectedin and clodronate, have been used to induce apoptosis of macrophages (Germano et al., 2013; Zeisberger et al., 2006). This macrophage depletion, however, turned out counterproductive as macrophages are essential for the therapeutic

efficacy of chemo- and immunotherapy (Guerriero et al., 2011; Gul et al., 2014). Therefore, reprogramming immunosuppressive tumor-infiltrating myeloid cells is being investigated and still holds great potential for cancer treatment (Mantovani & Allavena, 2015; Noman et al., 2014; Zhu et al., 2014). First candidate approaches, such as anti-CSF-1R, CD40 agonists and HDAC inhibition, show promising results, but still, druggable targets, particularly those targetable by small molecules have not yet been identified (Beatty et al., 2013; Evans et al., 2016; Wiehagen et al., 2017). However, despite the growing knowledge of key molecular determinants in macrophage biology, the molecular pathways and proteins involved in macrophage polarization to M1 and M2 have not been yet well characterized and therefore more research is necessary to improve our understanding.

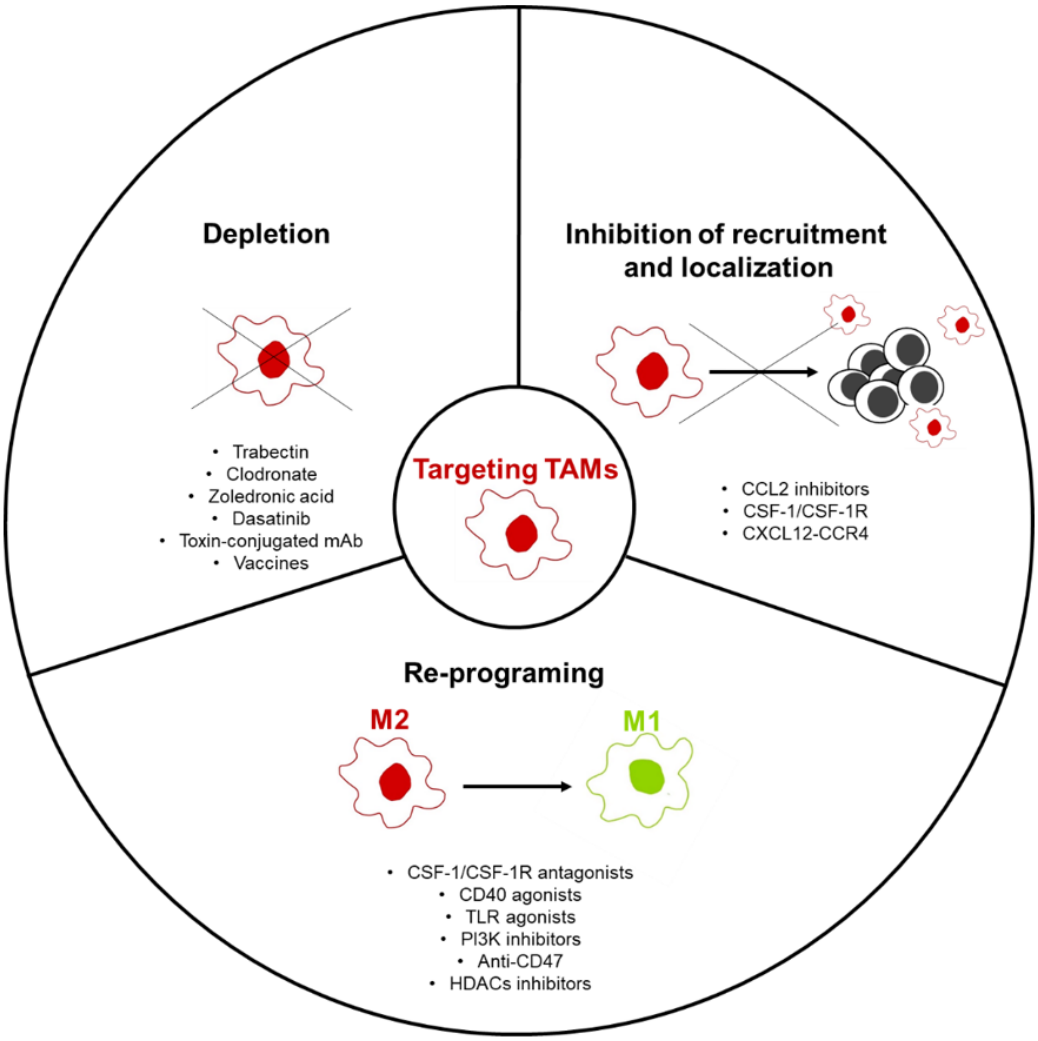

Figure 1.3. Therapeutic strategies targeting TAMs for cancer immunotherapy
Abbreviations: CSF-1, colony stimulating factor 1; CSF-1R, colony stimulating factor 1 receptor; CD40/CD47, Cluster of differentiation 40/47; TLR, Toll-like receptor; PI3K, phosphatidylinositol-4,5-bisphosphate 3-kinase-γ; HDAC, histone deacetylase; mAb, monoclonal antibody, CCL2, chemokine (C-C motif) ligand 2, CXCL12, C-X-C motif chemokine 12, CCR4, C-C chemokine receptor type 4, modified from (Guerriero, 2018).

Also, a better understanding of the links between TAMs and other cells in the TME is of great importance for further immunotherapies to improve clinical outcome. This also requires more

knowledge about the immunosuppressive myeloid cells. Furthermore, identifying modulators involved in the shaping of their dynamic phenotype will help steer the immune response against the tumor cells.

The example of the HDAC class IIa inhibitor TMP195, identified in a high throughput screening approach (Guerriero et al., 2017; Lobera et al., 2013), shows that unbiased research independent of mechanism or drug class is a powerful strategy to find new targets for immunotherapy and broaden our knowledge of macrophage biology.

An approach to extend the existing set of targets is a functional genomics-based screening method using CRISPR/Cas9 genome editing technology. This can elucidate the function of genes in a comprehensive and unbiased way and enable the identification of macrophage modulators and potentially also enable the development of novel cancer immunotherapies.

1.2 CRISPR/Cas9 screening for target identification

Loss-of-function genetic perturbation screens can provide information about gene functions in diverse cellular models, reflecting healthy and disease states.

Over the last years, many CRISPR screens have been carried out. A number of them show that CRISPR/Cas9 technology can be successfully used to identify functional pathway related genes which help in understanding biological processes. Also, new potential drug targets, drug-inhibitors, the mode of action and direct target of small-molecule inhibitors could be identified (Jost et al., 2017; Neggers et al., 2018). Very recently a genome wide CRISPR/Cas9 screen identified a new T cell receptor recognizing and killing human cancer types via the monomorphic MHC class I-related protein, MR1, a new candidate for HLA-independent, pan-cancer, pan-population immunotherapies (Crowther et al., 2020).

Gene silencing using RNA interference (RNAi) in *in vitro* or *in vivo* screens or CRISPR/Cas9 screens have already enabled the identification of potential key regulators of immune function and drug targets in the past. For example, Zhou and colleagues described an *in vivo* pooled shRNA screening approach leading to the identification of novel and druggable T cell specific targets to be used for cancer immunotherapy (Zhou et al., 2014). Shifrut et al. described the identification of key regulators of stimulation responses in primary human T cells in a CRISPR/Cas9 screen (Shifrut et al., 2018). They could identify signaling components and genes inhibiting proliferation after activation which extends our understanding of T cell function and their ability to overcome the TME.

When comparing RNAi and CRISPR/Cas9 screens, RNAi is limited by overwhelming off-target effects (Doench, 2018). The established gene editing technology using the CRISPR/Cas9 system is a valid alternative to these shRNA screens, with which even more efficient and accurate results can be achieved (Doench, 2018).

1.2.1 Mechanism of CRISPR/Cas9

The bacterial CRISPR (Clustered Regularly Interspaced Short Palindromic Repeats) – associated Cas9 (CRISPR-associated protein 9) nuclease provides an effective tool for introducing targeted loss-of-function mutations into the genome (Deltcheva et al., 2011; Jinek et al., 2012) and is a bacterial defense mechanism against pathogens (Shah et al., 2013). The bacterial Cas9 nuclease functions by inducing deoxyribonucleic acid (DNA) double-strand breaks within the target DNA sequence directed by a guide ribonucleic acid (RNA) (sgRNA or crRNA + tracrRNA). The single guide ribonucleic acid (sgRNA) consists of a 20-nucleotide targeting sequence and a scaffold sequence, which binds Cas9. The targeting sequence is 3-4 nucleotides upstream of a Protospacer Adjacent Motif (PAM, typically an NGG (G = guanine and N = any nucleotide)) which is necessary for Cas9 binding. When the Cas9-gRNA complex binds to the coding region of the gene it creates a double-strand break. This activates the endogenous error-prone non-homologous end joining DNA repair, which causes insertion/deletion (Indel) mutations. These Indels induce frameshift mutations that ultimately generate premature stop codons leading to gene knockout (KO).

1.2.2 Principle and approaches of CRISPR/Cas9 screening

CRISPR/Cas9 technology has been further developed and used over the last few years as a high throughput functional genomics screening method to elucidate the biological relevance of the expression of different genes in prokaryotic or eukaryotic cells.

The process can be simplified to a two-component system. First, it requires exogenous expression of an active bacterial Cas9 protein in the screening cell, which can be introduced stably or transiently. Secondly, a lentivirally packaged sgRNA library has to be transduced or synthetic gRNAs (crRNA + tracrRNA) have to be transfected into the screening cells. These serve as guides to direct the Cas9 to the desired genomic locations in order to generate a gene KO.

CRISPR/Cas9 screens can be carried out in an arrayed or in a pooled screening format (Figure 1.4). In the arrayed format, gRNAs are introduced separately into cells, one gRNA targeting one gene per culture well. The resulting phenotype of a specific gene KO can be directly

examined in the well, for example by means of high throughput imaging or luminescence or fluorescence-based readouts. In the pooled format a mixture of different sgRNAs targeting different genes (sgRNA library) is introduced on flasks of cells. Depending on the underlying biological question, selective pressure is applied to the transduced cells, which results in the accumulation or depletion of cells in response to the applied stimuli. At the end of the screen, cells harboring the desired phenotype are collected and the sgRNAs integrated in the genomic DNA serve as “barcodes” which are identified by next generation sequencing (NGS). Bioinformatic pipelines are then used to identify over- or underrepresented sgRNAs, and generate a list of candidate genes for further investigation.

The readout of pooled screens relies on the phenotypic separation of cells into population depleted or enriched in the phenotype of interest. A phenotype can be represented by reporter gene activity or by surface protein expression measured by flow cytometry. In pooled CRISPR screens detecting cell viability, the gene KO either leads to growth advantages over the selective pressure (positive selection screens) or cell death (drop-out screens) and thereby depletion of sgRNAs. Depending on these different types of screens, different experimental design, positive and negative controls, and appropriate representation of the screening library over the whole screening process is necessary to achieve statistically relevant screening results.

Alternative approaches to a CRISPRko (knockout) screen are CRISPRa (activation) and CRISPRi (interference) screens (Gilbert et al., 2014; Gilbert et al., 2013). In these screening formats a nuclease-deficient Cas9 (dCas9) is used to enable the activation or inhibition of the transcriptional initiation, thereby reversibly inducing (gain of function screen) or silencing gene expression (loss-of-function screen).

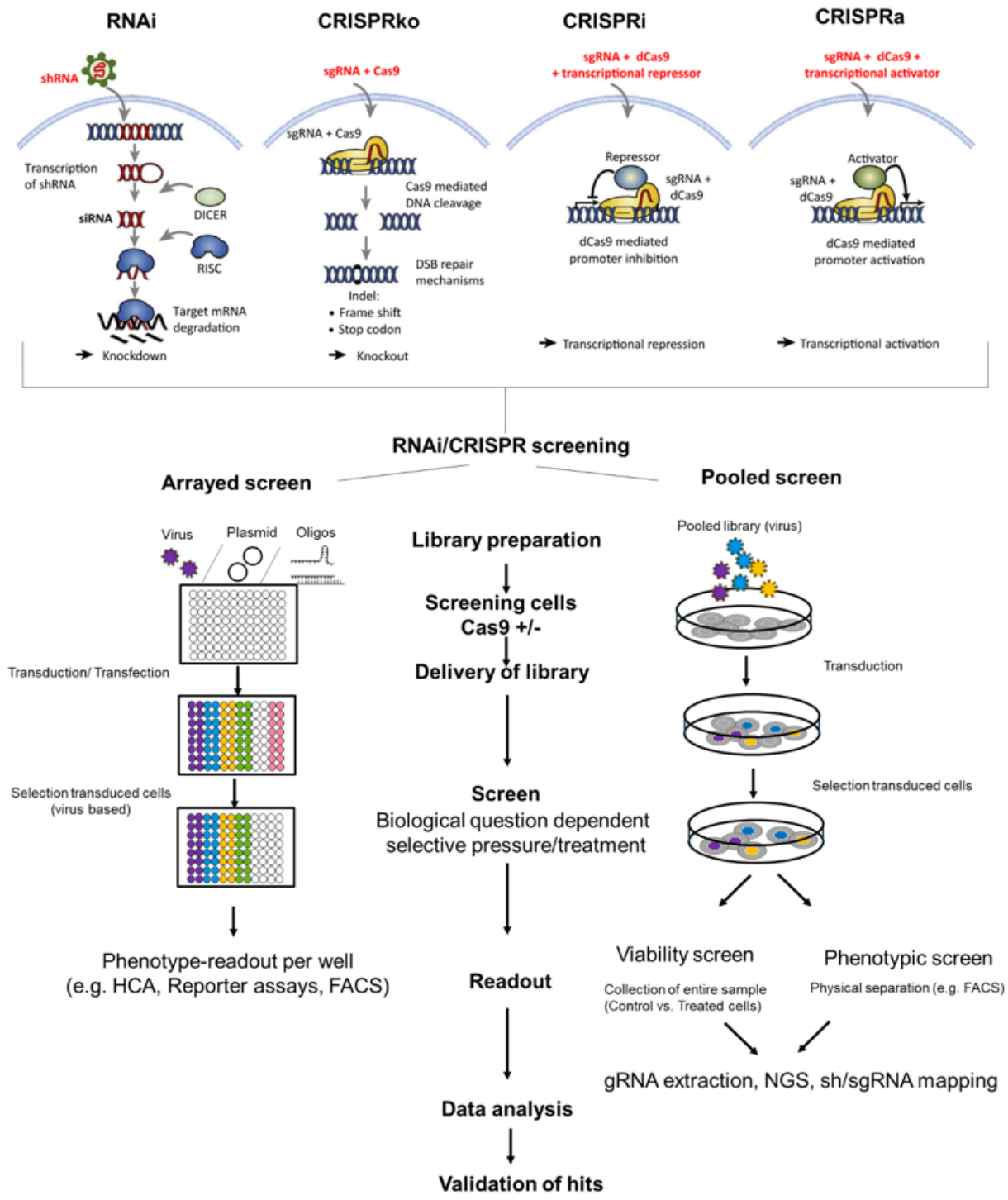

Figure 1.4. Overview of arrayed and pooled RNAi/CRISPR screening
RNA interference (RNAi) based knockdown of genes through shRNA (short hairpin RNA) with RISC (RNA-induced silencing complex) which leads to degradation of mRNA; CRISPRko results in gene knockout by Cas9 + sgRNA mediated double strand breaks (DSBs), leading to Indels (insertions/deletion), causing frame shift and premature stop codon; CRISPRi (interference) leading to transcriptional repression of genes through dCas9 (nuclease-deficient Cas9)+ sgRNA + transcriptional repressor which block the promotor, CRISPRa (activation) leading to transcription activation of genes with dCas9 + sgRNA + transcriptional activator, the latter binding to the promotor sequence of interest, Screening procedures described in text; HCA, high-content-analysis; FACS, fluorescent-activated sorting; NGS, next generation sequencing, modified from (Schuster et al., 2019)

These different CRISPR screening approaches can not only be performed in different cell types *in vitro*, which is the most commonly used format, but also *ex vivo* or *in vivo*, either by injecting viral particles into the *in vivo* system or implantation of cells transduced *in vitro* or *ex vivo* prior to implantation. This is especially important when investigating complex biological questions, such as the search for new drugs for cancer immunotherapy, where the TME is best recapitulated in the *in vivo* situation.

In summary, high-throughput genetic screens allow unbiased examination of phenotype-to-genotype relations in a systematic manner and show great potential for the identification of new targets which help in the understanding of the biology in different processes (depending on the biological question) and serve as starting points for possible drug development.

Aim of the study

Activating the intrinsic immune response is the main goal of immunotherapies in cancer. Therefore, the repolarization of immunosuppressive tumor-associated macrophages to proinflammatory M1-like macrophages is seen as a promising approach. However, the current understanding of relevant signaling pathways and specifically also potential therapeutically relevant genes involved in macrophage polarization is limited.

The aim of this thesis is to establish a CRISPR/Cas9-based screening approach in human monocytic cells enabling the identification of novel modulators of macrophage polarization in an unbiased fashion.

Therefore, the following points were addressed:

1. Establishment of the screening system by selecting the most suitable cell system and developing the protocols for polarization, genetic manipulation, FACS based readout, sorting strategy as well as sample processing for next generation sequencing.

2. Testing of the established conditions in a focused sgRNA screen targeting 171 genes known to be expressed in macrophages.

3. Performance of a whole genome targeting CRISPR/Cas9 screen, evaluation of screen quality, and the target hit selection.

4. Verification of screening results for top screening hits and first tests of their general role in macrophage polarization. Furthermore, assessment of suitability of some hits as good starting points for further *in vivo* investigation and drug development.

2 Results

To identify and validate novel targets in an *in vitro* pooled CRISPR screen in human myeloid cells the following aspects have been investigated and the results summarized in this chapter:

1. Establishment of the human myeloid cell CRISPR/Cas9 screening system
2. Evaluation of the established screening system with a focused sgRNA library
3. Performance of a whole genome CRISPR/Cas9 knockout screen
4. Hit identification
5. Hit verification

2.1 Establishment of the human myeloid cell CRISPR screening system

The use of pooled whole genome CRISPR/Cas9 screening for target identification allows comparatively fast screening but requires thorough assay development to obtain a robust system that yields reproducible and statistically significant results.

Therefore, protocols were established for an optimal human monocyte culture, their differentiation to macrophages and polarization into the M1/M2 phenotype. Also, a protocol was established for the transduction of these cells with the Cas9-sgRNA expression system. Furthermore, as screen readout, cells with different M1/M2 phenotype were FACS-sorted. For this purpose, a sorting strategy was defined to enable the proper discrimination of sgRNAs enriched or depleted in the respective populations subsequently to be subjected to deep sequencing. This included next generation sequencing (NGS) library preparation and sgRNA mapping as well as data analysis performed to enable identification of novel targets.

2.1.1 Evaluation of a suitable human cell system

Firstly, a suitable screening cell system had to be identified and established. Based on several features possibly determining technical success, the human monocytic THP-1 cells were tested alongside CD34+ hematopoietic stem cells (HSCs), human primary monocytes (HPMs) and human monocytic U937 cancer cells. As summarized in Table 2.1 the THP-1 cells were found to have the best characteristics to perform a large-scale screen.

Table 2.1. Evaluation of most suitable surrogate myeloid cell screening system
THP-1 cells show the best probabilities to perform a large-scale screening approach and are therefore considered as the best surrogate myeloid cell screening system.

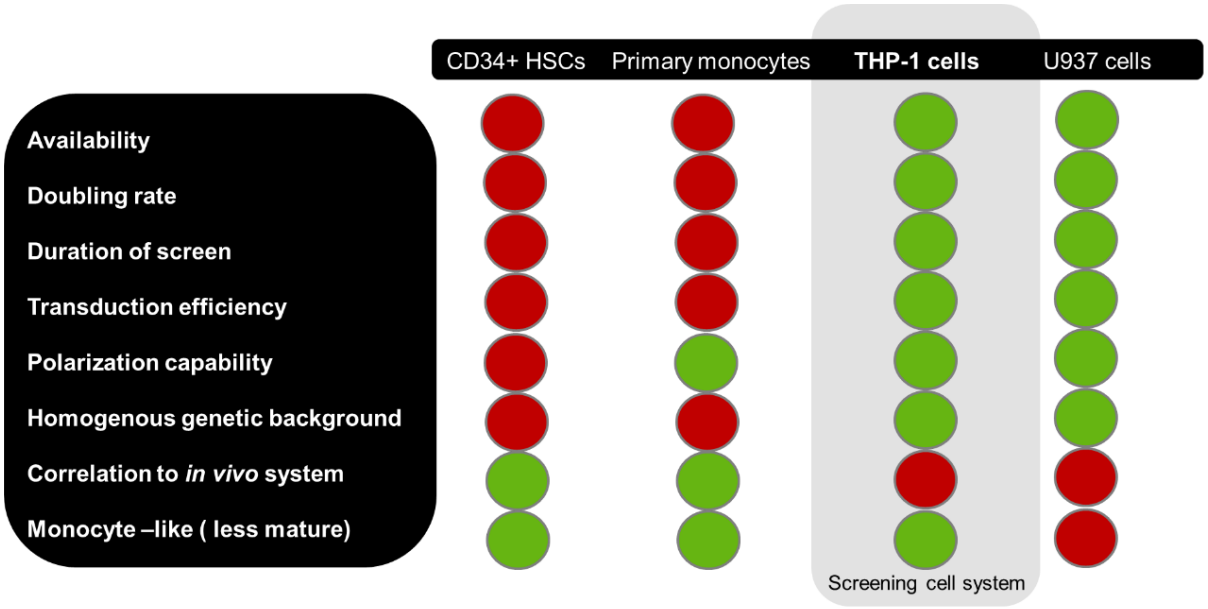

In technical terms, these cells have advantages over human primary monocytes as they are readily available and have growth characteristics ideal for large scale screening approaches not only regarding the duration of the screen but also the feasibility and technical reproducibility. Because more than one billion cells were needed to perform a six-week whole genome CRISPR screen, primary cells which are not immortalized could not be considered as screening cells as they cannot be cultivated *ex vivo* for such a long time. Furthermore, the homogenous genetic background of the THP-1 cells minimizes the phenotypic variability over the course of the screening project. Importantly, THP-1 cells have a significant higher transduction efficiency than the primary cells. In comparison to U937 cells, THP-1 cells are less mature and mimic more the monocyte-like phenotype. For this reason they are more commonly used to examine the cell biology of innate immune signaling (Chanput et al., 2014) than U937 cells.

The major disadvantage of THP-1 cells compared to HPMs is their cancerous origin. However, as described in chapter 2.1.2 and chapter 2.1.3, THP-1 cells show similar differentiation and polarization capabilities compared to HPMs and have therefore been considered a suitable surrogate to perform large-scale genetic screening. This said, the screening results require thorough validation of the identified targets in HPMs in an *ex vivo* approach to test for biological and therapeutic relevance and validity. Consequently, all the protocols established for the screening cells were also adjusted to be applicable for HPMs in parallel.

2.1.2 Polarization of human myeloid cells

To best mimic an *in vivo* situation with *in vitro* systems, HPMs were differentiated and polarized to monocyte derived macrophages (MDMs) following published protocols (Martinez et al., 2008). The combination of Macrophage colony-stimulating factor (MCSF) and Granulocyte-macrophage colony-stimulating factor (GMCSF) was used to differentiate HPMs for 7 days into M0 macrophages. Treating the M0 cells for 6 days with GMCSF and additional 24 h with LPS and IFN-γ generated M1 macrophages, while treating the cells with MCSF for 6 days and additional 24 h with IL-4, resulted in M2 macrophages.

To induce differentiation of THP-1 cells into macrophages, cells are treated for 48 h with Phorbol 12-myristate 13-acetate (PMA) (Genin et al., 2015). After differentiation, the cells were treated for additional 24 h with Lipopolysaccharide (LPS) and Interferon gamma (IFN-γ) to polarize the THP-1 cells into M1 and with Interleukin 4 (IL-4) to polarize them into M2 phenotype. Figure 2.1 shows the treatment regimen.

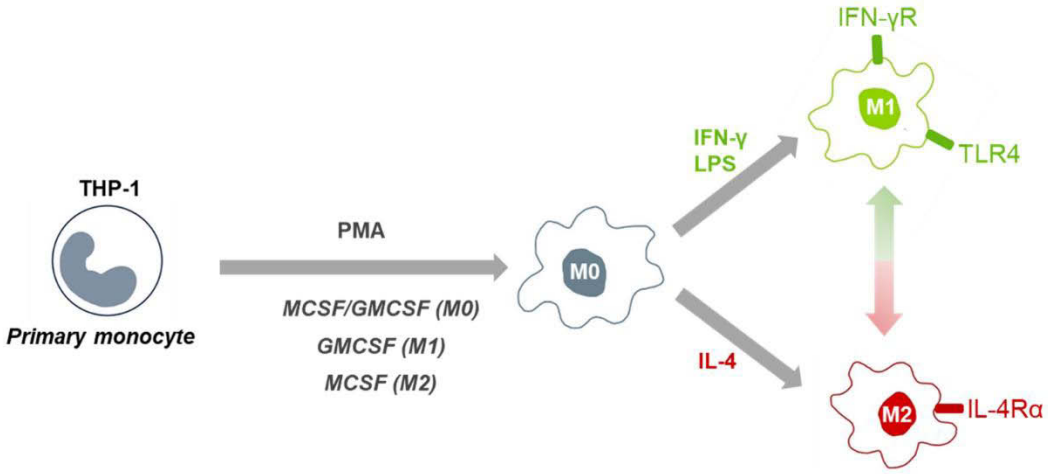

Figure 2.1. Schematic overview of differentiation and polarization conditions
Culture conditions were optimized to obtain M1 and M2 macrophages from primary human monocytes and THP-1 cells.

As cell morphology can serve as an indicator of macrophage polarization status and is associated with different functional stages of macrophages (Rostam et al., 2017; Tedesco et al., 2015) the resulting morphology of the cells was evaluated and compared after the different treatment regimens (Figure 2.2). The monocytic suspension cells were adhering when differentiating and polarizing to macrophages. After treatment with LPS and IFN-γ the cells started developing a predominantly spindle like shape, while IL-4 treatment promoted a round shape. The cell's growth and granularity increased, which was detected microscopically (Figure 2.2a) and by flow cytometry (Figure 2.2b). These morphological changes could be observed to similar degree in both the primary cells as well as the THP-1 monocytic cells suggesting a comparable cellular state.

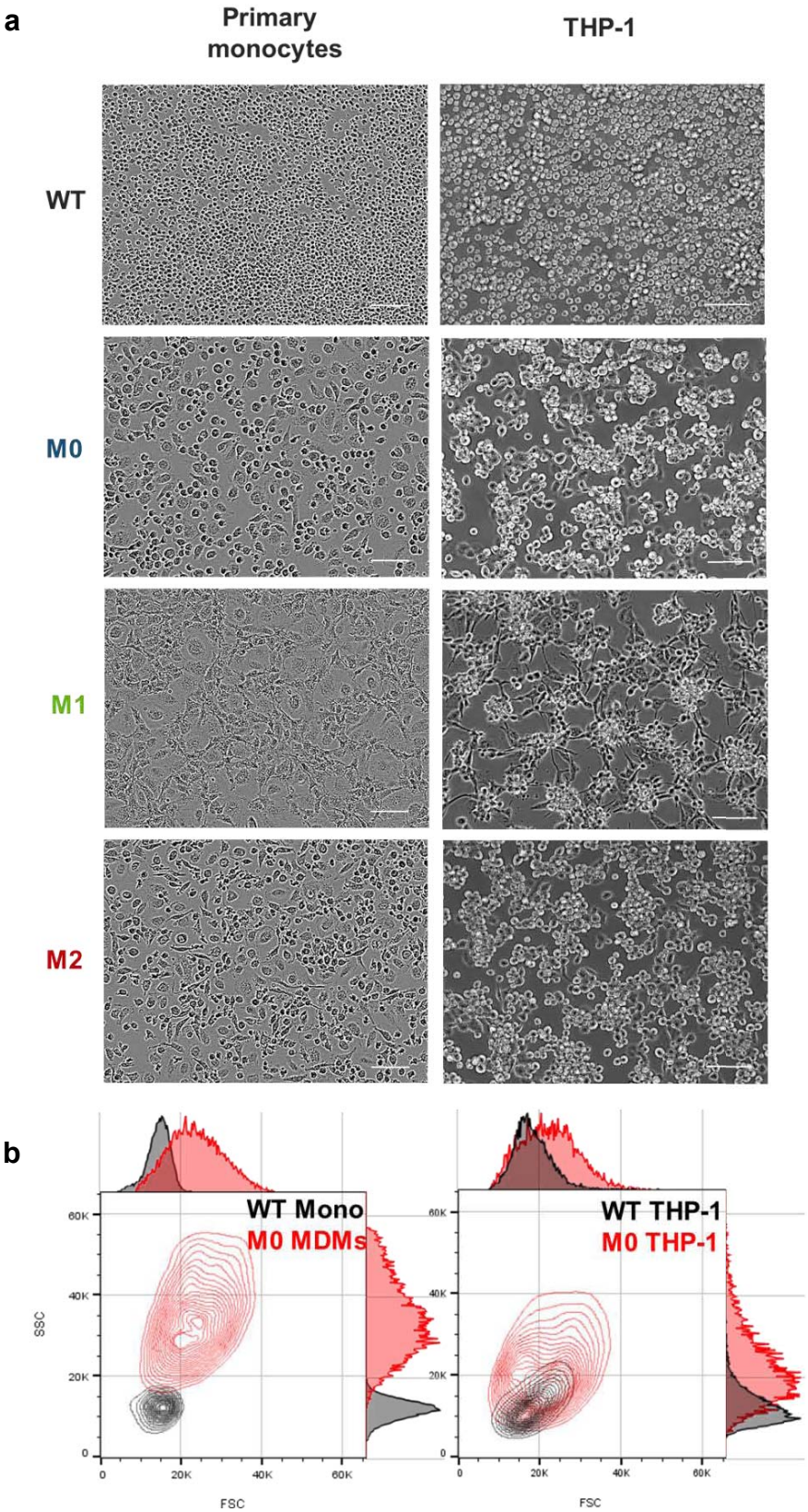

Figure 2.2. Morphology of wild type, differentiated and polarized THP-1 and primary monocytes
(a) Microscopic pictures of differentiated and polarized primary monocytes and THP-1 cells; wild type (WT) are unstimulated primary monocytes or THP-1 cells, M0 are differentiated monocytes and M1 and M2 are polarized monocytes; scale bar = 100 µM (b) FACS analysis of change in growth (FSC) and granularity (SSC) of cells when differentiated to macrophages; Mono = monocytes, MDMs = monocyte-derived-macrophages

To further evaluate the suitability of the THP-1 cells as surrogate myeloid cell screening system, the global transcriptional effects of polarizing THP-1 cells vs. HPMs were studied and compared in an RNA-sequencing (RNA-seq) approach.

Cells were cultured, differentiated and polarized as described before, RNA extracted and sequenced. Then, the 1,000 most highly expressed genes, ranked by Transcripts Per Million (TPM) value, were analyzed and compared between the differentiation only (M0) and polarization (M1, M2) conditions among MDMs and THP-1 cells (Figure 2.3a). The Venn-diagrams show that the different cell systems were sharing the expression of 666 to 696 genes in the M0, M1 and M2 state.

Additionally, sample variance analysis in the RNA-seq dataset using principal component analysis (PCA) was completed to assess the sample similarity of M0, M1 and M2 differentiated/polarized MDMs and THP-1 cells (Figure 2.3b). The base line gene expression profile of THP-1 cells and MDMs differ substantially, as shown by the shift along the axis of principal component 1 (PC1), which accounts for 26.5 % of the variance in the data. The induction of M1 and M2 polarization in both cell systems caused a similar gene expression profile defined by the PC2 axis (17.1 % variance). The highest variance within each cell system was found between M1 and M2 polarized cells. M0 and M2 conditions had the lowest variance for PC1 and PC2, but showed variance in PC3 in Figure 2.3c.

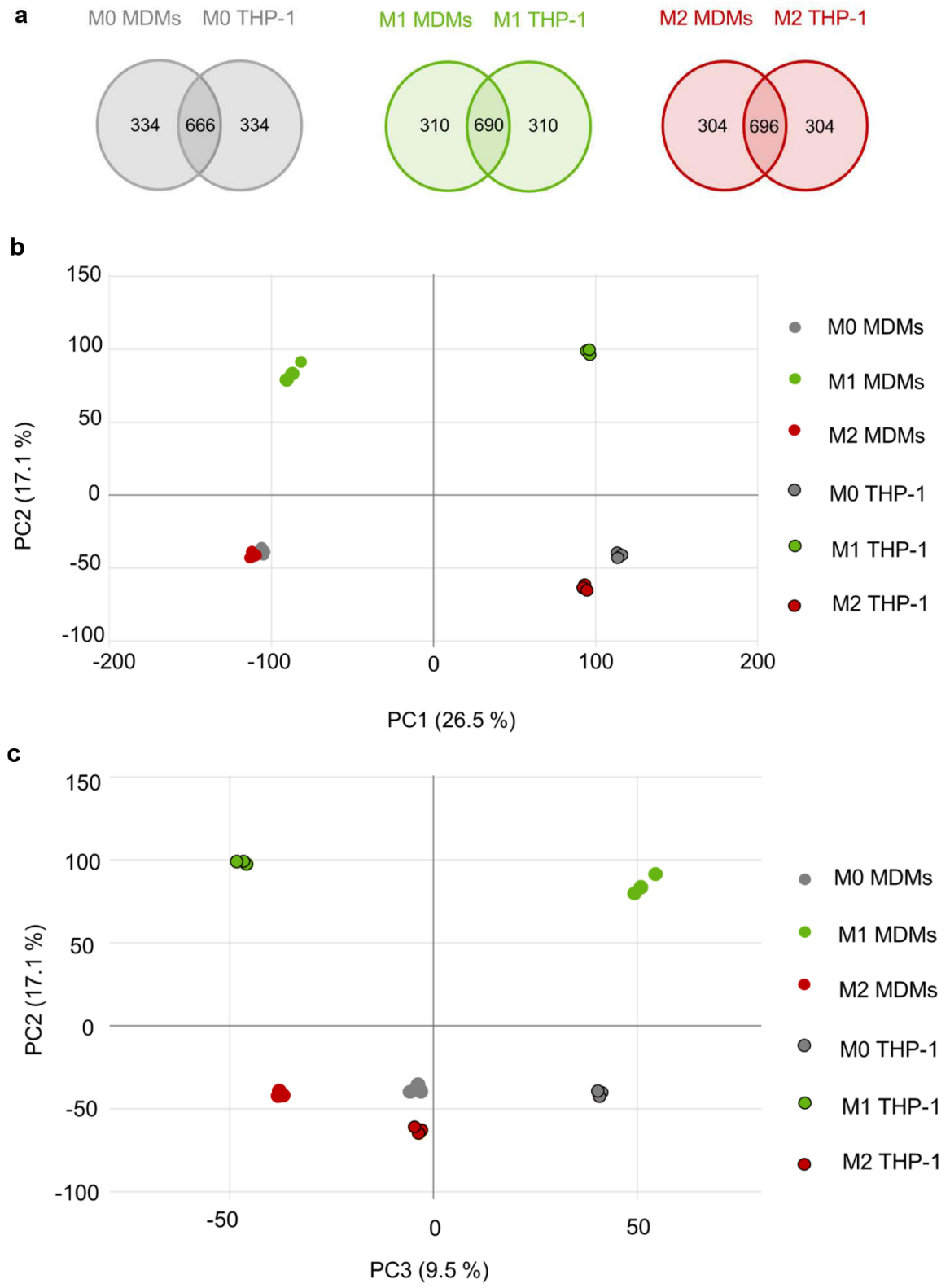

Figure 2.3. Similarity of MDMs and macrophages originating from THP-1 cells
(a) Venn diagram showing the numbers and the overlap of top 1,000 highly expressed genes in MDMs and THP-1 cells in M0, M1 and M2 conditions (b) and (c) Principal component analysis of RNA-seq data of M0, M1 M2 macrophages obtained from primary monocytes or THP-1 cells; n = 3 per sample, PC = Principal component, MDMs = monocyte-derived-macrophages; data analysis was performed by Dr. Helge Roider (Bayer Bioinformatics Department)

In order to define the different M1 and M2 macrophage specific transcriptomes, the top 150 differentially expressed genes (DEGs) ranked by log_2 fold change (FC) (M1/M2) were analyzed and compared between MDMs and THP-1 cells (Figure 2.4). 71 genes were equally regulated in the M1 condition and 30 genes under M2 condition. Importantly, the genes shared in these conditions are polarization markers, such as CD80, CCL19, CCL20, CXCL1, CXCL8-11, IDO1 and IL-6 for M1 conditions and CD209, ADORA3, ALOX15, CCL13, CCL26, and F13A1 for M2 conditions (Figure 2.4). The gene CD80, encoding for a well described M1 surface marker, was found on rank 25 of the DEGs in THP-1 cells and on rank 135 of DEGs in MDMs.

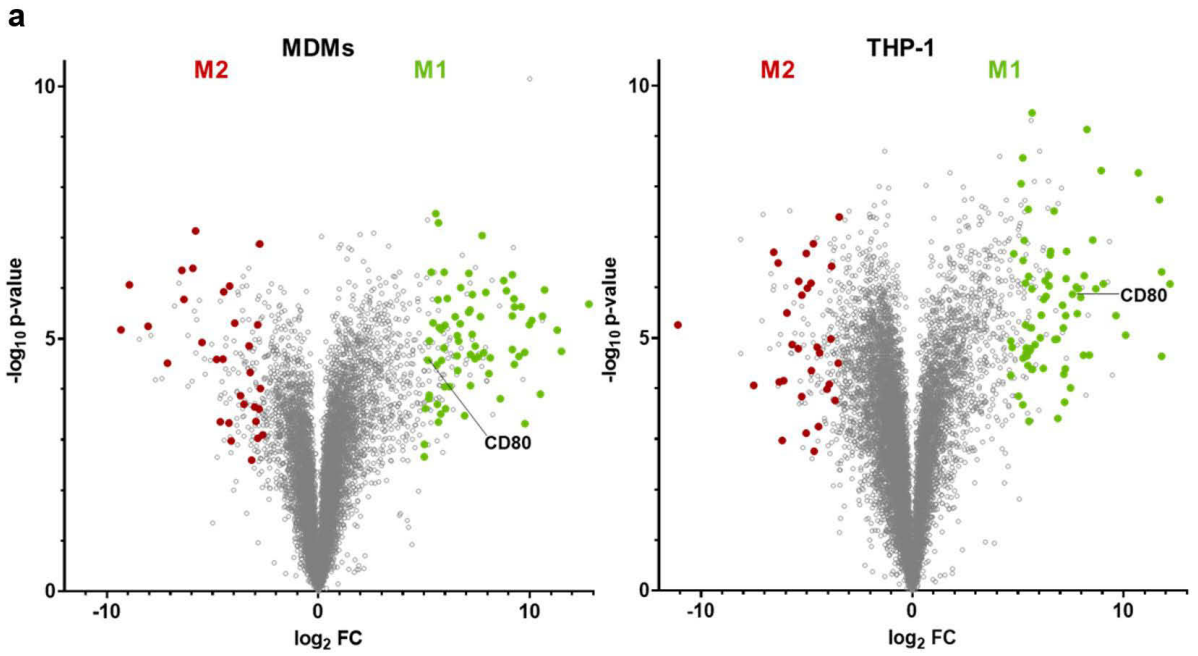

DEGs common in M1 MDMs and M1 THP-1

ACOD1	CD38	CXCL8	HERC5	IL15	LAG3	RSAD2	ZBP1
ADORA2A	CD80	CXCL9	HESX1	IL15RA	LAMP3	SECTM1	
AIM2	CLEC4E	EBI3	HSH2D	IL1B	MX1	SERPINB7	
APOBEC3A	CMPK2	EPSTI1	IDO1	IL23A	NCF1	SERPING1	
C1QTNF1	CXCL1	EREG	IDO2	IL32	OAS2	SIGLEC1	
C1R	CXCL10	ETV7	IFI27	IL36G	OASL	SOD2	
C1S	CXCL11	GBP4	IFI44L	IL6	PDE4B	STAT4	
CCL19	CXCL13	GBP5	IFIT1	IL7R	PLSCR1	TNFAIP6	
CCL20	CXCL2	GCH1	IFIT3	ISG15	PTGES	TNFSF10	
CCR7	CXCL3	HAPLN3	IFITM1	ISG20	PTGS2	UBD	

DEGs common in M2 MDMs and M2 THP-1

ADORA3	CD1E	HRH2
AKAP5	CD209	NFATC2
ALOX15	CD300LB	NRGN
ANKH	CLEC10A	NT5DC2
CCL13	CR1	SNAI3
CCL26	CREG2	TMIGD3
CD180	CTNNAL1	TSPAN7
CD1A	F13A1	TUBA1A
CD1B	FCER2	TUBA8
CD1C	GALNT12	WNT5B

Figure 2.4. Differentially expressed genes between M1 and M2 polarized macrophages originating from primary monocytes or THP-1 cells

(a) Vulcano plot for differential expressed genes (DEGs) of M1 polarized cells compared to M2 polarized monocyte-derived-macrophages (MDMs) or THP-1 cells. Dots depict genes (n = 3), y-axis shows the significance of differential expression, x-axis displays magnitude and direction of the log_2 fold change (FC) in transcript abundance. Red dots represent significantly DEGs shared by M2 MDMs and M2 THP-1 cells and green dots represent significantly DEGs shared by M1 MDMs and M1 THP-1 cells, plot generated with GraphPad Prism 8 (b) Venn diagrams showing numbers and overlap of top 150 DEGs shared by MDMs and THP-1 in M1 and M2 polarization conditions, shared genes are labeled in table below, displaying many macrophage polarization markers; data analysis was performed by Dr. Helge Roider (Bayer Bioinformatics Department)

The expression of common M1 and M2 macrophage markers (based on literature research) in MDMs and THP-1 cells is depicted in the heatmap in Figure 2.5. Highly upregulated genes found in M1 polarized THP-1 cells and MDMs are consistent with M1 genes published to be upregulated in MDMs (HLA-DRA, CD80, TLR2, IDO1, IL-1B, IL-6, IL-12B, TNF, IL-23A, CXCL8-10, CXCL16, CCR7, CCL3, CCL5 and CCL19) and so are genes found in M2 polarized THP-1 cells and MDMs (MRC1, CD209, CD200R1, FCER2, ALOX15, F13A1, CCL13, CCL22, CCL24, CCL26 and CLEC4A) (Mantovani et al., 2002; Murray et al., 2014). These genes are consistently expressed in MDMs and THP-1 derived macrophages.

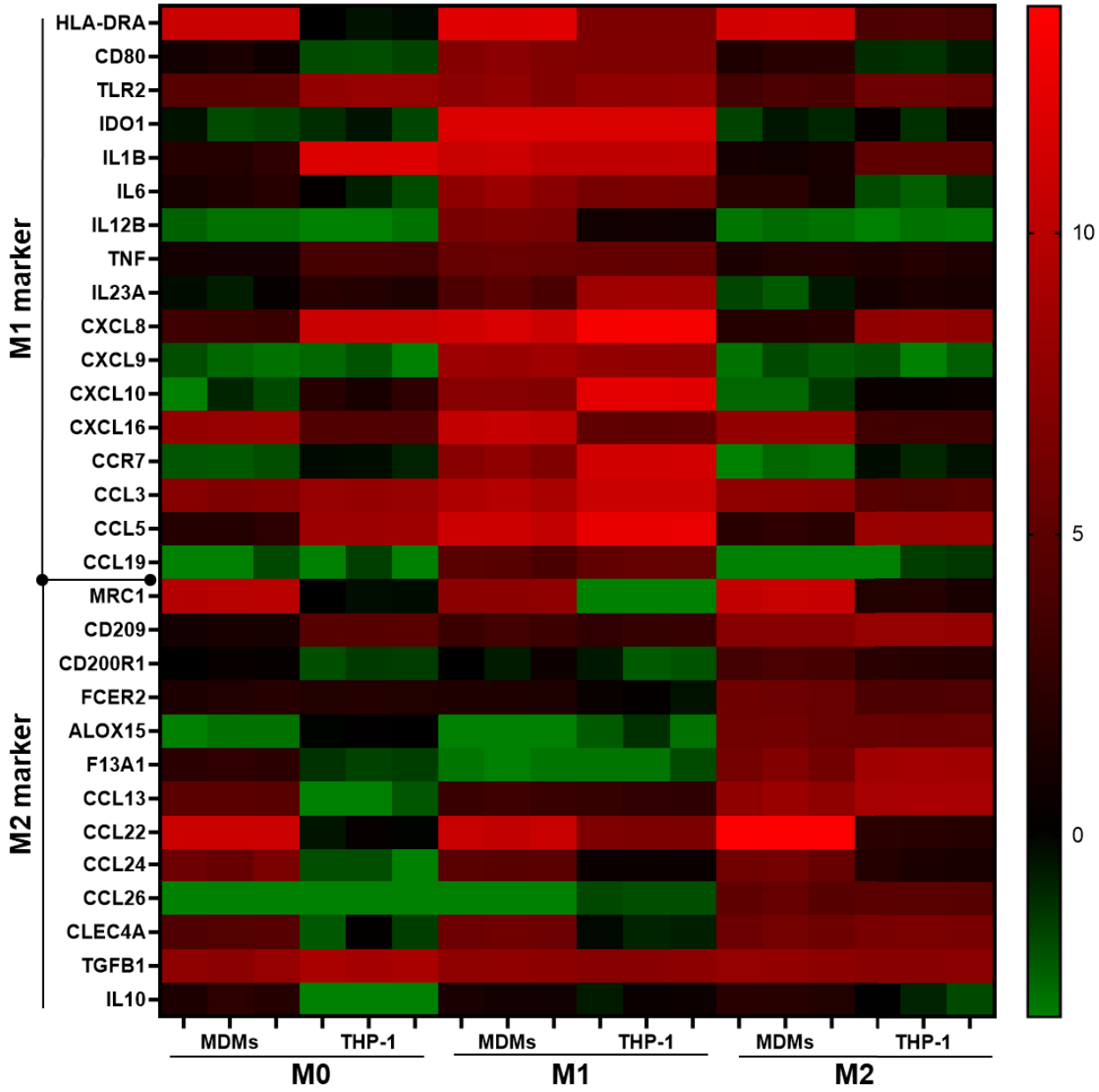

Figure 2.5. M1 and M2 marker gene expression in M0, M1 and M2 MDMs and THP-1 cells derived macrophages
Heat map representing color-coded expression of common M1 or M2 marker genes after RNA-seq analysis of M0, M1 or M2 monocyte-derived macrophages (MDMs) or M0, M1 or M2 THP-1 cells (log_2 TPM). M1 marker gene expression and M2 marker gene expression was found to be upregulated in the M1 or M2 polarization sample respectivetly. n = 3 per sample; data analysis was performed by Dr. Helge Roider (Bayer Bioinformatics Department)

As an additional approach to study differences in the functionality of the M1 and M2 macrophage subsets, their production of proinflammatory cytokines was examined (Figure 2.6). The protein concentration of the cytokines TNF, IL-6, IL-1β and IL-12(p40) was deterimed by enzyme-linked immunosorbent assay (ELISA) and showed significantly higher concentrations in the generated M1 macrophages originating from both, HPMs or THP-1 cells.

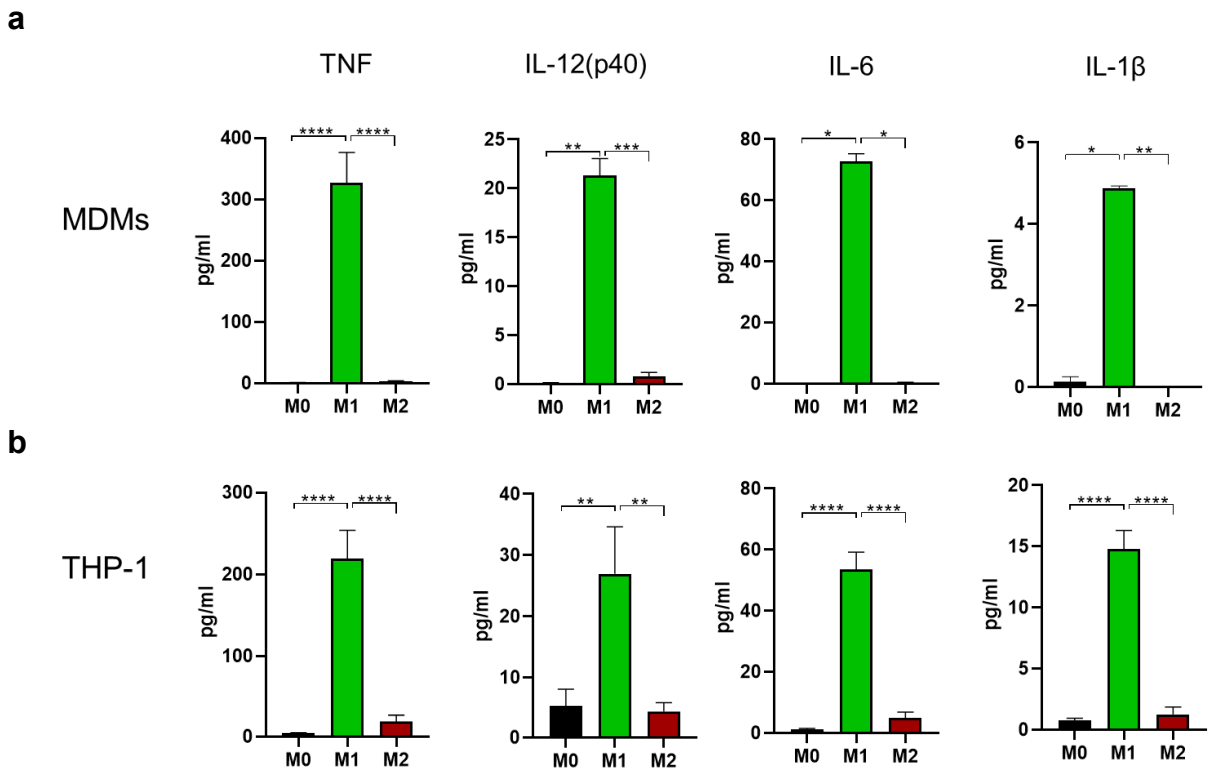

Figure 2.6. Proinflammatory cytokine secretion of MDMs and THP-1 derived macrophages
(a) Primary human monocytes were differentiated to M0 macrophages with MCSF/GMCSF and polarized to M1 with IFN-γ and LPS and to M2 macrophages with IL-4 (b) THP-1 cells were differentiated to M0 macrophages with Phorbol 12-myristate 13-acetate (PMA) and polarized to M1 macrophages with IFN-γ and LPS and to M2 macrophages with IL-4. Cell culture supernatant was harvested, and ELISA analysis was performed for the proinflammatory cytokines TNF, IL-12(p40), IL-6 and IL-1β [pg/ml]. n ≥ 3. Mean ± SEM, paired t-test, * p ≤ 0.05, ** p ≤ 0.01, *** p ≤ 0.001, **** p ≤ 0.0001

Coculture experiments were performed to characterize the functionality of the macrophage phenotypes regarding the activation and proliferation of primary T cells as well as the activation of Jurkat cells. Therefore, M0, M1 or M2 macrophages were cocultured with primary T cells from different donors and the activation of T cells was assessed by ELISA of IFN-γ. The proliferation of T cells was determined using FACS-based analysis of Carboxyfluorescein succinimidyl ester (CFSE) dilution due to T cell division. The M1 and M2 polarized THP-1 cells were cocultured with Jurkat IL-2 promoter_NLucP reporter cells (Axxam). These cells were engineered to express NanoLuc® luciferase under the control of the IL-2 promoter. The IL-2 expression after coculturing the cells with polarized THP-1 cells was assessed with the Nano-Glo® Luciferase Assay System (Promega). As shown in Figure 2.7 IFN-γ secretion and proliferation of T cells were stronger induced in primary T cells cocultured with M1 MDMs than with M2 MDMs. Similar results are seen for coculturing M1 or M2 THP-1 cells with Jurkat cells, which is detected by increased IL-2 expression in Jurkat cells cocultured with M1 THP-1 cells.

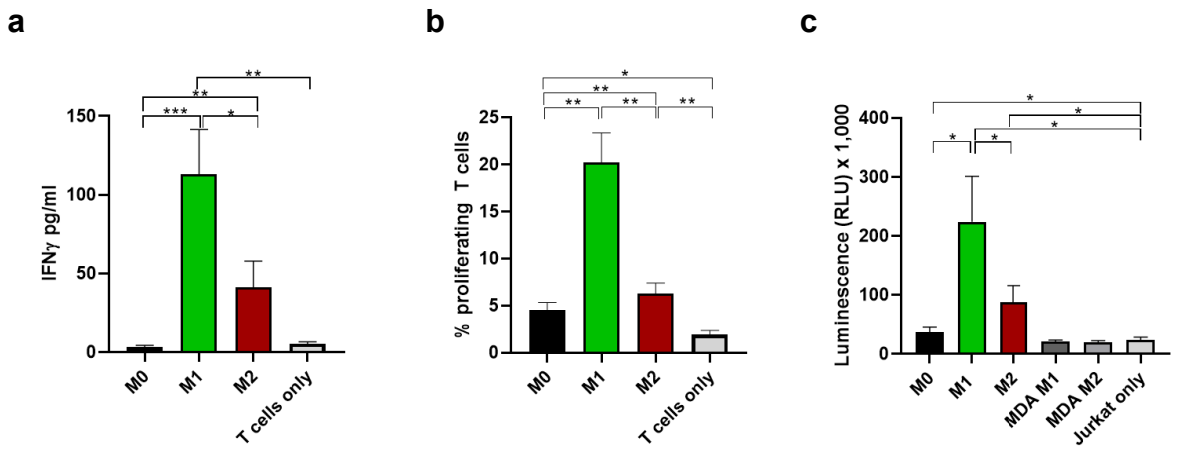

Figure 2.7. T cell activation and proliferation after coculture with M0, M1 or M2 MDMs or THP-1 cells
(a) ELISA of IFN-γ secretion by primary human T cells cocultured with M0, M1 or M2 MDMs for 5 days (b) FACS analysis of proliferating T cells stained with CFSE (Carboxyfluorescein succinimidyl ester) and cocultured with M0, M1 or M2 MDMs for 5 days. (c) Nano-Glo® Luciferase Assay detecting NanoLuc® luciferase under the control of the IL-2 promoter in Jurkat IL-2 promoter NLucP reporter cell line (Axxam) after 24 h coculture with M0, M1 or M2 macrophage derived from THP-1 cells, or cocultured with M1/M2 stimulated MDA MB231 cells as a negative control. Jurkat cells cultured without macrophages are named "Jurkat only" and serve also as a control. n ≥ 3. Mean ± SEM, paired t-test; * p ≤ 0.05, ** p ≤ 0.01, *** p ≤ 0.001, **** p ≤ 0.0001

In summary, both THP-1 cells and primary monocytes showed comparable profiles of generated M1 and M2 phenotypes not only on M1 and M2 markers, but also in their functionality to secrete proinflammatory cytokines and activate T cells, confirming the suitability of studying macrophage polarization with the established polarization protocols in THP-1 cells as well as in primary monocytes.

2.1.3 Genetic manipulation of THP-1 cells

2.1.3.1 Generation of the THP-1-Cas9 screening cell line

To increase the reproducibility of performing CRISPR-based experiments a stable Cas9 expressing THP-1 cell clone was generated. To do so, THP-1 cells were transduced with a lentiviral packaged Cas9 expression vector, selected with hygromycin B, and single cell sorted. After expansion and further hygromycin B selection Cas9 expression was examined with western blot analysis. Out of 12 clones that could be expanded, clone 2 and 8 showed Cas9 protein expression (Figure 2.8a) and were further tested for Cas9 cutting activity (Figure 2.8b). Therefore, the CRISPRtest™ Functional Cas9 Activity Kit from Cellecta (#CRUTEST) was used. This assay is based on the co-transduction of cells with sgRNAs targeting the essential gene PCNA (proliferating cell nuclear antigen), co-expressing green fluorescent protein (GFP) and sgRNAs against a control gene co-expressing red fluorescent protein (RFP) in a specific limiting ratio. High Cas9 cutting activity in these cells leads to cell death due to efficient PCNA knockout (KO) and reduction in GFP abundance which is compared to the RFP expression of

the non-toxic control sgRNA. The ratio of GFP:RFP cells enables the calculation of Cas9 cutting activity.

Clone 8 showed highest Cas9 expression and a Cas9 activity of 73 %, which shows to be sufficient to efficiently edit genes leading to gene KO.

a

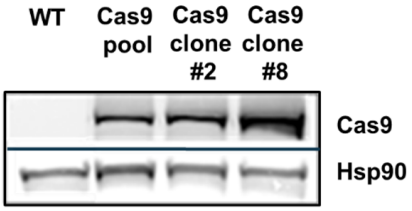

b

% KO = Cas9 activity

WT	Cas9 pool	Cas9 clone #2	Cas9 clone #8
0 %	77 %	73 %	73 %

Figure 2.8. Generation of a THP-1 clone stably expressing Cas9
(a) Determination of Cas9 protein level by western blot analysis of wild type (WT) THP-1 cells, THP-1 cells with heterogenous Cas9 expression in a pool of cells (Cas9 pool) and in the two clonal selected THP-1 Cas9 cell lines (Cas9 clone #2 and Cas9 clone #8) including Hsp90 (heat shock protein 90) loading control (b) Cas9 activity tested in a functional assay from Cellecta (CRISPRtest^{TM} Functional Cas9 Activity Kit (#CRUTEST))

To ensure that the selected clone had retained the THP-1 parental cells' polarization capabilities determined before, the mRNA expression of major M1 and M2 markers were compared between the parental THP-1 cells and the THP-1 Cas9 clone 8. The expression profile of these cells examining M1 and M2 markers was comparable, as shown in the heat map in Figure 2.9.

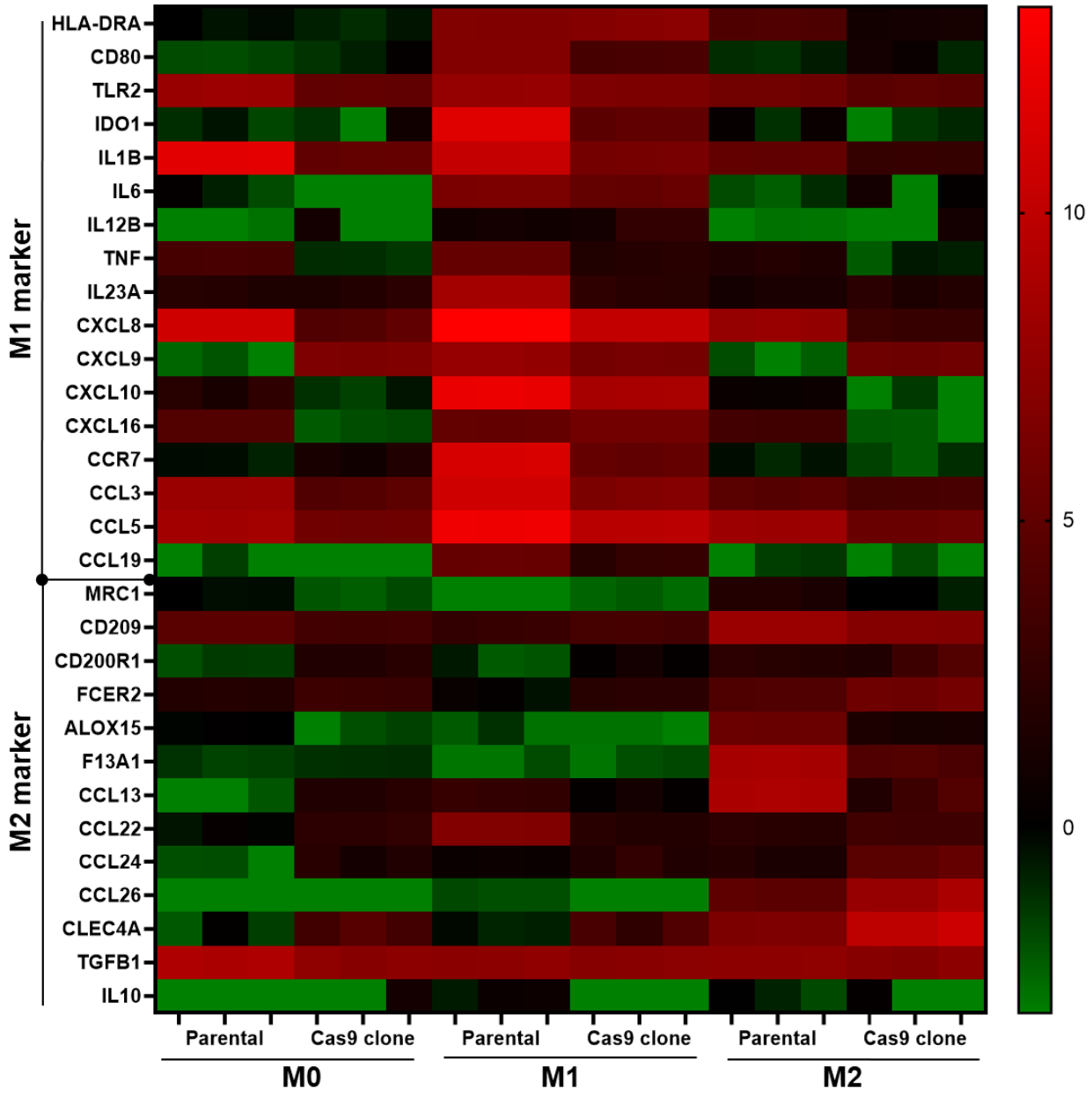

Figure 2.9. M1 and M2 gene marker expression in polarized THP-1 parental and THP-1 Cas9 clone 8 cells

Heat map representing color-coded expression of common M1 or M2 marker genes after RNA-seq analysis of M0, M1 or M2 THP-1 parental cells or M0, M1 or M2 THP-1 Cas9 clone 8 cells (log_2 TPM), M1 marker gene expression and M2 marker gene expression was found to be upregulated in the M1 or M2 polarization sample respectivetly and comparible in both parental and Cas9 clone 8 THP-1 cells; n = 3 per sample; data analysis was performed by Dr. Helge Roider (Bayer Bioinformatics Department)

2.1.3.2 Transduction of pooled sgRNA library in THP-1 clone 8 screening cells

Pooled CRISPR/Cas9 screening relies on a direct phenotype-sgRNA expression relation. This requires that each cell is transduced by only one virus, leading to a single sgRNA being integrated and expressed per cell, and ensuring that the induced KO causes the observed phenotype. To achieve this single sgRNA integration, a transduction rate of less than 30 % is

recommended (Doench, 2018; Sanson et al., 2018). Different cell systems show differences in their sensitivity to viral infections. Therefore, the multiplicity of infection (MOI), equaling the number of viral particles needed to infect a given number of cells, must be determined experimentally for every screening cell system using a given sgRNA library. Based on the viral titer of 1.23×10^9 TU/ml (transduction units per ml) Cellecta had determined for whole genome pooled sgRNA library module 3, increasing MOIs were tested. As RFP is co-expressed with the sgRNA transcribed from the viral DNA the percentage of RFP+ cells increased with increasing MOI values. Fig 2.10 shows that transduction of the THP-1 Cas9 clone 8 with one viral particle of the used sgRNA library per cell was necessary to achieve 30 % of the transduced cells to express RFP. These results suggest that a MOI of 1 is optimal to perform a pooled CRISPR screen using this library.

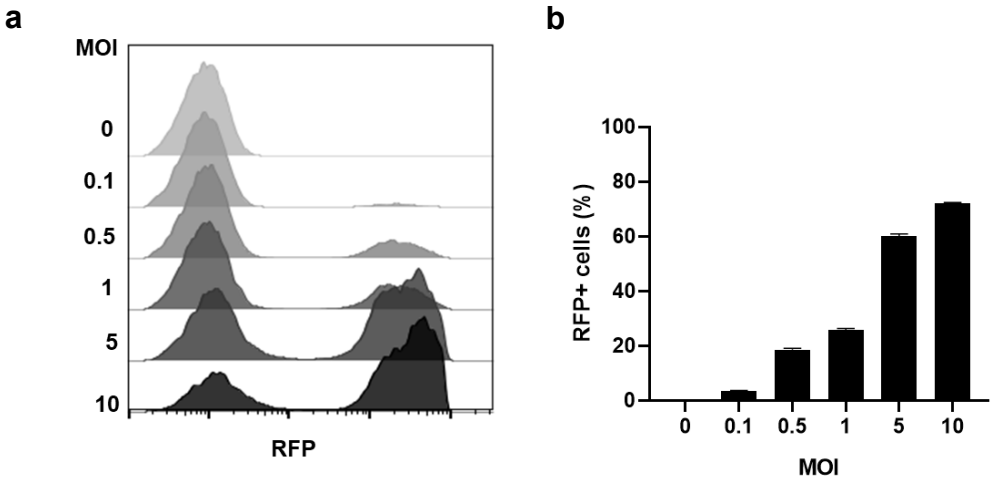

Figure 2.10. Multiplicity of infection (MOI) determination for pooled sgRNA library screening
THP-1 Cas9 clone 8 cells were transduced with different MOIs of the lentiviral whole genome sgRNA pooled library (module 3) particles co-expressing RFP. Three days post transduction the transduction efficiency was analyzed by FACS analysis. (a) Successfully transduced cells with different lentiviral particle load express RFP which was assessed by flow cytometry and displayed in a histogram (b) bar plot shows percentage of RFP+ THP-1 Cas9 clone 8 cells detected by flow cytometry as mean ± SD, n = 3; An MOI of 1, resulting in 30 % of the examined cells to be successfully transduced, was used for performing the CRISPR/Cas9 pooled screens.

To select the 30 % transduced cells with a single sgRNA integration the cells were treated with puromycin, for which a resistance gene was also co-expressed with the sgRNAs. The optimal puromycin concentration was determined to be 2 µg/ml (data not shown).

2.1.3.3 Electroporation of THP-1 cells using gRNAs

As an alternative to the viral-based sgRNA delivery method used in the screen, conditions were defined to electroporate THP-1 cells using the Amaxa 4D Nucleofector. The Figure 2.11 shows that a gRNA (pre-complexed tracrRNA + crRNA) targeting the gene PLK1 (polo-like kinase 1), essential for cell fitness, and electroporated into untreated Cas9-positive THP-1 cells. This causes significant reduction in cell viability in comparison to non-targeting gRNAs

or cells which only received the electrical pulse but no gRNA, indicating successful electroporation.

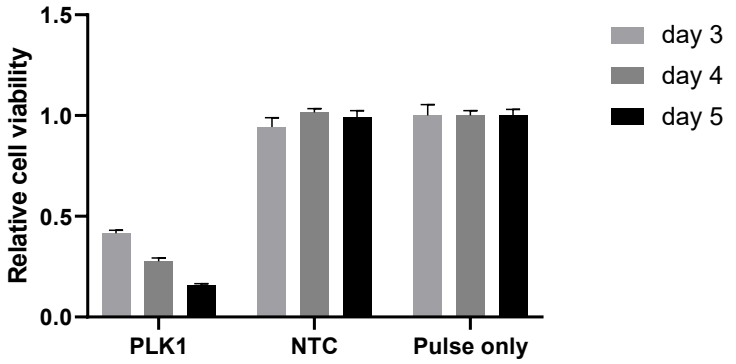

Figure 2.11. gRNA electroporation efficiency in THP-1 cells
Electroporation of crRNA and tracrRNA complexes (gRNAs) into THP-1 Cas9 cells targeting the gene PLK1, essential for cell viability, non-targeting gRNAs (NTC) or no gRNAs (Pulse only). Relative cell viability was measured using CellTiter-Glo® Luminescent Cell Viability Assay at 3, 4 or 5 days post electroporation. The KO of the essential gene PLK1 resulted in a relative reduction of cell viability to 16 % in comparison to NTC or Pulse only cells at day 5 post electroporation.

This method was used for target validation purposes as crRNAs are readily available and cost-effective compared to lentiviral sgRNA delivery.

2.1.4 Genetic manipulation of human primary monocytes

Even though THP-1 cells served as a suitable model system to study monocyte polarization under screening conditions, to understand the biological role of the targets identified in the screen it is necessary to confirm the data in a physiologically more predictive cell system, the HPMs. For most of the screening hits no specific chemical agent is known that could block the target protein and be used to verify the effects detected in the THP-1 cells. Thus, it is necessary to use genetic perturbation methods to study the biology of the targets.

Therefore, conditions had to be identified to directly manipulate primary monocytes, ideally, to establish conditions to allow CRISPR-based experimentation. The standard methods to achieve genetic perturbation are viral-based transduction, lipid-mediated transfection or electroporation of cells. All these methods have been thoroughly tested to function in HPMs.

2.1.4.1 Transduction optimization of primary monocytes

Genetical manipulation of primary myeloid cells has proven to be very difficult. As a starting point, several conditions were tested to transduce HPMs virally. The optimization strategy included promoting co-localization of the monocytes and virions using RetroNectin-coated

plates and spinoculation for differing durations. Also, polybrene, known to improve transduction efficiencies in many cell types (Davis et al., 2002), was tested at varying concentrations to identify the optimal concentration to increase retrovirus gene transfer efficiency. The limiting factor of all the above-mentioned methods and transduction-enhancing-substances is the possible induction of toxicity which was assessed microscopically (data not shown). Thus, it was also tested if the fitness of the cells affected the transduction results significantly by comparing freshly isolated and thawed monocytes and determining optimal growth factor concentrations.

Using the optimized conditions, lenti-virally packaged sgRNAs co-expressing GFP and RFP could be transduced into HPMs with a transduction efficiency of about 25 % (Figure 2.12). This is equivalent to an experimental MOI of 0.25 which would be suitable for the planned experiments. However, for CRISPR/Cas9-based experiments also the 160 kDa Cas9 protein has to be introduced and expressed in the cells. Probably due to the large size of the construct (11,537 bp) packaging and integration efficacy are very low. Even after extensive testing of various parameters possibly affecting transduction efficiencies no Cas9 expression could be detected in these cells. Since the HPMs could be successfully transduced, the alternative method to achieve genetic perturbation is using RNA interference (RNAi), specifically virally packaged shRNAs. This induces target knockdown (KD) without the need of Cas9 expression. Figure 2.12 shows the successful transduction of an shRNA co-expressing RFP into monocytes with an efficiency of 27 % using the optimized transduction protocol. As the aim of the study is to harness the advantages of CRISPR screening, this technique would serve as an optional method for validation of identified targets but is not suitable for performing the pooled screen.

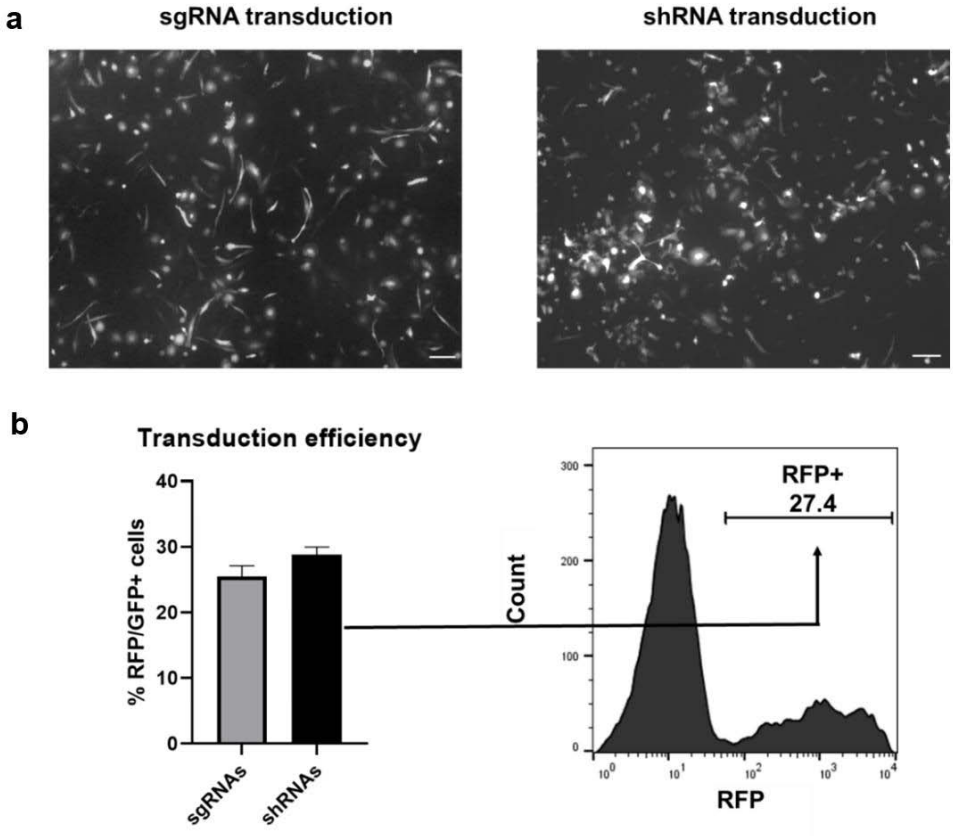

Figure 2.12. Efficiency of sgRNA and shRNA transduction in human primary monocytes
Fluorescent microscopy of lenti-virally packaged sgRNAs co-expressing GFP and RFP or lenti-virally packaged sgRNAs co-expressing RFP transduced human primary monocytes (HPMs) 7 days post transduction; 25 % of transduced cells were GFP or RFP positive, scale bar = 100 µM (b) Barplot of percentage of GFP+/RFP+ transduced cells with sgRNAs or shRNAs and FACS histogram displaying RFP+ fraction of shRNA transduced HPMs; n = 3 with each technical triplicates; Mean ± SD

2.1.4.2 gRNA and RNP electroporation of human monocytes

In parallel to testing viral transduction methods to manipulate HPMs, also the use of RNA oligos such as crRNAs (CRISPR RNA) or siRNAs (small interfering RNA) was investigated. These small RNAs could be either transfected using lipids or be introduced into the cells by electroporation. Electroporation might also be an option to introduce an active Cas9 protein, RNA or ribonucleoproteins (RNPs) into the cells. RNPs consist of a preformed complex of Cas9-protein and gRNA (tracrRNA + crRNA). A great advantage of this method is that the CRISPR-based method can be used without stable expression of Cas9 in the cells. This is optimal for the validation of targets but is not enabling pooled CRISPR/Cas9 screening, as the gRNAs are not stably integrating into the DNA and cannot be identified by deep sequencing anymore.

Many parameters were tested to find optimal settings to transfect HPMs or even THP-1 cells using lipids and RNPs. However, neither of the two cell types could be transfected with

reasonable efficiency and viability using the lipid-based method. All the lipids tested to transfect HPMs were cytotoxic to the cells or resulted in no gene KO (data not shown).

To establish conditions for electroporation, the electrical pulse, the efficiency of different available recombinant Cas9 proteins (from Streptococcus pyogenes) was determined and the gRNA/Cas9 ratio was optimized to reduce toxicity and increase electroporation efficiency in HPMs. Figure 2.13 shows that a gRNA targeting an essential gene ("Lethal"), complexed with active Cas9 protein and electroporated into HPMs using optimized conditions, causes significant reduction in cell viability down to 8 % in comparison to non-targeting gRNAs or the pulse only control (no gRNA/Cas9 complex), indicating successful electroporation without negative effects on cell viability.

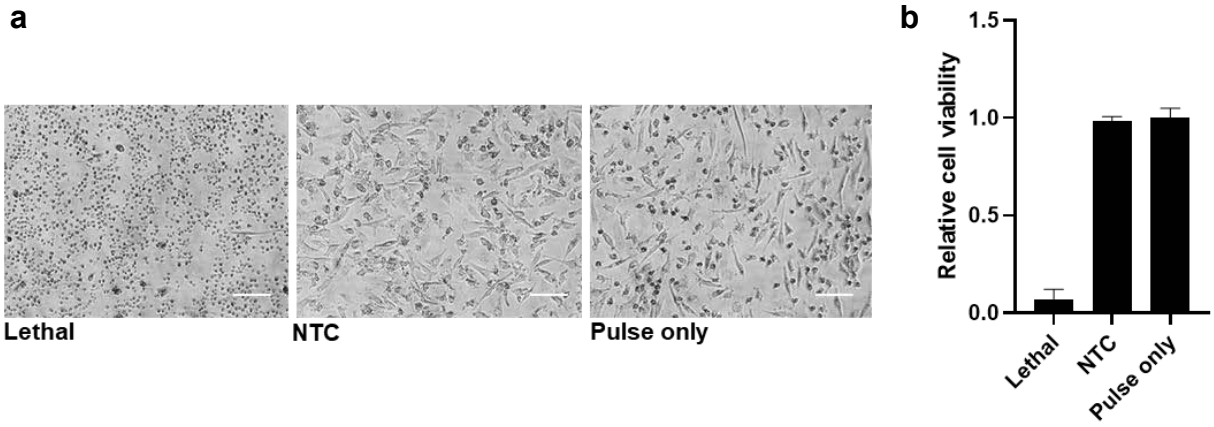

Figure 2.13. RNP electroporation efficiency in primary monocytes
Electroporation of preformed ribonucleoproteins (RNPs) in primary human monocytes (HPMs) and examination of the relative cell viability by CellTiter-Glo® Luminescent Cell Viability Assay (Promega) 5 days post electroporation. The knockout of an essential gene (Lethal) resulted in a relative reduction of cell viability to 8 % in comparison to non-targeting gRNAs (NTC) or the pulse only control (no gRNA/Cas9 complex), where almost 100 % of the cells were viable, (a) Representative microscopical picture of electroporated cells; scale bar = 100 µM, (b) Bar blot depicting quantification of viable cells from n = 3; Mean ± SD

2.1.5 Establishment of a FACS based readout

One possible method for a phenotypic readout for pooled CRISPR screens is the physical separation of the cells into subpopulations which show distinct protein expression detected by flow cytometry (Doench et al., 2014). Therefore, a highly sensitive and stable expression-based readout system for surface markers suitable for FACS-based cell sorting has been established.

The advantage of the separation based on surface marker expression is, that it does not require permeabilization and beforehand Brefeldin A treatment, as it would be necessary for cytokine staining for example. Due to the complexity of the screening procedure, the most important characteristic of the readout is its technical feasibility to obtain robust results. The

readout system must be highly sensitive and stable to enable identification of enrichment or depletion of the phenotype after gene KO.

For this purpose, well described M1 and M2 surface markers, such as CD80, MHC-II and CD86 for the M1 phenotype and CD163, CD206 and CD209 for the M2 phenotype, were examined based on flow cytometry analysis.

In Figure 2.14 the FACS blots for the protein expression of the surface markers CD80, MHC-II, CD163 and CD209 are displayed, which have been described to discriminate best both M1 and M2 polarizing conditions in THP-1 derived macrohages and MDMs based on their expression of surface markers (Mantovani et al., 2002; Murray, 2017). Among these markers CD80 was found to best discriminate M1 and M2 polarized THP-1 cells and MDMs which was detected on mRNA level in Figure 2.4 as well as on protein level in Figure 2.14. The M2 marker CD209 was distinct expressed in M1 and M2 MDMs and THP-1 cells on mRNA level (Figure 2.4), but not on protein level detected with FACS analysis (Figure 2.14). Another M2 marker, CD163, could also not enable the clear separation of M1 and M2 polarized macrophages in THP-1 cells as it could in primary macrophages (data not shown). These findings are consistent with data already reported, indicating that THP-1 cells can be better characterized by M1 phenotype marker than by M2 marker (Shiratori et al., 2017; Tedesco et al., 2018).

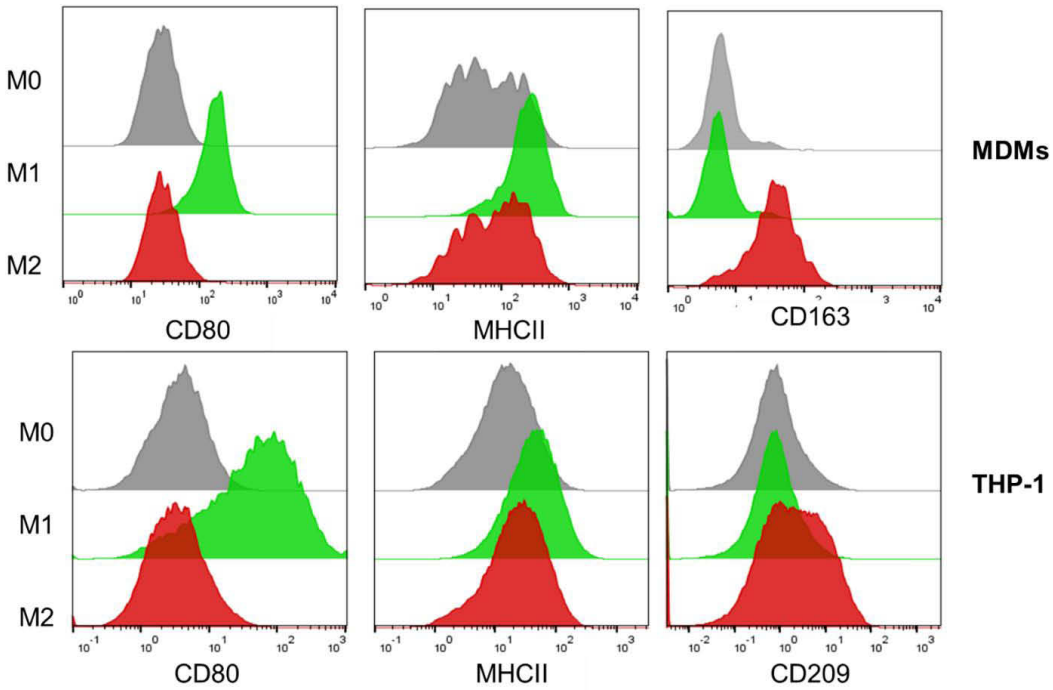

Figure 2.14. M1 and M2 surface marker analysis of MDMs and THP-1 derived macrophages
Primary human monocytes (HPMs) were polarized into M0, M1 or M2 monocytes derived macrophages (MDMs) and THP-1 cells were polarized into M0, M1 and M2 macrophages as described before. The best surface marker for differentiating between M1 and M2 polarized THP-1 screening cells was determined as CD80 (M1 marker), the M1 marker MHC-II and M2 marker CD209 could not distinguish the two polarizing phenotypes well, unlike in MDMs where both CD80 and M2 marker CD163 enabled good discrimination of M1 and M2 macrophages.

CD80 is known to be a robust M1 macrophage marker in the murine and human system (Mantovani et al., 2013) and determined to be the most significant M1 and M2 discrimination maker for our screening purpose. But also, CD80 is known to play a crucial role in T cell activation and thereby the activation of the immune response in a tumor microenvironment (TME) with anergic T cells. CD80 together with CD86 is a costimulatory molecule for T cell activation, survival and IL-2 production, therefore the modulation of CD80/CD86 expression on antigen presenting cells (APCs) as macrophages may alter the development of the immune response. Furthermore, the expression level of CD80 and not only its presence was shown to having an influence on tumor growth (Yu et al., 1998).

For testing the applicability of the chosen anti-human CD80 BV421 antibody conjugate (BD, # 564160), gRNAs targeting CD80 were electroporated into the screening THP-1 Cas9 cells. Assessing the difference of the mean fluorescence intensity (MFI) of CD80 expressing cells electroporated with non-targeting control (NTC) gRNAs or gRNAs against CD80, it could be shown that the antibody used, detected the different expression levels in CD80 wild type vs. CD80 KO cells implicating the feasibility to use this specific CD80 antibody conjugate for screening purposes in M1 and M2 polarizing conditions (Figure 2.15).

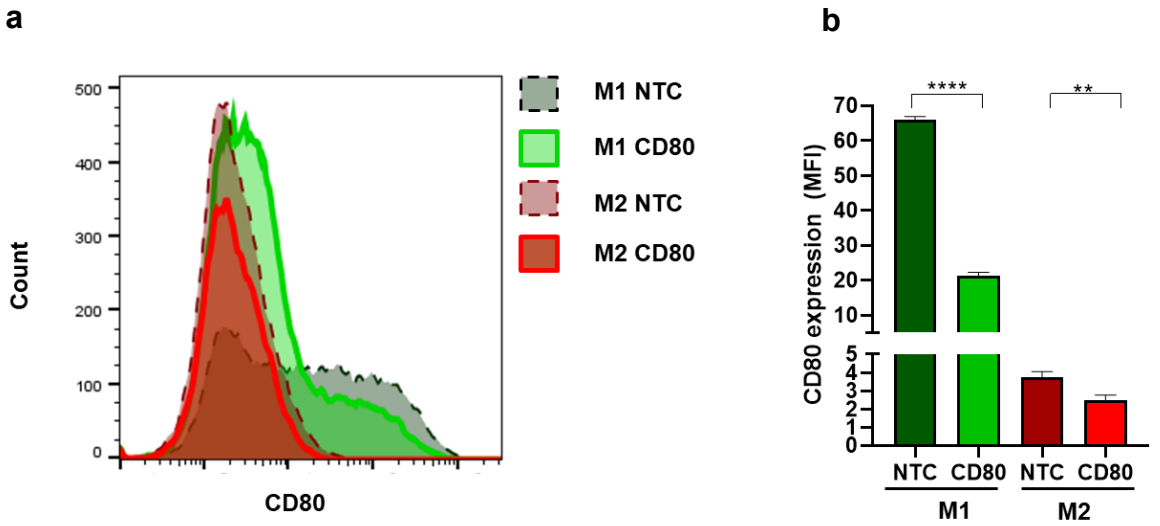

Figure 2.15. Effects of electroporated CD80 targeting gRNAs in THP-1 Cas9 screening cells on CD80 expression using FACS based readout
THP-1 Cas9 screening cells were electroporated with gRNAs against CD80 and non-targeting control gRNAs (NTC), differentiated and polarized to M1 and M2 macrophages, and stained for CD80 expression (a) Flow cytometry analysis of CD80 expression; overlaid histograms as a representative; (b) Quantified mean fluorescence intesity (MFI) of CD80 expression in experiment displayed in a), Mean ± SD (technical triplicate), unpaired t-test; * $p \leq 0.05$, ** $p \leq 0.01$, *** $p \leq 0.001$, **** $p \leq 0.0001$

For a pooled screening approach, ideally a positive or negative selection screen could be done. Figure 2.16 shows that distinct subpopulations representing distinct CD80 marker -expressing cell populations would be best to be detected via FACS. The discrete cell population could then be gated, collected and sequenced to identify the sgRNAs enriched in this population

causing the observed CD80 expression. Performing the pilot experiment with the focused library targeting 171 genes expressed in myeloid cells, none such distinct separation could be observed (data not shown). Therefore, the bin gating or also known as percentage gating was performed. Using this approach, the 10 % of the cells with highest and lowest CD80 expression levels are collected. sgRNAs not affecting polarization remain randomly distributed between this “collection bins” (Figure 2.16) while sgRNAs enriched in the 10 % of the cells with highest vs. lowest CD80 expression might address potential targets. To guarantee reaching statistical significance of enrichment or depletion of sgRNAs, this bin gating strategy requires a significantly higher sgRNA representation per bin than a positive selection screen would, thereby increasing the required cell culture work of the screen significantly.

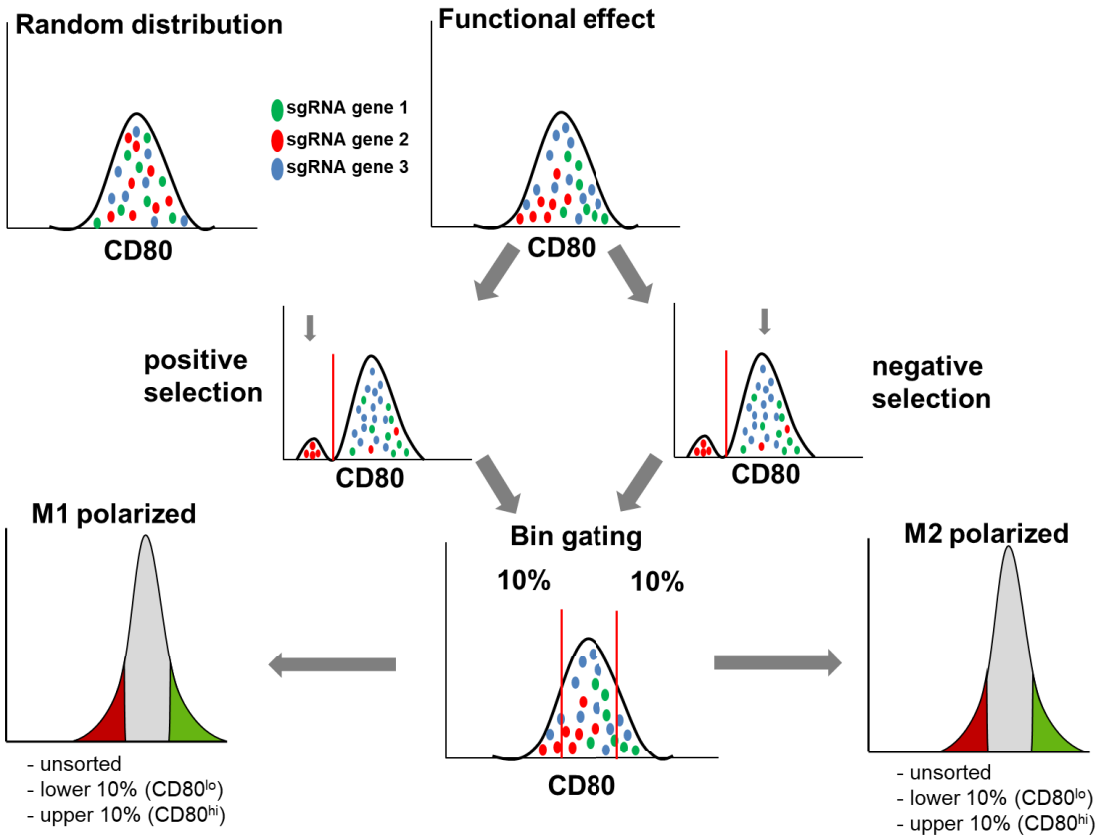

Figure 2.16. FACS-based bin gating strategy
In the human CRISPR THP-1 Cas9 screen the 10 % of high and low CD80 marker expressing cells are collected enabling the identification of sgRNAs enriched in one or the other population by next generation sequencing.

2.1.6 Sample processing for next generation sequencing

To identify the abundance of sgRNAs in CD80^{hi} and CD80^{lo} sorted cells and thereby sgRNAs affecting polarization in the described pooled screening format, genomic DNA (gDNA) had to be extracted from paraformaldehyde (PFA)-fixed cells, and the sgRNAs inserts had to be amplified to perform Illumina based NGS.

As described above, billions of cells had to be sorted per bin to ensure the required representation of sgRNAs. The library representation is defined as the absolute number of a single sgRNA in the pool of cells over the whole period of the screening procedure. Maintaining adequate library representation over the whole CRISPR screen is ensuring accurate quantification of sgRNAs. 500 – 1,000-fold representation of the sgRNAs was shown to be necessary to allow statistically relevant identification of even small changes in cell phenotype readout caused by sgRNA driven KO of a particular gene (Joung et al., 2017; Strezoska et al., 2012).

Sorting the necessary number of cells to ensure adequate representation using the available FACS Jazz Cell sorter from BD took about 9 days per replicate. Therefore, life cell staining was not an option and cells had to be fixed with PFA. This causes covalent crosslinks between intracellular proteins and thus required the establishment of a special protocol for isolation of gDNA from fixed cells (Figure 2.17).

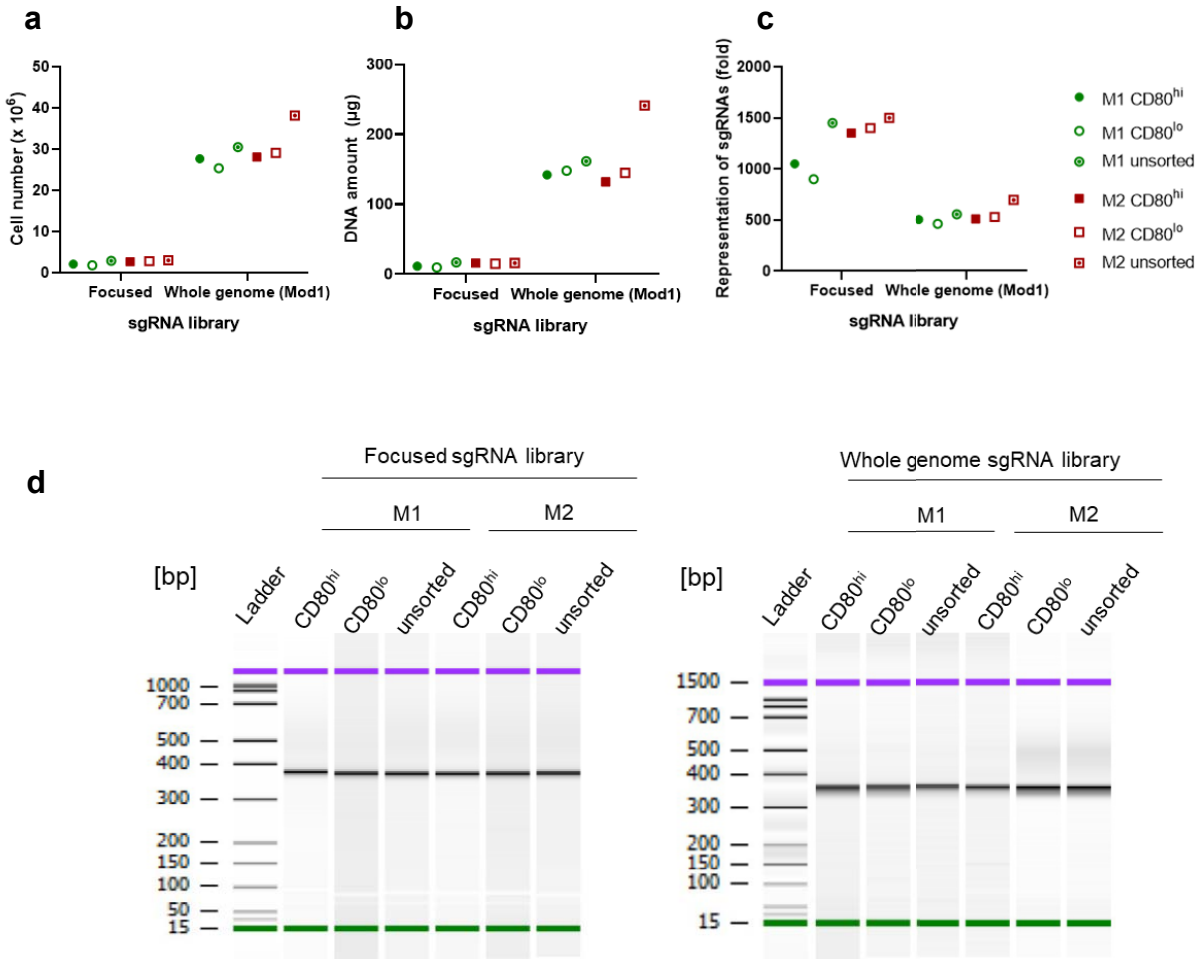

Figure 2.17. Quality criteria analysis during sample processing for NGS

(a) Cell yield of sorted and unsorted samples (b) DNA amount after isolation of DNA from PFA-fixed cells (c) representation of sgRNAs from M1 polarized or M2 polarized focused screen or whole genome screen with module 1 (d) Gel-like densitometry plot of purified PCR amplicons of sgRNA inserts after two-step PCR with annealed sequences which are complementary to P5 and P7 Ilumina primers as well as unique indices primers to tag individual samples enabling multiplexed sequencing. The final PCR product consists of 359 bp.

The feasibility of the protocol was proven showing that extracted amounts of DNA correlated with the cell number of the input samples from both, the focused screen and whole genome screen. The obtained DNA could be correlated to cell counts that ensured an sgRNA representation in the focused as well as whole genome screen of at least 500 cells/sgRNA (Figure 2.17c).

In the subsequent two-step PCR, first the 20 bp sgRNA insert was amplified and then sequences annealed complementary to the P5 and P7 Illumina primers necessary for Illumina based NGS. Also index primers were annealed to tag individual samples, which enables multiplexed sequencing. The two step PCR product should result in 359 bp which was confirmed by the gel-like densitometry plot shown in Figure 2.17 demonstrating pure amplification products with the expected fragment length. These could be subsequently used for NGS with the Illumina platform.

2.2 Performance of the CRISPR/Cas9 screen with a target-focused sgRNA library

To test all the before described established protocols for their suitability to perform CRISPR/Cas9-based target screening, a screen was performed using a focused sgRNA library targeting a limited number of genes known to be expressed in myeloid cells.

This focused library consists of 2,000 sgRNAs targeting 171 different genes known to be involved in myeloid cell function (supplementary S1 Materials), as well as positive and negative controls (200 sgRNAs). Each gene is addressed by 10 individual sgRNAs. Positive controls target genes described to be essential for survival (T. Wang et al., 2015) and negative controls target sequences known to not code for human genes or sgRNAs targeting gene's introns. This library was transduced as a lentiviral pool at a multiplicity of infection determined to transduce and integrate only single sgRNAs/cell. This was thought to induce a distinct gene KO per cell. After treating the cell population with puromycin to select for sgRNA expressing cells, the cells were differentiated to macrophages and polarized into M1 and M2 phenotype as described above. These M1 and M2 cells were then stained for the surface marker CD80 and FACS-sorted for the 10 % low and 10 % high CD80 expressing cells. After extraction of gDNA from the sorted cells NGS was performed. Then the read counts for each sgRNA are

mapped and fold changes (FC) are calculated. Thereby, sgRNAs which promote M1 or inhibit M2 polarization will be identified as potential targets.

The strategy for the established pooled CRISPR/Cas9 screen in THP-1-Cas9 human myeloid cells is shown in Figure 2.18.

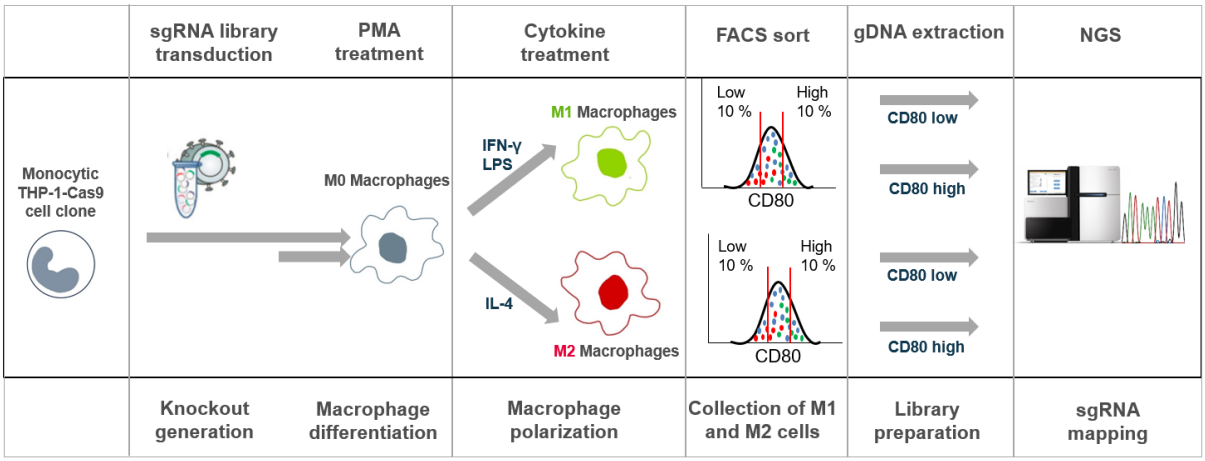

Figure 2.18. Strategy of the established pooled CRISPR/Cas9 screen in human myeloid cells
THP-1 Cas9 cells were transduced with the sgRNA library (focused or whole genome library) on day 0. After knockout generation, on day 11 (focused screen) or day 33 (whole genome screen) cells were differentiated for 2 days to M0 macrophages and polarized one additional day to M1 and M2 macrophages. M1 and M2 macrophages were stained for CD80 expression and PFA-fixed on day 14 (focused screen) and day 36 (whole genome screen). Sorting of cells from focused screen lasted 1 day and for cells from the whole genome screen 9 days. After 3 days of library preparation of both screens the samples were sequenced and sgRNA mapped.

2.2.1 Evaluation of screening performance

To understand the quality of the technical performance of the screening approach and the specificity of CRISPR/Cas9 induced effects the sgRNA library was transduced into both, THP-1 cells expressing Cas9 or not, named Cas9 positive and negative THP-1 cells. The abundance of each individual sgRNA (as reads per million – RPM) was plotted against the number of sgRNAs represented in the library as given by the provider. Significant enrichment of sgRNAs in cells with high or low CD80 expression after library transduction could only be detected in Cas9 positive but not negative cells indicating specific KO effect and the ability to detect effects of KO on polarization by using the established bin gating strategy (Figure 2.19).

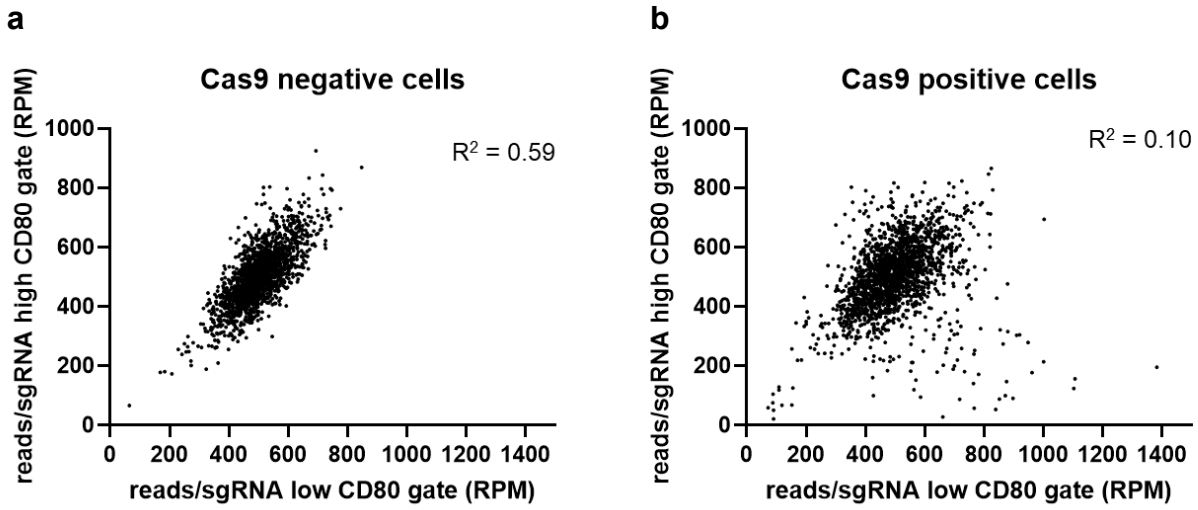

Figure 2.19. Correlation of sgRNA abundance in high or low CD80 level sorted population after transduction of THP-1 Cas9 positive or Cas9 negative cells
Data was collected analyzing sgRNA representation in 10 % CD80 high and low sorted cells. sgRNA read counts were normalized to reads per million (RPM). (a) indicates sgRNA abundance found in Cas9 negative cells and (b) in Cas9 positive cells. Depicted R^2 values are calculated from linear regression analysis.

The abundance of individual sgRNAs between the selected 10 % high and low CD80 expressing cell population was examined and normalized reads per sgRNA were plotted. Several sgRNAs were found to be overrepresented either in the selected high or low sorted fraction of the M1 or M2 polarized cells in Cas9 positive cells only.

2.2.2 Evaluation of CD80 knockout as technical control

The proof of concept for the developed screening conditions and the bin gating sorting strategy was performed by identification of the prior defined technical control CD80. CD80 gene KO was prior tested and resulted in a decreased CD80 expression analyzed by FACS (Figure 2.15). Therefore, the cells expressing sgRNAs targeting CD80 were expected to be enriched in the CD80 low fraction. The FCs of the abundance of individual sgRNAs in the CD80 high and CD80 low sorted population showed that 8 of 10 sgRNAs targeting CD80 were enriched in the CD80 low fraction (Figure 2.20).

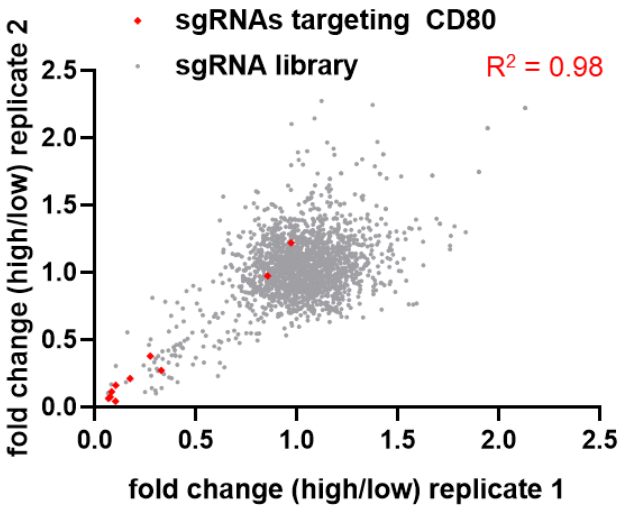

Figure 2.20. Fold changes of effects by sgRNAs targeting the technical control CD80 in CD80 high vs. low cell population
8 of 10 sgRNAs targeting the readout marker CD80 from the focused screen in both replicates were enriched in the CD80 low cell population with high correlation between the replicates. Depicted R^2 values are calculated from linear regression analysis.

2.2.3 Reproducibility

The established screening protocol and the optimized conditions yielded highly reproducible results. In Figure 2.21 the correlation of the results of the screen performed as 2 biological replicates is shown. The correlation coefficient between the replicates of R^2 = 0.92 for M1 polarization conditions and R^2 = 0.86 for M2 polarizing conditions indicates the reliability of the screening conditions.

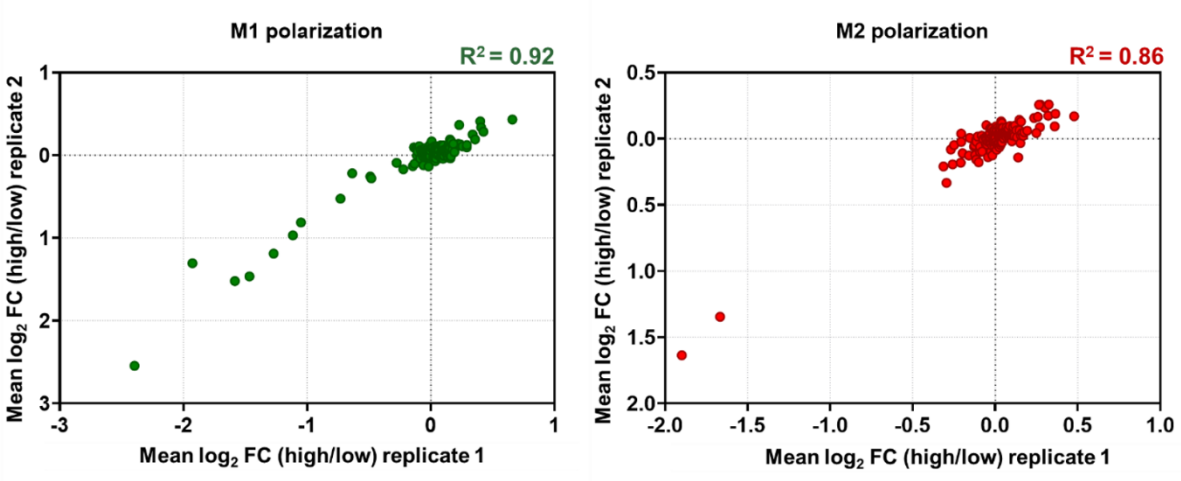

Figure 2.21. Correlation of mean log_2 fold changes of effects on CD80 expression induced by sgRNAs in CD80 high vs. low population
THP-1 Cas9 clone 8 cells were transduced with the focused pooled lentiviral sgRNA library targeting 171 genes. sgRNAs were quantified via Illumina MiSeq analysis and the mean log_2 fold changes were calculated (CD80 high/CD80 low population). Significant outliers regarding sgRNA abundance are detected between both populations in the M1 polarized (green) as well as the M2 polarized cells (red). Depicted R^2 values were calculated by linear regression analysis

2.2.4 Data analysis to identify hits

The above described data confirms the potential of this screening strategy to identify targets involved in the polarization of macrophages.

In Figure 2.22 the FACS plots from the target-focused screen are shown, depicting CD80 low expressing-cells (red) which have the more M2 like phenotype and CD80 high expressing-cells (green) which have acquired the M1-like phenotype. As the focused library consists of sgRNAs targeting 171 genes, 171 dots are shown on this plot. In the upper right quarter, the mean effect of sgRNAs is depicted enriched in the CD80 high fraction of M1 and M2 polarized cells and in the lower left quarter the sgRNAs are shown that are enriched in the CD80 low expressing cell fraction. Dots centered in the middle are depicting targets KO of which does not specifically affect CD80 expression either way.

a

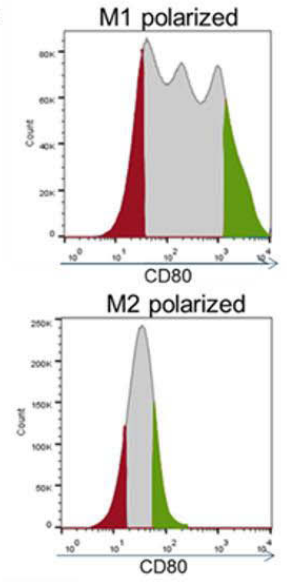

b

sgRNAs promoting CD80 expression when M1 polarized

Top 10	M1 log_2 FC	M2 log_2 FC
TNFAIP3	0.63	0.25
IL1B	0.44	0.08
TBK1	0.39	0.10
MKNK1	0.32	0.18
SLC11A1	0.30	0.41
PAK2	0.25	0.36
FCGR1A	0.23	0.22
MMP9	0.20	0.14
ITGAL	0.05	0.19
ICAM1	0.04	0.31

c

sgRNAs inhibiting CD80 expression when M1 polarized

Top 10	M1 log_2 FC	M2 log_2 FC
CD80	-2.42	-0.19
STAT1	-1.82	-0.01
WARS	-1.62	-1.62
CD14	-1.50	0.05
STK40	-1.27	-0.26
TLR4	-1.09	-0.04
RPS6KA1	-0.77	0.16
CSK	-0.47	-0.50
JAK2	-0.46	0.04
PTGS1	-0.31	-1.93

d

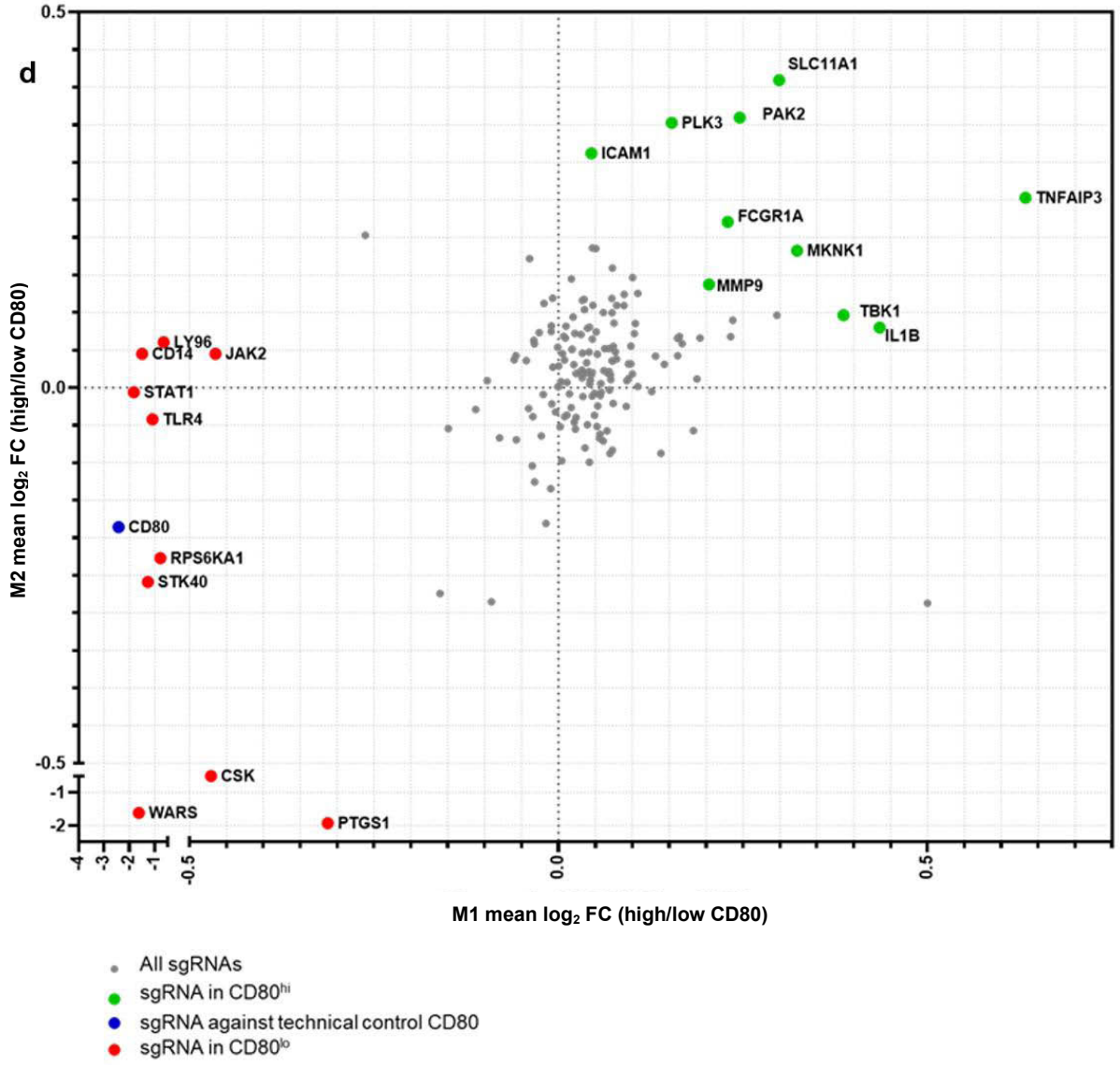

Figure 2.22. The CRISPR/Cas9 screen targeting 171 genes known to be expressed in myeloid cells identified sgRNAs targeting genes known to regulate M1 and M2 polarization and CD80 marker expression
(a) FACS profile is shown for M1 polarized and M2 polarized THP-1 Cas9 cells. Cells with 10 % low CD80 expression (red population) and 10 % high CD80 expression (green population) were sorted and gDNA sequenced. (b) and (c) show the top 10 hits for M1 polarized and M2 polarized cells which inhibit or promote M1 polarization when knocked out and their corresponding log_2 mean fold change values (high/low CD80 expression) (d) The log_2 mean fold changes (high/low CD80 expression) of the number of all sgRNAs targeting the respective gene in M1 polarized vs. M2 polarized cells are plotted. Green dots are sgRNAs enriched in $CD80^{hi}$ cell population indicating genes, when knocked out, promoting M1 polarization, Red dots are sgRNAs enriched in $CD80^{lo}$ cell population indicating genes, when knocked out, inhibit M1 polarization (CD80 downregulation) Blue dot depicts sgRNAs against CD80, when knocked out found enriched in $CD80^{lo}$ fraction serving as technical control of the screen.

sgRNAs targeting TNFAIP3 were found significantly enriched in the CD80 positive M1-like phenotype cell fraction. Since TNFAIP3 is believed to be a key player in the negative feedback regulation of NF-κB signaling, the identification that its inhibition promotes M1 polarization and thus the inflammatory response supports the validity of the screening conditions (Shembade & Harhaj, 2012; Verhelst et al., 2012).

Furthermore, sgRNAs targeting CD80 were found enriched in the CD80 low cell population serving as technical control of the screening procedure as CD80 expression was used as phenotypic readout system. As biological controls such genes targeted by sgRNAs were found causing changes in polarization behavior due to KO. For M1 activation the sgRNAs against TLR4, CD14, Signal transducer and activator of transcription 1 (STAT1) and Lymphocyte antigen 96 (LY96) were found enriched in the CD80 low cell fraction implicating their crucial role for correct M1 polarization. In M1 polarization with LPS and IFN-γ, LPS binds to the TLR4, whereby CD14 acts as coreceptor along with TLR4 and LY96 for the detection of bacterial LPS (Kitchens, 2000; Re & Strominger, 2002; Tapping & Tobias, 2000). STAT1 is downstream of the IFN-γ receptors and is activated by IFN-γ and important for further IFN-γ signaling. Inhibition of all these genes leads to inhibition of M1 polarization and reduction in CD80 expression.

sgRNAs against WARS for example were found enriched in the CD80 low cell population which is in concordance with published data as WARS acts together with IDO1 through the tryptophan pathway in proinflammatory processes, and inhibiting WARS may therefore cause a more M2-like phenotype (Bao et al., 2013).

All in all, in the focused screen genes, such as TNFAIP3, CD14, STAT1, TLR4, LY96 and WARS, were identified known to have a putative role in M1 or M2 polarization implicating that the established protocol could be used to perform a genome-wide screen to identify novel targets with a role in myeloid cell polarization.

2.3 Whole genome sgRNA CRISPR/Cas9 screen

To take full advantage of the high-throughput capacities of the established screening conditions, a CRISPR/Cas9 screen was conducted in the THP-1-Cas9 cells targeting the whole genome with the exact same strategy as outlined in Figure 2.18.

2.3.1 sgRNA library composition

The sgRNA library used is provided in 3 modules. Each module covers approximately 6,300 genes with up to 8 sgRNA per gene. The modular format allows a screening-feasible library complexity. Each module contains the same 260 non-targeting, intron targeting and essential genes targeting sgRNAs, allowing for cross-module correlation and the empirical testing of screen performance beyond values of technical reproducibility.

2.3.2 Quality parameters and comparison with focused screen

The results of the focused screen had shown that ensuring maintenance of a certain sgRNA representation throughout the screening procedure and high enough sequencing depth are crucial for the quality of the screen and to achieve statistically relevant data.

Therefore, throughout the entire screen a minimum average of 500 cells per sgRNA have been maintained to be collected in the final FACS-sort. Thus, 90 million cells per module were transduced at the start of the screen and over 1 billion cells in total subsequently have been FACS sorted by CD80 intensity. Using next generation sequencing, an sgRNA read count depth of over 1,000 reads per sgRNA had to be achieved.

In order to control for functionality of the performed screen positive and negative controls are introduced into the sgRNA library. These sgRNAs should cause expected effects on viability. The positive control sgRNAs are targeting the essential genes CDC16, GTF2B, HSPA5, HSPA9, PAFAH1B1, PCNA, POLR2L, RPL9, SF3A3 and SF3B3. KO of these genes leads to cell death through the loss of protein functions essential for fundamental biological processes, such as DNA replication (CDC16) or RNA transcription (POLR2L, GTF2B). 80 different sgRNAs targeting those 12 genes were used to study the effect of the KO of these lethal genes in the THP-1 screening cells. In Figure 2.23 the sgRNA read counts for the unsorted sample of Module1 are compared to the sgRNA read counts of the original library, clearly showing a depletion of sgRNAs targeting essential genes (red). sgRNAs targeting non-essential genes (blue) or are supposedly not targeting any known human genes (green) have no effect on sequence abundance. These controls not only demonstrate the efficiency of KO generation

while screening but also enable the comparison of these controls across the three sub-screens which ensures comparability between the three modules and thereby indicates the quality of whole genome screen. This was supported by the high correlation of the 260 positive and negative controls across the 3 different modules (correlation coefficients: R^2 = 0.87 Mod1/Mod2, R^2 = 0.90 Mod1/3 and R^2 = 0.85 Mod2/Mod3).

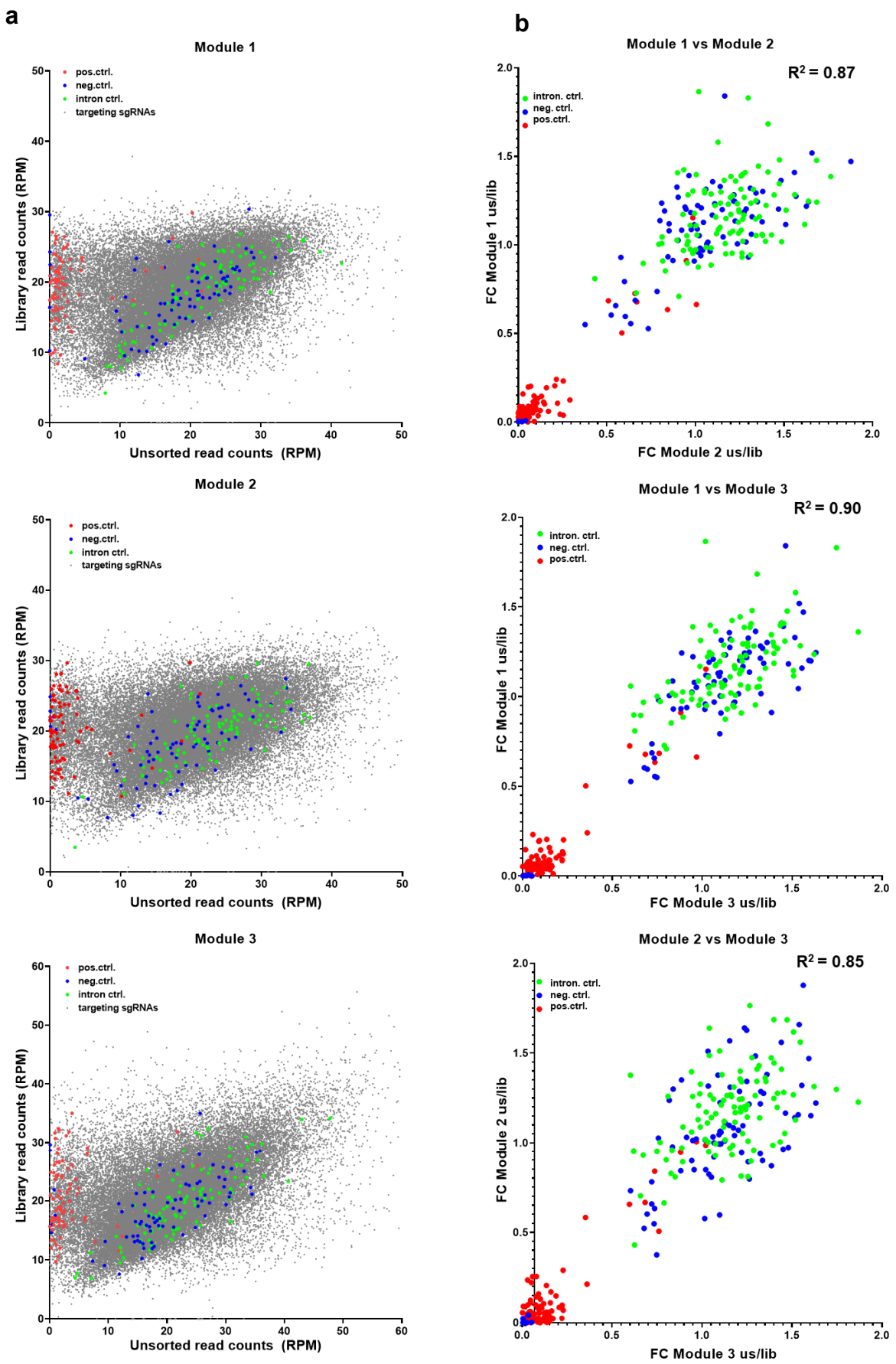
a
Module 1
pos.ctrl.
neg.ctrl.
intron ctrl.
targeting sgRNAs
Library read counts (RPM)
Unsorted read counts (RPM)
Module 2
pos.ctrl.
neg.ctrl.
intron ctrl.
targeting sgRNAs
Library read counts (RPM)
Unsorted read counts (RPM)
Module 3
pos.ctrl.
neg.ctrl.
intron ctrl.
targeting sgRNAs
Library read counts (RPM)
Unsorted read counts (RPM)
b
Module 1 vs Module 2
R² = 0.87
intron. ctrl.
neg. ctrl.
pos.ctrl.
FC Module 1 us/lib
FC Module 2 us/lib
Module 1 vs Module 3
R² = 0.90
intron. ctrl.
neg. ctrl.
pos.ctrl.
FC Module 1 us/lib
FC Module 3 us/lib
Module 2 vs Module 3
R² = 0.85
intron. ctrl.
neg. ctrl.
pos.ctrl.
FC Module 2 us/lib
FC Module 3 us/lib

Figure 2.23. Library representation and cross module correlation of control sgRNAs
(a) Normalized read counts (reads per million = RPM) of sequenced sgRNAs from the whole genome CRISPR/Cas9 screen in THP-1 Cas9 cells of the unsorted sample at the end of the screen compared to read counts given by the provider; positive control sgRNAs targeting lethal genes are depleted (red), while sgRNAs targeting non-essential genes (blue) or supposedly not targeting any known human genes (green) have no effect on sequence abundance. (b) Cross-module comparison of control sgRNAs showing high correlation. Depicted R^2 values are calculated from linear regression analysis.

Another criterium of screening quality is the specificity of sgRNA-mediated gene targeting. To analyze this, the global gene expression in THP-1 macrophages was compared to the mean $\log_2$ FC (high/low) effects of the mapped sgRNAs. 12,357 of 19,000 genes (mean mRNA expression > 0.5 $\log_2$ TPM) targeted by the whole genome sgRNA library are expressed in the screening cells. Figure 2.24 shows that indeed only these genes in the THP-1 cells (mean mRNA expression > 0.5 $\log_2$ TPM) are affected by sgRNAs (mean $\log_2$ FC >/< ± 0.3).

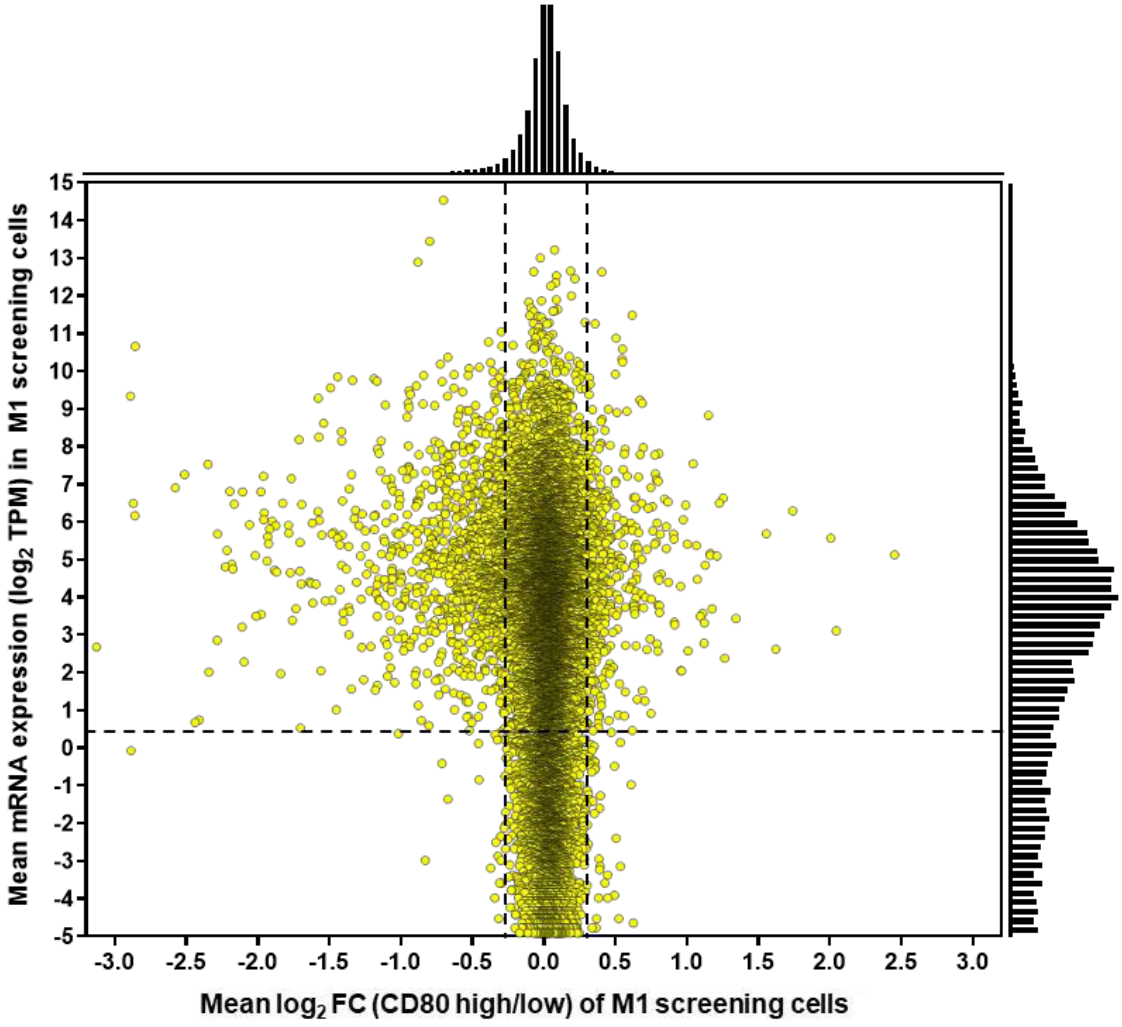

Figure 2.24. Expression of genes targeted by sgRNAs causing effect on CD80 expression from whole genome library
12,357 genes of 19,000 are expressed in screening cells (mean mRNA expression > 0.5 $\log_2$ TPM). Non-expressed genes show no enrichment (mean mRNA expression < 0.5 $\log_2$ TPM). Expressed genes are affected by sgRNAs (mean $\log_2$ FC >/< ± 0.3) Dashed lines indicate thresholds

To evaluate the reproducibility of the data generated in distinct performed CRISPR screens, the focused and whole genome screen, effects induced by the 171 sgRNAs from the focused screen were correlated with the effect induced by sgRNAs targeting the same genes but with distinct sgRNA sequences in the whole gnome screen (Figure 2.25). The effects of the sgRNAs from the top hits from the focused screen (Figure 2.22) were correlating with the effects of the sgRNAs targeting the same genes by the whole genome library. This supports the earlier noted reproducibility of data generated, using the established screening conditions (R^2 = 0.84 for M1 polarized cells and R^2 = 0.57 for M2 polarized cells).

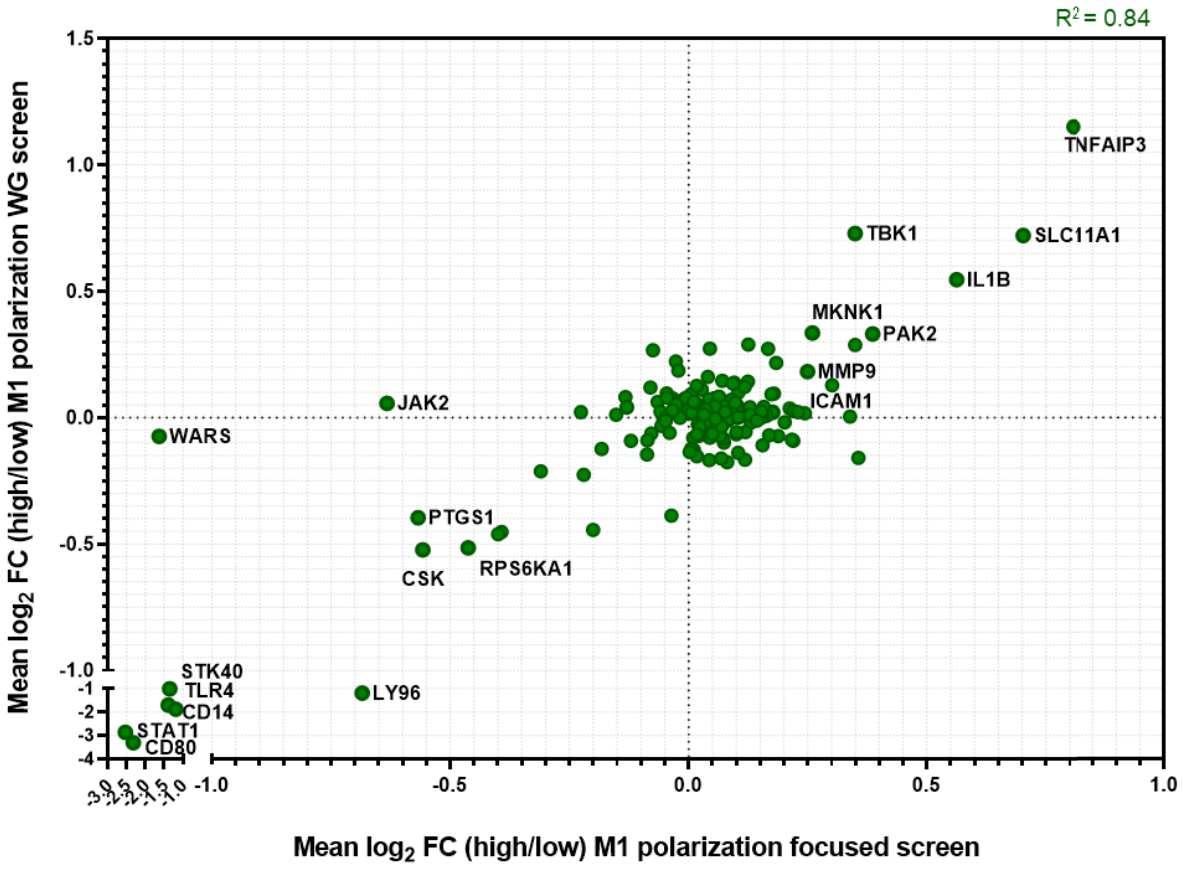
R² = 0.84
TNFAIP3
TBK1
SLC11A1
IL1B
MKNK1
PAK2
MMP9
ICAM1
JAK2
WARS
PTGS1
CSK
RPS6KA1
STK40
TLR4
CD14
STAT1
CD80
LY96
Mean log2 FC (high/low) M1 polarization WG screen
Mean log2 FC (high/low) M1 polarization focused screen

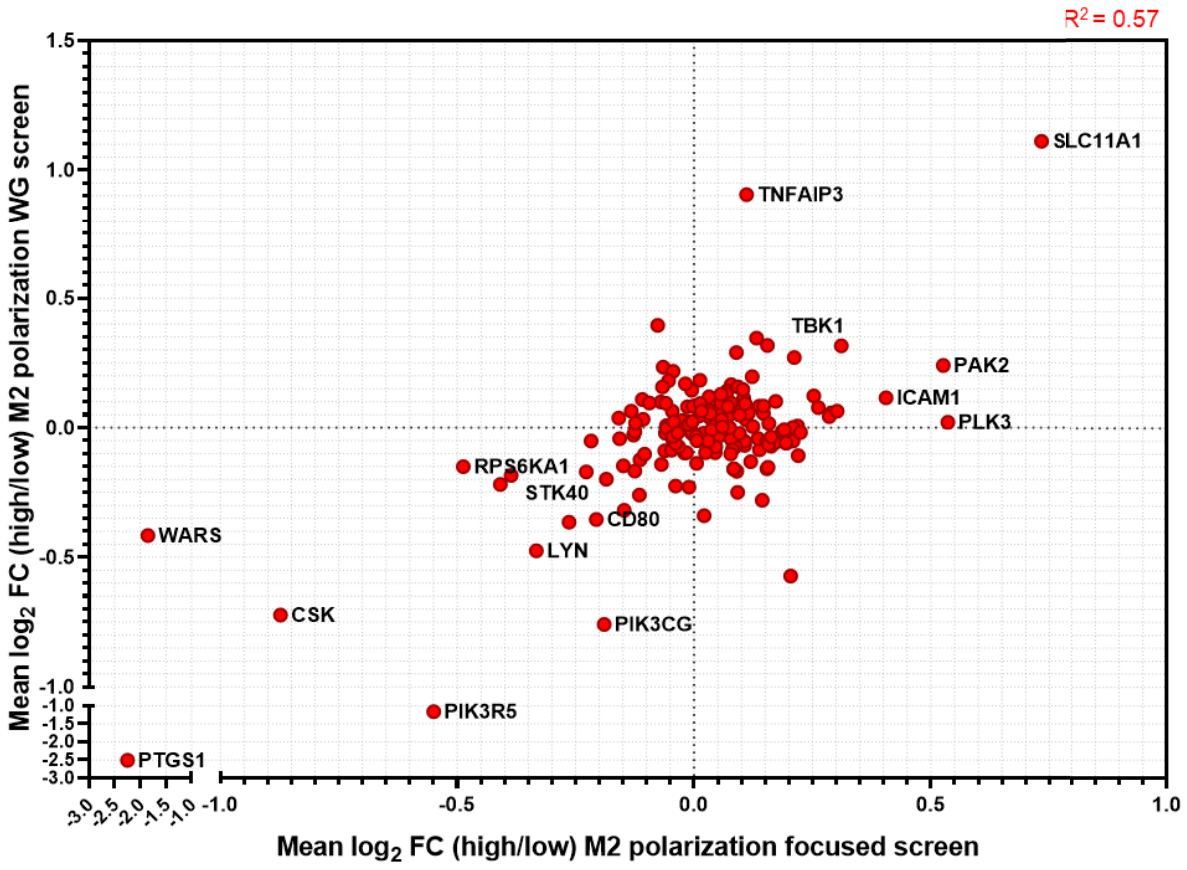
R² = 0.57
SLC11A1
TNFAIP3
TBK1
PAK2
ICAM1
PLK3
RPS6KA1
STK40
CD80
WARS
LYN
CSK
PIK3CG
PIK3R5
PTGS1
Mean log2 FC (high/low) M2 polarization WG screen
Mean log2 FC (high/low) M2 polarization focused screen

Figure 2.25. Reproducibility of results obtained in focused CRISPR/Cas9 screen compared to whole genome screen
The CRISPR/Cas9 screens were performed in THP-1 Cas9 cells with the focused sgRNA library and the whole genome (WG) sgRNA library. The focused library targets 171 genes known to be expressed in myeloid cells. The same 171 genes are also targeted in the whole genome screen with 8 instead of 10 sgRNAs. These sgRNAs target different sequences of the same genes. The effects of the sgRNAs in M1 (green) and M2 (red) polarized screening cells was calculated as the mean $\log_2$ fold change (FC) of the abundance of the sgRNAs found in the 10 % CD80 high expressing cells and 10 % CD80 low expressing cells. These mean $\log_2$ FC from the focused screen and the whole genome (WG) screen correlate highly for the M1 polarizing condition ($R^2 = 0.84$) and modest for M2 polarizing condition ($R^2 = 0.57$)

2.3.3 Hit identification

To identify sgRNAs affecting M1/M2 polarization in differentiated THP-1 Cas9 cells, the sgRNA distribution was analyzed as shown in Figure 2.26 using the normalized reads per million (RPM) of every sgRNA detected in the respective collected “bin” of high vs. low CD80 expressing cells. sgRNAs enhancing CD80 expression are supposed to be enriched in the defined “high” sorted population and sgRNAs causing inhibition of CD80 expression are to be found in the “low” sorted fraction (Figure 2.26a). The unsorted sample is used to evaluate the overall sgRNA representation at the end of the screen. Comparing this to the representation of the sgRNAs in the library at the beginning of the screen, whereby this information is provided by the manufacturer of the library, enables to detect effects on cell viability caused by the gene’s KO. sgRNAs not being detectable in the unsorted sample have most likely been depleted over the course of screening due to cell death and were excluded from further analyses.

Figure 2.26b shows how the data matrix enables the identification of sgRNAs effects on cell viability and CD80 marker expression. This data matrix enables the distinction whether for example CD80 KO causes changes in CD80 expression or cell viability and shows that sgRNA effects on cell viability do not correlate with CD80 enrichment. Furthermore, it shows that effects of sgRNAs targeting CD80 are highly correlated. Only one sgRNA (sg_5) of eight was not functional and is not affecting CD80 expression. As the majority of the sgRNAs showed high correlation of their effects on CD80 expression (data not shown), the mean $\log_2$ FC of all sgRNAs targeting one gene was calculated to allow gene level comparison. To ensure that the observed enrichment of sgRNAs in CD80 high expressing cells was not hampered by generally low read counts or caused by viability effects of the sgRNAs, all sgRNAs against one gene were excluded when more than 3 out of 8 sgRNAs caused cell death. The threshold used was based on the overall effects of positive control sgRNAs depleted over the course of the screen ($\log_2$ FC (unsorted/library) < -1).

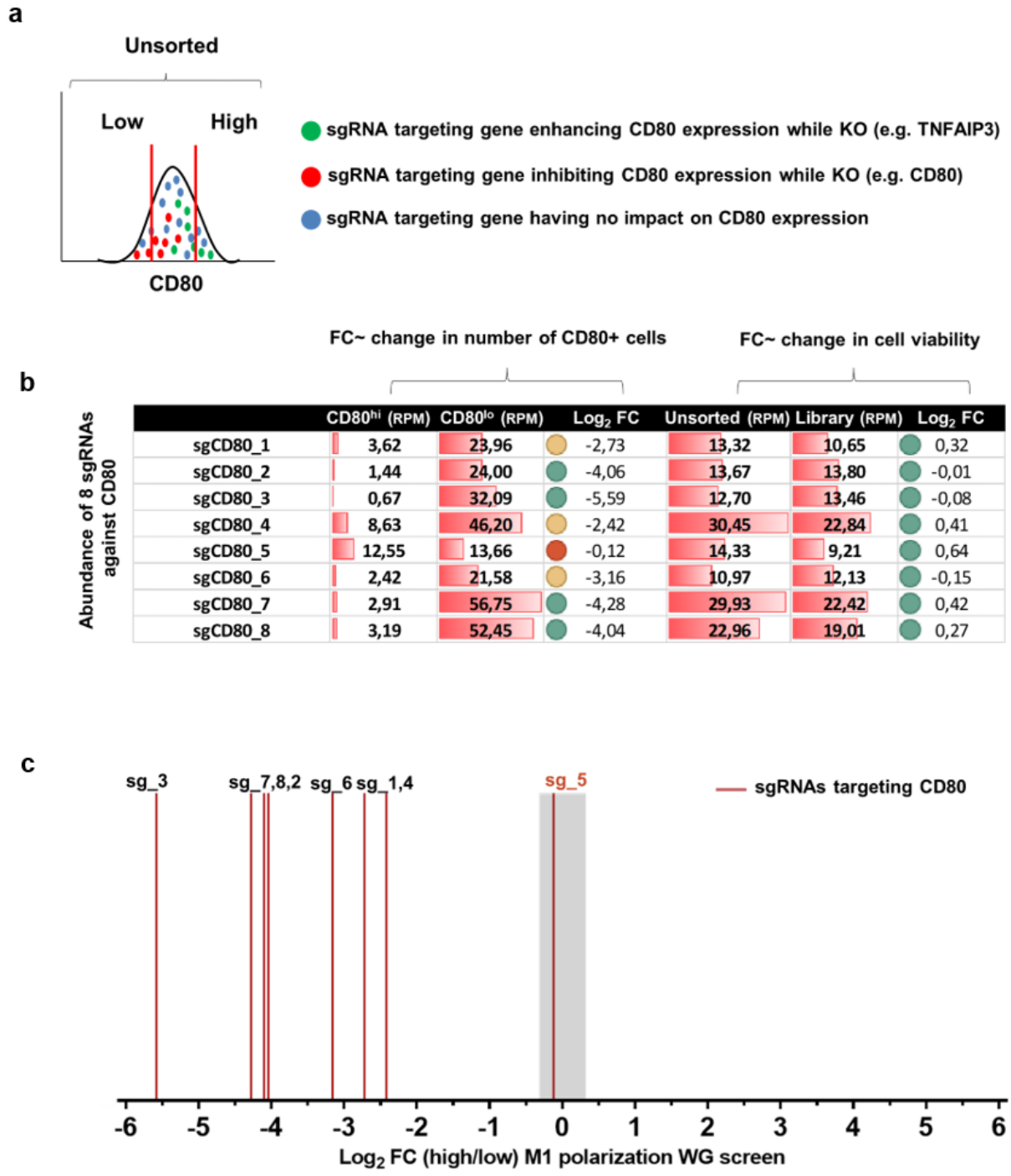

Figure 2.26. Identification of sgRNA effects on number of CD80+ cells and cell viability
(a) Principle of bin sorting strategy and expected output. sgRNAs (green) enhancing CD80 expression accumulate in the high population, such as sgRNAs targeting TNFAIP3. sgRNAs enriched in the low fraction, such as sgRNAs targeting CD80, decrease CD80 expression and sgRNAs having no impact on CD80 expression (blue) are found equally distributed. (b) Data matrix with reads per million (RPM) values enables identification of hits by mean fold change analysis of read counts of sgRNAs in high and low CD80 expressing cells. Changes in cell viability due to KO of essential genes are detectable by FC calculation of RPMs in unsorted vs. library RPMs for each sgRNA (c) Distribution of log_2 fold change (high/ow CD80) values for all eight sgRNAs targeting CD80 enriched in the low fraction in the whole genome CRISPR screen; grey bar depicts that most sgRNAs accumulated have no or marginal effects on CD80 expression (log_2 FC (high/low) -0.3 - + 0.3)

The hitlist of the whole genome screen is derived from the data of sgRNA effects on cells promoting M1 macrophage phenotype under M1 polarization conditions and of sgRNA effects on cells promoting M1 macrophage phenotype under M2 polarizing conditions. These conditions are designed to mimic the exposure of macrophages to polarized CD4+ T cells which produce distinct cytokine combinations. T helper 1 (T_H1) cells produce IFN-y and T helper 2 (T_H2) cells IL-4 and IL-13 (Munder et al., 1998; Munder et al., 1999).

In Figure 2.27 the graph shows the mean log_2 FC of the read counts in M1 polarized cells on the x- axis and on the y- axis the mean log_2 FC of the read counts in M2 polarized cells. The dots depict the mean of the effects of all sgRNAs targeting a single gene. For hit selection the focus was on the sgRNAs enriched in the CD80 high fraction of both the M1 and M2 polarized cells hitting potential direct targets to induce a therapeutic effect. The top 100 hits with the highest mean log_2 FC of M1 and M2 polarized cells were selected as the sgRNAs with the strongest effects on CD80 expression, whereby sgRNAs targeting 30 specific genes were hits under both conditions. This sums up to a hitlist with 170 potential targets, displayed as labeled green dots in Figure 2.27, involved in M1 and/or M2 polarization. The gene lists with the top 100 targets and their log_2 FC values in M1 and M2 polarizing conditions can be found in the supplement S2 Hit list in Table 6.3.

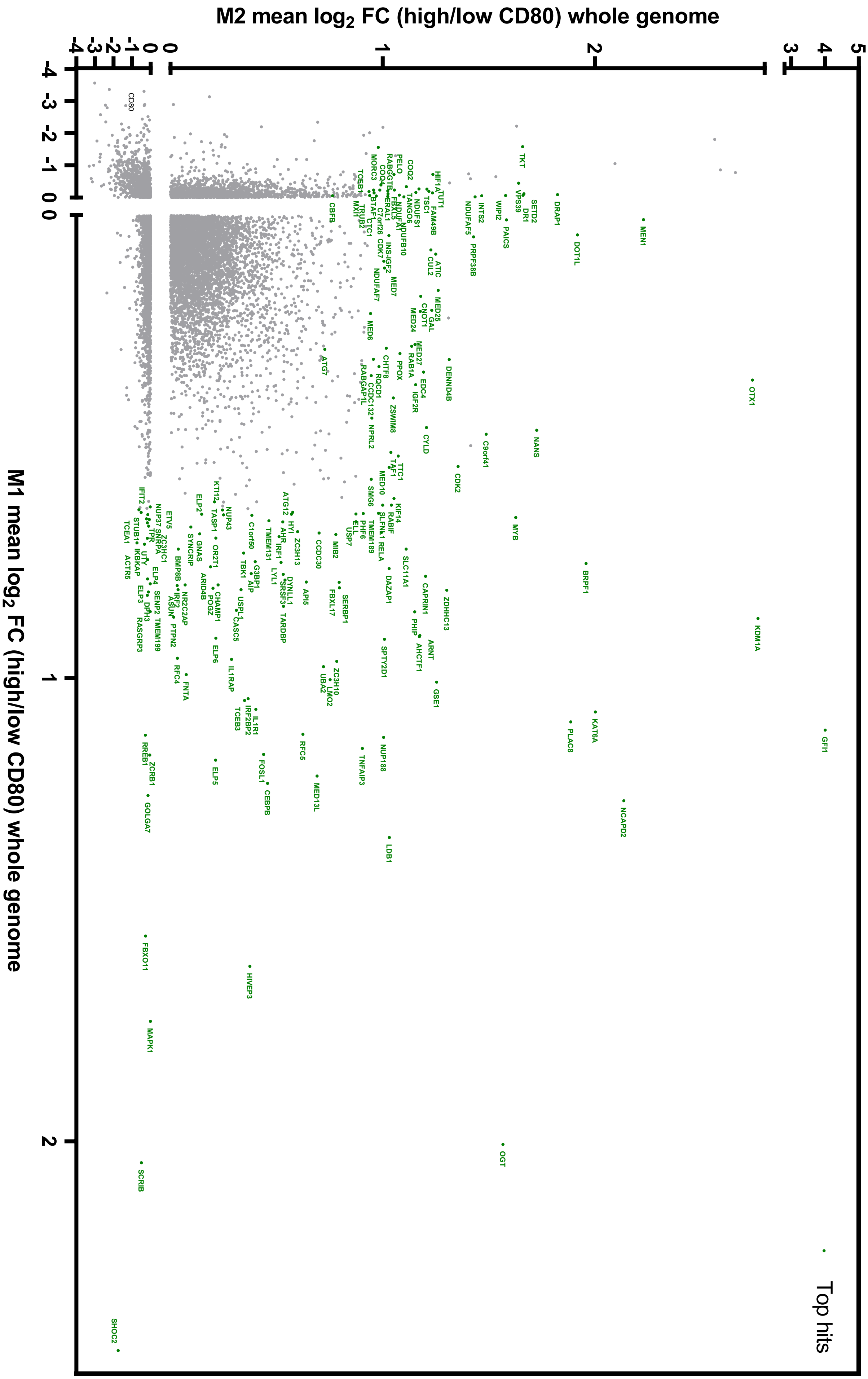
M2 mean log2 FC (high/low CD80) whole genome
M1 mean log2 FC (high/low CD80) whole genome
Top hits

Figure 2.27. Top hits from whole genome CRISPR/Cas9 screen
Whole genome (WG) CRISPR/Cas9 screen was performed in THP-1 Cas9 cells and enabled the identification of 170 potential M2 promoting targets, which when inhibited enhance the M1-like phenotype.The WG sgRNA library targets 19,000 genes with in total 150,000 sgRNAs, i.e. about 8 different sgRNAs per gene.The screen was performed under M1 polarizing conditions (IFN-γ and LPS) and M2 polarizing conditions (IL-4) and the hitlist is merged from the top 100 hits from both conditions, whereby 30 targets are shared among both polarization approaches. The effects of gene knockout on polarization capability are monitored via CD80 expression changes. Therefore 10 % CD80 high expressing and 10 % CD80 low expressing cells were sorted and the abundance of the sgRNAs in each population detected by next generation sequencing. The x-axis depicts the mean log_2 FC (high/ low CD80) of sgRNA abundane in M1 polarized cells and the y-axis depictes the mean log_2 FC (high/low CD80) in M2 polarized cells. Potential targets are found enriched in the CD80 high population and are marked green.

2.4 Hit verification

The comparison of data obtained in the focused and whole genome CRISPR screen implicated a relatively high reproducibility of the screening results within the THP-1 cell system. To understand the relevance of the targets for general macrophage polarization it was necessary to not just verify the hits in the THP-1 cells but also in other relevant cell models, namely primary cells. Therefore, a rather complex hit verification strategy was developed including testing the effects of hit-knockout firstly in the screening cells, then in U937 cells, and also in primary macrophages as well as using synthetic gRNAs instead of sgRNAs and several readouts detecting effects on mRNA and internal protein as well as secreted protein levels.

To establish and test this hit verification strategy, the initial hit verification was restricted to 20 of the 170 identified potential targets. These were selected based not only on a significant screening effect but also on relevance in macrophage biology, putative druggability, and novelty. The following targets had been selected:

ARNT, BRPF1, CBFB, CD80 (technical control), CEBPB, DENND4B, GFI1, HIF1A, IKBKAP, IRF2BP2, KDM1A, MAPK1, OTX1, PLAC8, PTPRC, RASGRP3, RELA, SCRIB, SHOC2, TNFAIP3.

2.4.1 Verification of selected top 20 hits

The following protocol was used in the THP-1 Cas9 screening cells: the THP-1 Cas9 cells were electroporated using gRNAs against the targets. After 4 days of KO generation the cells were differentiated to macrophages and polarized to M1 or M2 for the final 24 hours.

As the hits were selected based on their effect on CD80 protein expression this expression was compared to the CD80 gene expression after target KO in the verification process. After single KO of the 20 targets CD80 expression was examined via TaqMan and the results compared to the values of log_2 FC obtained for the corresponding sgRNA in the screen (Figure 2.28) under the M1 polarizing (Figure 2.28a+b) and M2 polarizing conditions (Figure 2.28c+d).

Figure 2.28a and Figure 2.28c show the relative CD80 gene expression ($-2^{(\Delta\Delta CT)}$) normalized to the Non-targeting control (NT.CTRL). Figure 2.28b and Figure 2.28d show the distribution of $\log_2$ FC values from the whole genome screen of CD80 high and low expressing cells for eight sgRNA per gene, representing the effect of KO on CD80 protein expression. The results depict that the KO effect of the sgRNAs increased CD80 expression and this correlates highly with the $\log_2$ FC detected in the whole genome screen, under both M1 and M2 polarizing conditions. Thereby, the KO of TNFAIP3, KDM1A, OTX1 and GFI1 showed not only the most significant effect on CD80 gene expression but the targeting sgRNAs were also most strongly enriched in the CD80 high cell population under screening conditions, especially when M2 polarized.

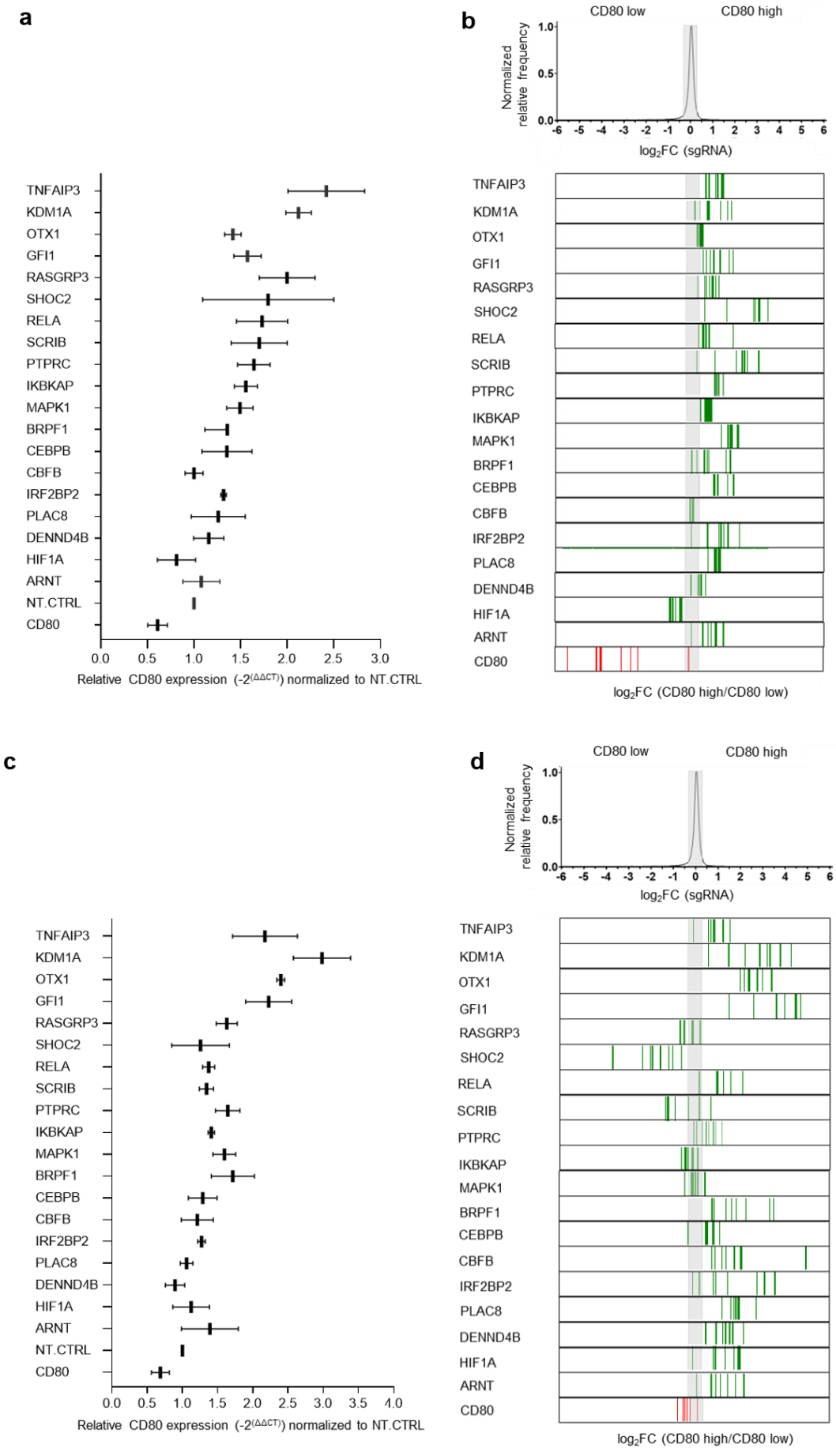
a
TNFAIP3
KDM1A
OTX1
GFI1
RASGRP3
SHOC2
RELA
SCRIB
PTPRC
IKBKAP
MAPK1
BRPF1
CEBPB
CBFB
IRF2BP2
PLAC8
DENND4B
HIF1A
ARNT
NT.CTRL
CD80
0.0 0.5 1.0 1.5 2.0 2.5 3.0
Relative CD80 expression (-2(ΔΔCT)) normalized to NT.CTRL
b
CD80 low
CD80 high
Normalized relative frequency
1.0
0.5
0.0
-6 -5 -4 -3 -2 -1 0 1 2 3 4 5 6
log2FC (sgRNA)
log2FC (CD80 high/CD80 low)
c
0.0 0.5 1.0 1.5 2.0 2.5 3.0 3.5 4.0
Relative CD80 expression (-2(ΔΔCT)) normalized to NT.CTRL
d
CD80 low
CD80 high
Normalized relative frequency
log2FC (sgRNA)
log2FC (CD80 high/CD80 low)

Figure 2.28. CD80 gene expression after target KO and correlation with distribution of corresponding log_2 FC values of M1 promoting sgRNAs in the whole genome screen in THP-1 Cas9 cells
(a) Relative CD80 expression ($-2^{(\Delta\Delta CT)}$) of cells with top20 target KO normalized to non-targeting control (NT.CTRL) in M1 polarizing conditions (a) and M2 polarizing conditions (c); n = 3 with each technical triplicates; Mean ± SEM (b) + (d) Top: Distribution of log_2 FC values of CD80 high over CD80 low expressing cells for > 150,000 guides in the whole genome library. Bottom: log_2 FC for all eight genes enriched in CD80 high expression and CD80 low expression, gray bar depicts -0.3 – 0.3 log_2 FC interval of screening results

For further verification of the 20 screening hits, the CD80 protein expression after target KO was analyzed via FACS. The CD80 expression in the non-targeting control expressing THP-1 Cas9 cells was compared to the KO THP-1 Cas9 cells (Figure 2.29). Especially under M1 polarized conditions the CD80 expression was increased as strongly as found in the screen. Also, in these experiments, KO of TNFAIP3, GFI1, KDM1A and OTX1 induced the strongest readout effects (Figure 2.29).

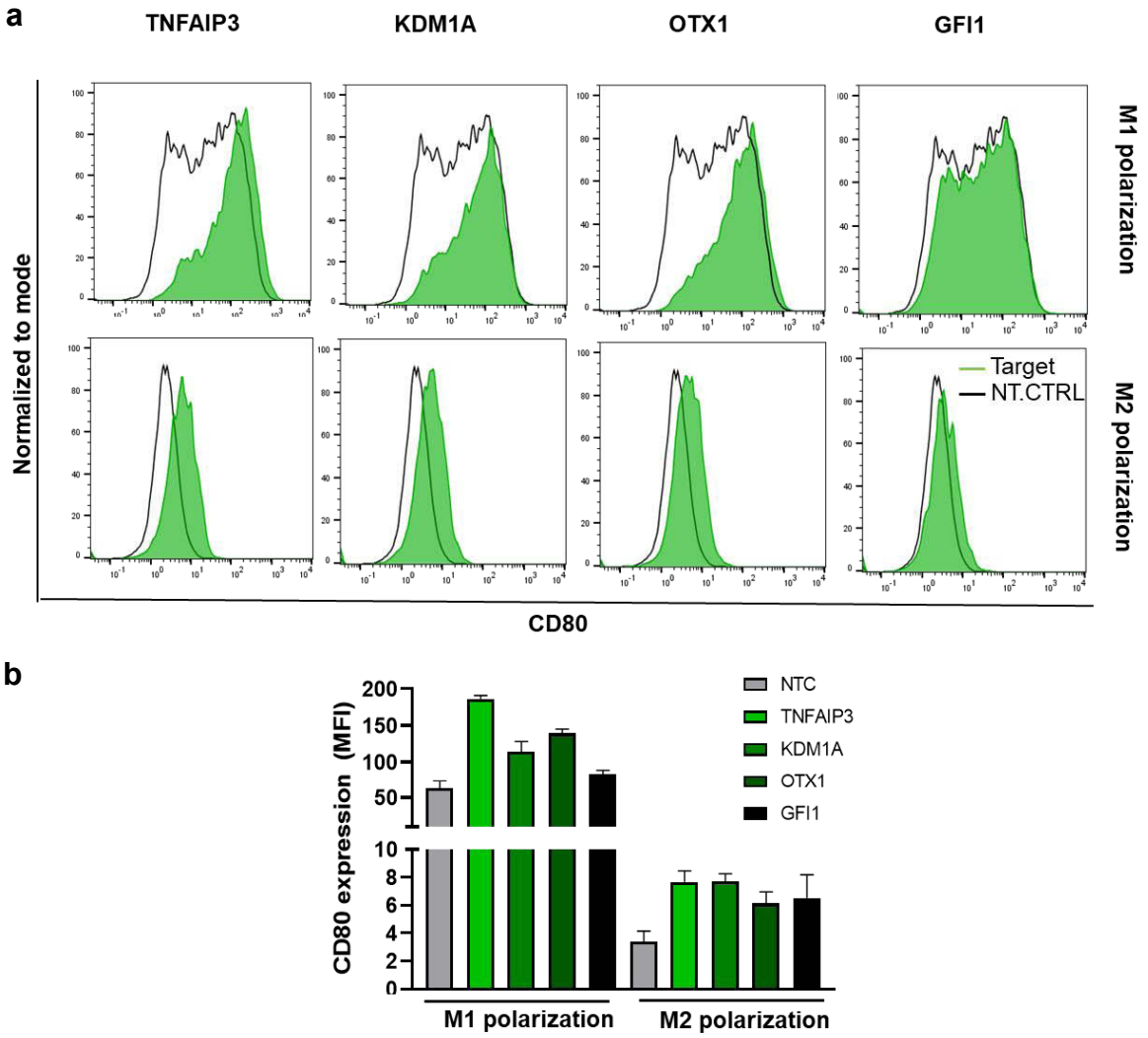

Figure 2.29. Validation of CD80 protein expression in THP-1 Cas9 cells
CD80 protein expression after target KO of TNFAIP3, GFI1, KDM1A and OTX1 in THP-1 Cas9 cells was analyzed via FACS under M1 and M2 polarization conditions. The CD80 expression of the KO cells was compared with the non-targeting control (NTC) expressing cells. (b) CD80 expression from a) was quantified by analyzing the mean fluorescent intensity (MFI) of CD80 expressing cells, n = 3; Mean ± SD

To measure KO effects on mRNA level, gene expression analysis using TaqMan was performed to detect the M1 markers CD80, CD86 and HLA-DRA and the proinflammatory cytokines TNF, IL-1B, IL-12B and IL-6. The mean of the relative expression ($-2^{(\Delta\Delta CT)}$) of the surface markers and proinflammatory cytokines are highly correlating under M1 and M2 polarization conditions, as shown in Figure 2.30. Strongest effects on both surface and cytokine expression were observed for the KO of TNFAIP3, GFI1, KDM1A and OTX1. For detailed information, the effects of the KO of these 4 genes on all marker and cytokine gene expression measured are depicted in Figure 2.30c+d.

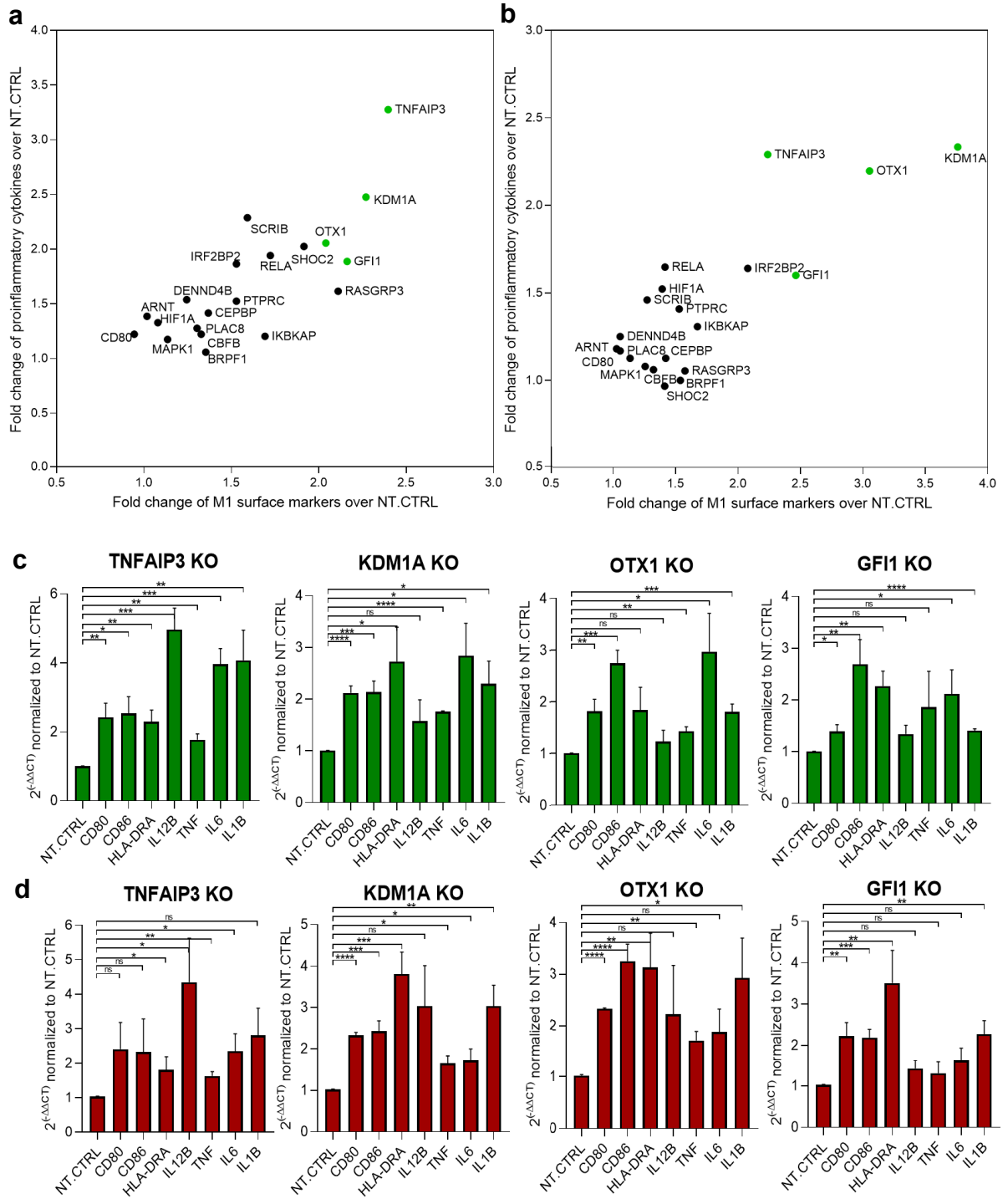

Figure 2.30. Validation of top 20 hits in THP-1 Cas9 cells – mRNA expression
Gene expression analysis using TaqMan was performed to detect the target's KO effect in THP-1 Cas9 cells on the M1 markers CD80, CD86, and HLA-DRA (x-axis shows mean of at least three biological replicates, each consisting of 3 technical replicates of $-2^{(\Delta\Delta CT)}$ values normalized to NT.CTRL of surface markers). Also the effect on the expression of proinflammatory cytokines TNF, IL-1B, IL-12B, and IL-6 was examined (y-axis shows mean of at least three biological replicates, each consisting of 3 technical replicates of $-2^{(\Delta\Delta CT)}$ values normalized to NT.CTRL (of these proinflammatory cytokines) (a) in M1 polarizing condition (IFN-γ and LPS) (b) in M2 polarizing conditions (IL-4) (c) data shown in a) is displayed as a single parameter analysis, (d) data shown in d) is displayed as single parameter analysis; n ≥ 3, Mean ± SEM, unpaired t-test; * p ≤ 0.05, ** p ≤ 0.01, *** p ≤ 0.001, **** p ≤ 0.0001

Besides mRNA expression analyses of proinflammatory cytokines described before, TNF-α, IL-12p40, IL-6, and IL-1β protein expression were measured in the supernatant of the NT.CTRL and TNFAIP3, GFI1, KDM1A and OTX1 KO THP-1 Cas9 cells using a cytokine-specific ELISA (Figure 2.31). Independent of the polarization conditions ((a) green: M1 and b) red: M2) the KO cells induced more TNF-α, IL-12(p40), IL-6, and IL-1β than detectable in the NT.CTRL cells.

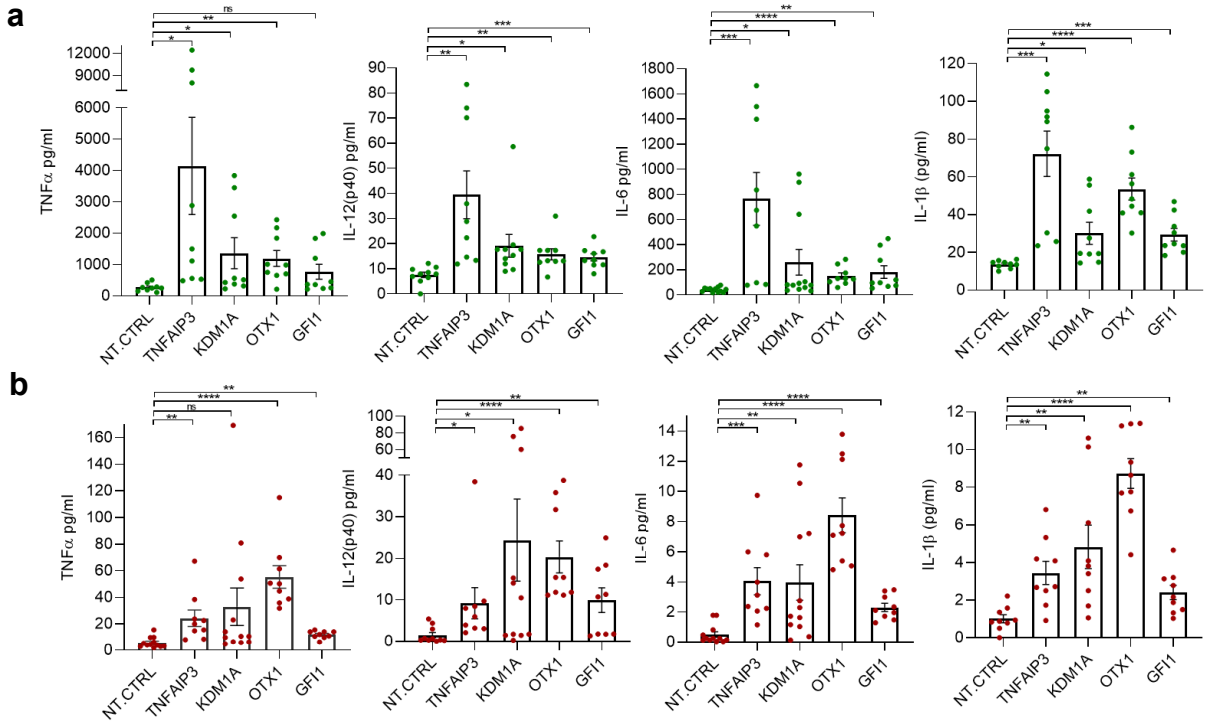

Figure 2.31. Validation of hits in THP-1 Cas9 cells – Cytokine secretion
ELISA of proinflammatory cytokines IL-6, IL-12p(40), and TNF-α (pg/ml) comparing supernatant of non-targeting control (NT.CTRL) THP-1 Cas9 cells and TNFAIP3, GFI1, KDM1A and OTX1 KO THP-1 Cas9 cells cultured under different polarization conditions (M1: green (a) and M2: red (b); n ≥ 9. Mean ± SEM, unpaired t-test; * p ≤ 0.05, ** p ≤ 0.01, *** p ≤ 0.001, **** p ≤ 0.0001

2.4.2 TNFAIP3 validation

The screening and hit validation data strongly implicated a role of TNFAIP3 in macrophage polarization. TNF Alpha Induced Protein 3 (TNFAIP3) is a known key player in the negative feedback regulation of NF-κB signaling (Shembade and Harhaj, 2012; Verhelst, 2012) and it has already been shown that TNFAIP3-silenced macrophages drastically induced granzyme B expression in CD4+ T cells (L. Wang et al., 2012). Taken this data together, TNFAIP3 was considered a potentially highly interesting immunoncology target. To better understand its function and elucidate the therapeutic potential of targeting specifically the TNFAIP3 de-ubiquitinase activity, further validation of the protein's role in macrophage polarization was carried out.

2.4.2.1 Verification of TNFAIP3 in U937 cells and primary monocytes

As shown before, KO of TNFAIP3 induced a marked M1 phenotype in THP-1 Cas9 cells detected by an increase in mRNA expression of not only M1 surface markers but most importantly increased proinflammatory cytokine expression (IL-12B, TNF, IL-6, and IL-1B). This could be detected in cells under M1 polarizing conditions (a) and M2 polarizing conditions (b) (Figure 2.30). Furthermore, KO of TNFAIP3 in U937 and MDMs confirmed that TNFAIP3 has a role in macrophage polarization and that the results regarding TNFAIP3 KO obtained in THP-1 Cas9 cells were not cell type specific artefacts (Figure 2.32). TNFAIP3 found as a hit in the screen and being a relevant target also in primary monocytes further indicates that the used CRISPR/Cas9 screening approach allows the identification of possible targets, inhibition of which might promote M1 polarization of macrophages.

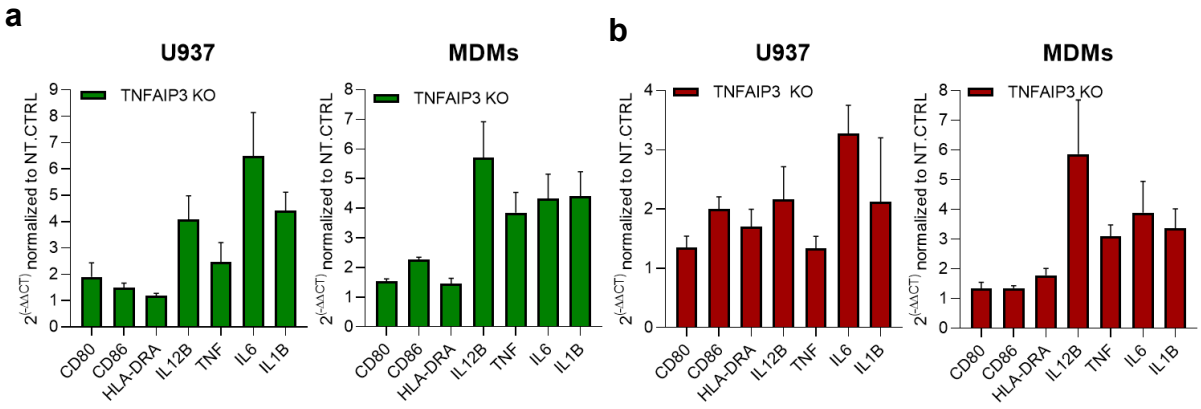

Figure 2.32. Gene expression analysis to examine effects of TNFAIP3 KO on polarization of U937 cells and human primary monocyte derived macrophages (MDMs)
U937 cells or primary human monocytes were electroporated with gRNAs or RNPs targeting TNFAIP3 to generate TNFAIP3 KO cells. Then, U937 cells were differentiated for 2 days with PMA and polarized with LPS and IFN-γ to M1 macrophages or with IL-4 to M2 macrophages for 24 h. Primary monocytes were differentiated for 6 days with MCSF/GMCSF to macrophages and polarized with LPS and IFN-γ to M1 macrophages or with IL-4 to M2 macrophages for 24 h. Proinflammatory cytokine expression and M1 surface marker expression in M1 polarized (a) and M2 polarized (b) TNFAIP3 KO U937 cells and MDMs was determined by TaqMan analysis and normalized to the NT.CTRL of each polarizing condition ($2^{(-\Delta\Delta CT)}$), n ≥ 3. Mean ± SEM, paired t-test; * p ≤ 0.05, ** p ≤ 0.01, *** p ≤ 0.001, **** p ≤ 0.0001

2.4.2.2 Verification of role of TNFAIP3 in macrophage polarization using TNFAIP3 homozygous KO THP-1 cell clones

The beforehand described validation experiments using the gRNA or RNP electroporation to generate TNFAIP3 KO result in a heterogenous population of cells exhibiting different genotypes of TNFAIP3 hemizygously, heterozygously, and homozygously deleted cells, and cells without any KO. To allow clear interpretation if the observed effects are indeed caused by TNFAIP3 KO, THP-1 cell clones homozygously deleted of TNFAIP3 were purchased from Horizon Discovery. Figure 2.33. shows in a western blot analysis that in comparison to parental THP-1 cells the TNFAIP3 KO clones do not express any detectable levels of TNFAIP3 protein.

Furthermore, it also shows that the loss of TNFAIP3 can be detected by the loss of TNFAIP3's molecular function as an ubiquitinating enzyme targeting RIP1 and RIP2 for degradation. RIP1 and RIP2 protein expression was examined in these TNFAIP3 KO THP-1 cells after activation with LPS. It could be shown that both proteins were not degraded upon LPS stimulus due to the lack of TNFAIP3 expression.

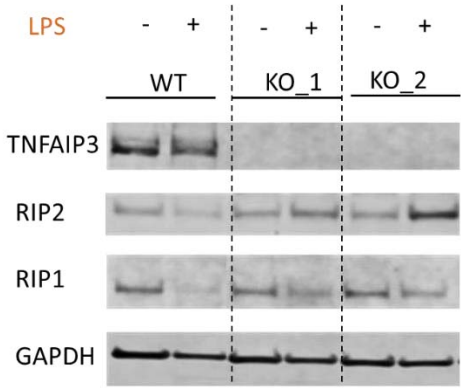

Figure 2.33. RIP1 and RIP2 stabilization in TNFAIP3 KO THP-1 cells after LPS activation
THP-1 wild type and TNFAIP3 KO THP-1 clones (KO_1 and KO_2) were treated with 100 ng/ml LPS or vehicle and further processed for western blot analysis of RIP1 and RIP2 expression. TNFAIP3 KO stabilizes the expression of both proteins after LPS stimulus, representative of n = 3; GAPDH was used as loading control

Next, the effects of the complete TNFAIP3 KO on the expression of additional M2 markers and chemokines were investigated in an RNA-seq experiment. In Figure 2.34 the expression of M1 associated genes (green) and M2 associated genes (red) is examined in THP-1 parental cells (WT) and the two THP-1 cell clones with homozygously deleted TNFAIP3 (TNFAIP3 KO #1 and KO#2) after IFN-γ and LPS polarization (a) or polarization with IL-4 (b). It could be shown that TNFAIP3 KO not only blocked M2 differentiation detected by decreased expression of the M2 associated genes CD163, MRC1, F13A1, CCL13, CCL24 and IL-10, but also could redirect differentiated THP-1 TNFAIP3 KO cells to immune stimulating M1 like macrophages. This was observed not only under proinflammatory conditions but even in the presence of immunosuppressive IL-4 by upregulating significantly several M1-associated genes (IL-23A, CXCL8, CXCL9, CXCL10, CCL3), besides markers described before such as CD80, IL-1B, IL-6, IL-12B, and TNF.

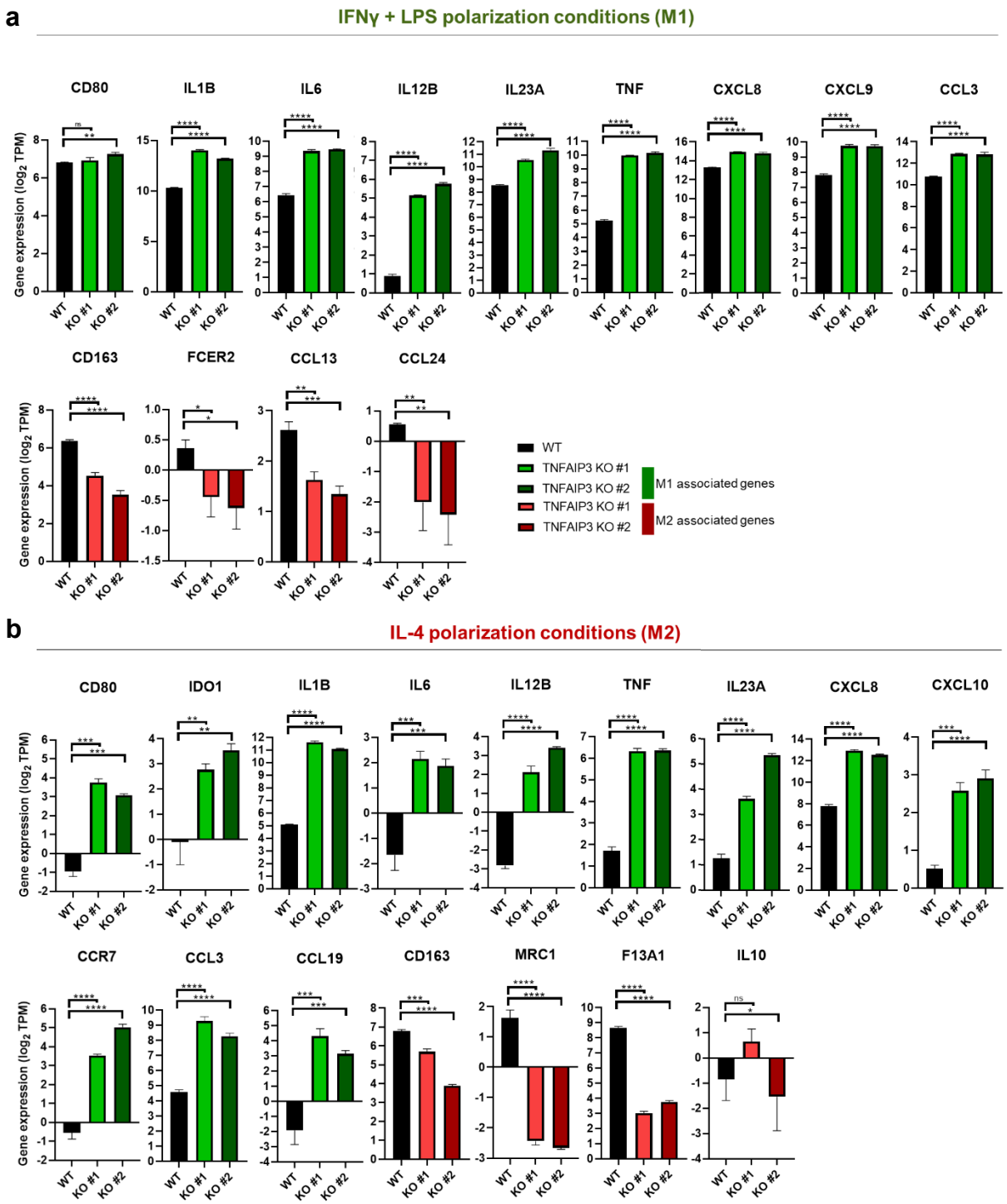

Figure 2.34. Transcriptomic analysis of THP-1 cells homozygously deleted of TNFAIP3 after M1 and M2 polarization

RNA-seq analysis in THP-1 cells homozygously deleted of TNFAIP3 (clone 1 and clone 2) after M1 polarization (IFN-γ and LPS) (a) and M2 polarizing (IL-4) (b). Shown are the $\log_2$ TPM values specifically for the M1 macrophage markers and M2 markers, n ≥ 3. Mean ± SD, unpaired t-test; * p ≤ 0.05, ** p ≤ 0.01, *** p ≤ 0.001, **** p ≤ 0.0001; data analysis was performed by Dr. Helge Roider (Bayer Bioinformatics Department)

2.4.2.3 Functional evaluation of TNFAIP3 KO in primary human macrophages

To allow evaluation of the global effects of TNFAIP3 KO on primary macrophages an RNA-seq analysis was performed with TNFAIP3 KO and control macrophages. Analyzing the results first for polarization marker expression, Figure 2.35 shows that primary macrophages with TNFAIP3 KO exhibited increased M1 marker expression (surface marker, proinflammatory cytokines and chemokines) and decreased expression of the M2 markers CD163 and IL-10.

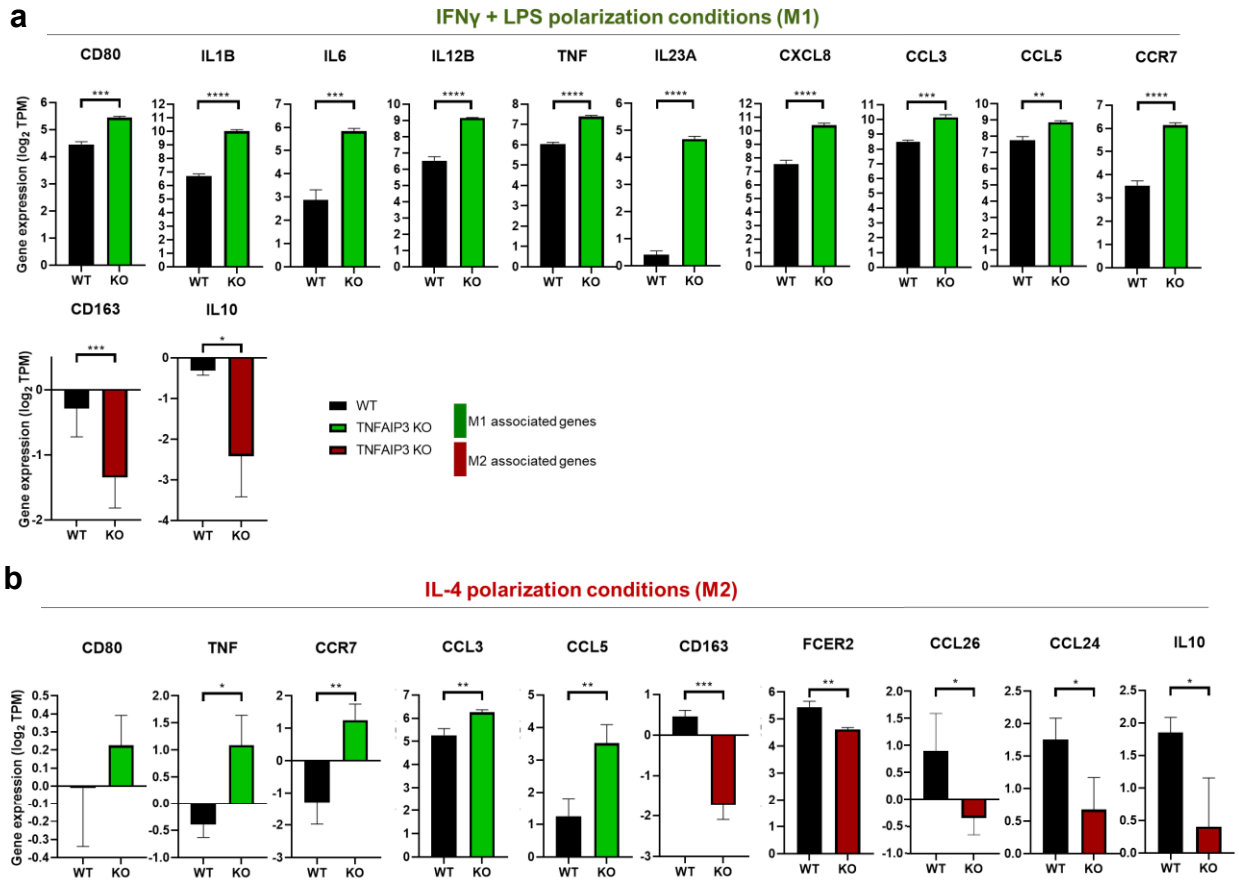

Figure 2.35. Transcriptomic analysis of primary human monocytes deleted of TNFAIP3 after M1 and M2 polarization
RNA-seq analysis in primary human monocytes deleted of TNFAIP3 (KO) after M1 polarization (IFN-γ and LPS) (a) and M2 polarizing (IL-4) (b). Shown are the log_2 TPM values specifically for the M1 macrophage markers and M2 markers. n ≥ 3. Mean ± SD, unpaired t-test; * p ≤ 0.05, ** p ≤ 0.01, *** p ≤ 0.001, **** p ≤ 0.0001; data analysis was performed by Dr. Helge Roider (Bayer Bioinformatics Department)

Next, the effects of the induced proinflammatory phenotype of TNFAIP3 KO primary macrophages on primary T cell stimulation were tested. TNFAIP3 KO M1 and M2 macrophages were cocultured with primary T cells and T cell activation was measured by their effect on T cell proliferation analyzed using a CFSE proliferation assay and on IFN-γ production (Figure 2.36). T cells showed increased proliferation activity when cocultured with M1 polarized macrophages than with M2 polarized macrophages. In these polarized macrophages, TNFAIP3 KO further enhanced the effect on proliferation of the T cells from 30 % proliferating T cells co-cultured with control M1 macrophages (NTC) to 55 % proliferating T cells when

cocultured with TNFAIP3 KO M1 macrophages. When T cells were grown in culture with M2 macrophages 15 % proliferated. Even, when TNFAIP3 was knocked out in M2 macrophages the amount of proliferating T cells increased to 40 % (Figure 2.36a+b). This activation of the T cells by cocultured TNFAIP3 KO macrophages under different polarization conditions could also been shown when T cell IFN-γ secretion was analyzed. The effect of TNFAIP3 KO on the T cell activation correlated significantly with the effects observed on proliferation (Figure 2.36 c). Furthermore, macrophages were examined before cocultured for their capacity to secrete the proinflammatory cytokines such as IL-6, TNF-α, IL-12(p40), IL-8 and IL-1β. TNFAIP3 KO caused a significant increase in the secretion of these cytokines in comparison to control macrophages (NTC) under both, M1 and M2 polarizing conditions (Figure 2.36 d). The efficiency of TNFAIP3 KO in the primary macrophages was confirmed by western blot analysis (Figure 2.36 e). Overall, this data shows that TNFAIP3 KO in macrophages primes these cells to an M1-like proinflammatory phenotype which in turn stimulates T cells.

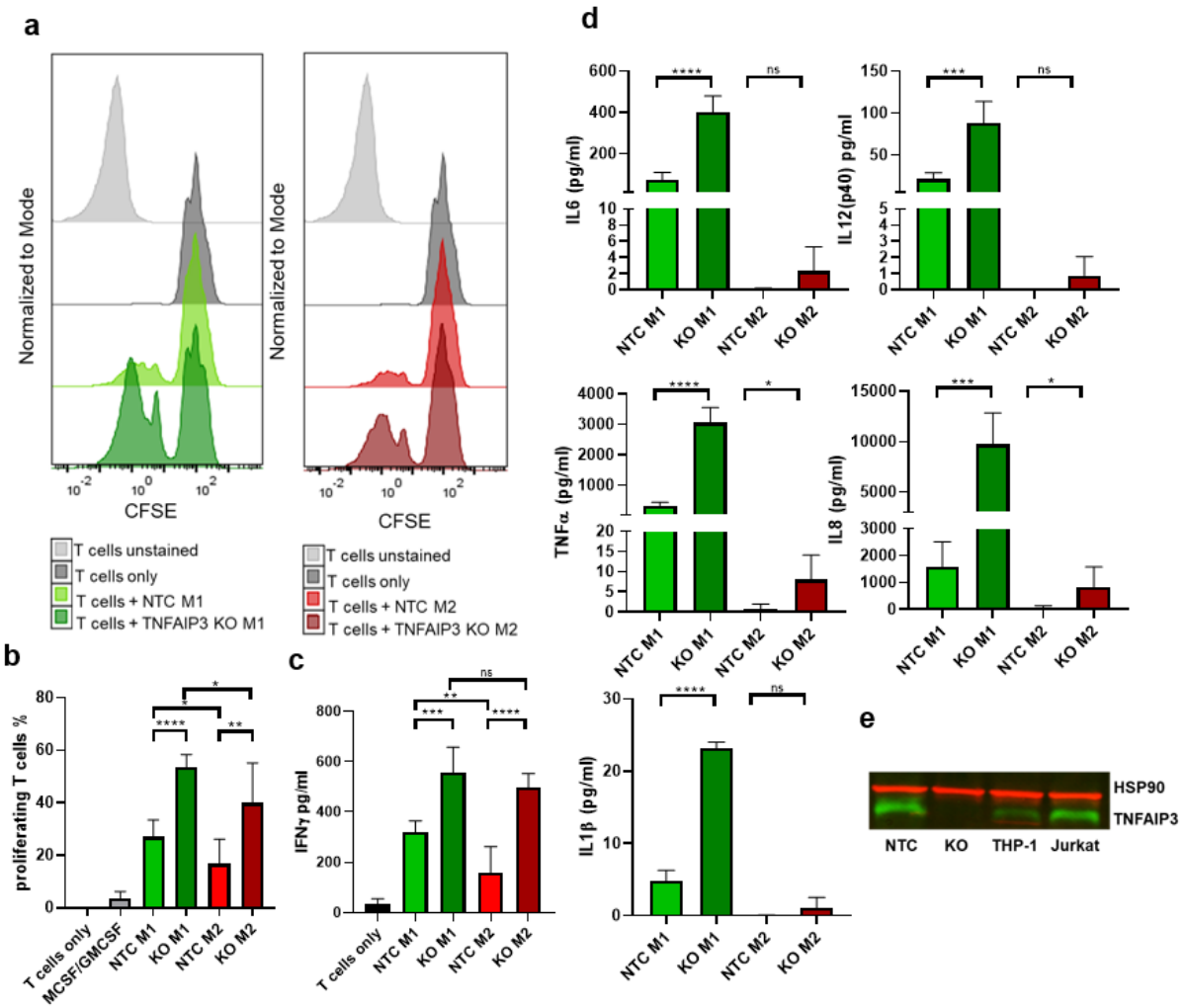

Figure 2.36. Coculture of primary human T cells with TNFAIP3 KO M1 or M2 primary human macrophages

(a) Primary human T cells were stained for CFSE and cocultured for 7 days with primary human M1 and M2 polarized macrophages which had been electroporated 7 days before the start of coculture with ribonucleoproteins (RNPs) against a non-targeting control (NTC) or TNFAIP3 (TNFAIP3 KO) (b) The proliferation of CFSE stained T cells from a) was quantified by determining the percentage of proliferating T cells, T cells without coculture (T cells only) T cells coculture with differentiated but not polarized macrophages (MCSF/GMCSF) and cocultured with NTC M1/M2 or TNFAIP3 KO M1/M2 macrophages n = 3, Mean ± SEM, paired t-test; * $p \leq 0.05$, ** $p \leq 0.01$, *** $p \leq 0.001$, **** $p \leq 0.0001$ (c) after 5 days of coculture the supernatant was analyzed for IFN-γ, determining the activation of T cells cultured without macrophages (T cells only), or cocultured with NTC M1/M2 or TNFAIP3 KO M1/M2 macrophages; n = 3, Mean ± SEM, paired t-test; * $p \leq 0.05$, ** $p \leq 0.01$, *** $p \leq 0.001$, **** $p \leq 0.0001$, (d) proinflammatory cytokine secretion of NTC M1/M2 vs. TNFAIP3 KO M1/M2 macrophages before cocultured with T cells; ; n = 3, Mean ± SEM, paired t-test; * $p \leq 0.05$, ** $p \leq 0.01$, *** $p \leq 0.001$, **** $p \leq 0.0001$, I determination of TNFAIP3 KO in TNFAIP3 KO macrophages (KO) in comparison to NTC macrophages and THP-1 and Jurkat cells; HSP90 serves as a loading control

2.4.3 Evaluation of the therapeutic potential of targeting specifically the TNFAIP3 de-ubiquitinase activity

The complete KO of TNFAIP3 in mice causes a severe inflammatory phenotype leading to multiple organ damage and premature death (E. G. Lee et al., 2000). In contrast, mice with a bi-allelic knock-in (KI) of a C103A point mutation in the TNFAIP3 gene, inducing a specific inactivation of the TNFAIP3 de-ubiquitinase activity, did either not show an inflammatory phenotype at all (De et al., 2014) or a mild proinflammatory phenotype (Lu et al., 2013). Therefore, the aim was to evaluate if a specific inhibition of the de-ubiquitinase activity of TNFAIP3 would be therapeutically relevant and, like the complete KO could prime these cells to an M1-like proinflammatory phenotype which in turn stimulates T cells.

To test this, Jurkat cells and THP-1 cells with a bi-allelic KI of a point mutation C103A into the TNFAIP3 gene, which abolishes the deubiquitinase activity of TNFAIP3, were purchased from Horizon Discovery.

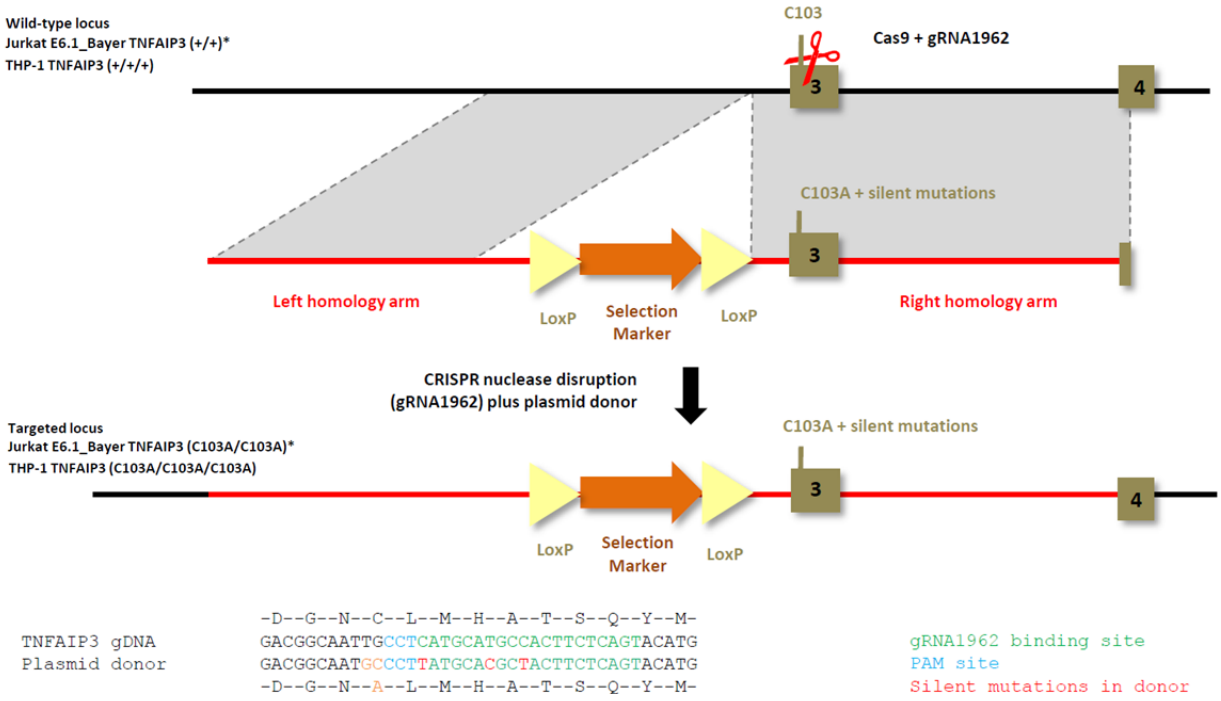

Figure 2.37. Vector design for TNFAIP3 (C103A) KI point mutation in THP-1 and Jurkat cells
gRNA 1962 binds to the green site in sequence. Blue indicates the PAM site which is also required for cutting activity. The plasmid donor contains a selection cassette and the C103A mutation (TGC > GCC). In addition, the plasmid donor contains silent mutations (highlighted in red) which will disrupt the green region. These will prevent re-cutting of the donor once it is integrated. *SNP6.0 data for HD held (ATCC sourced) Jurkat HD PAR-840 indicates that TNFAIP3 has a copy number of 2N but following isolation of clonal population, the copy number was adjusted to 4N (provided by Horizon Discovery)

Clones with the following genotype were obtained:

Table 2.2 Genotype of obtained KO and KI TNFAIP3 THP-1 and Jurkat cell clones

Cell line		Genotype
Jurkat E6.1	Parental	TNFAIP3 (+/+/+/+)
Jurkat E6.1	KO	TNFAIP3 (+/-/-/-)
Jurkat E6.1	KI clone 1	TNFAIP3 (C103A/-/-/-)
Jurkat E6.1	KI clone 2	TNFAIP3 (C103A/C103A/-/-)
THP-1	Parental	TNFAIP3 (+/+/+)
THP-1	KO clone 1+2	TNFAIP3 (-/-/-)
THP-1	KI clone	TNFAIP3 (C103A/+/+)

Generating cell lines with homo- or hemizygous knockin of a mutation is a well-established procedure with a success rate of about 5 % in diploid cells (S. H. Lee et al., 2018). However, based on prior analysis, Jurkat cells found to have 4 alleles of the TNFAIP3 locus and THP-1 cells 3. This requires simultaneous editing of all alleles. For the Jurkat cells Horizon Discovery successfully generated hemizygous cell clones expressing either one or two C103A mutated transcripts on an otherwise genetic KO background. This allows, genotype to phenotype analysis based specifically on the expression of different levels of TNFAIP3 mutated transcripts

(data not shown). However, even after extensive testing, no such cell clones could be obtained for the THP-1 cells. Instead, in these cells only clones could be generated with a mutation in one of the alleles while the other two remained to be wild type for TNFAIP3. Therefore, for further analyses to determine the role of the deubiquitinase domain in a potential therapeutic setting only the Jurkat TNFAIP3 C103A KI cells could be used.

Figure 2.38a shows the effects of C103A KI on activation of the Jurkat cell clones. TNFAIP3 is known to regulate TCR/CD28 mediated NF-κB activation (Duwel et al., 2009; Malewicz et al., 2003). Therefore, wild type (WT), TNFAIP3 KO and TNFAIP3 KI (C103A) Jurkat cells were stimulated with anti-CD3/anti-CD28 to activate TCR signaling. To gain more insight into the effects on gene expression induced by TNFAIP3 KO or KI, RNA-seq analysis was performed. Thereby, genes such as IL-2, IL-2RA, TNF, TNFRSF9 and NFKB1 were shown to be significantly differentially expressed (Figure 2.38).

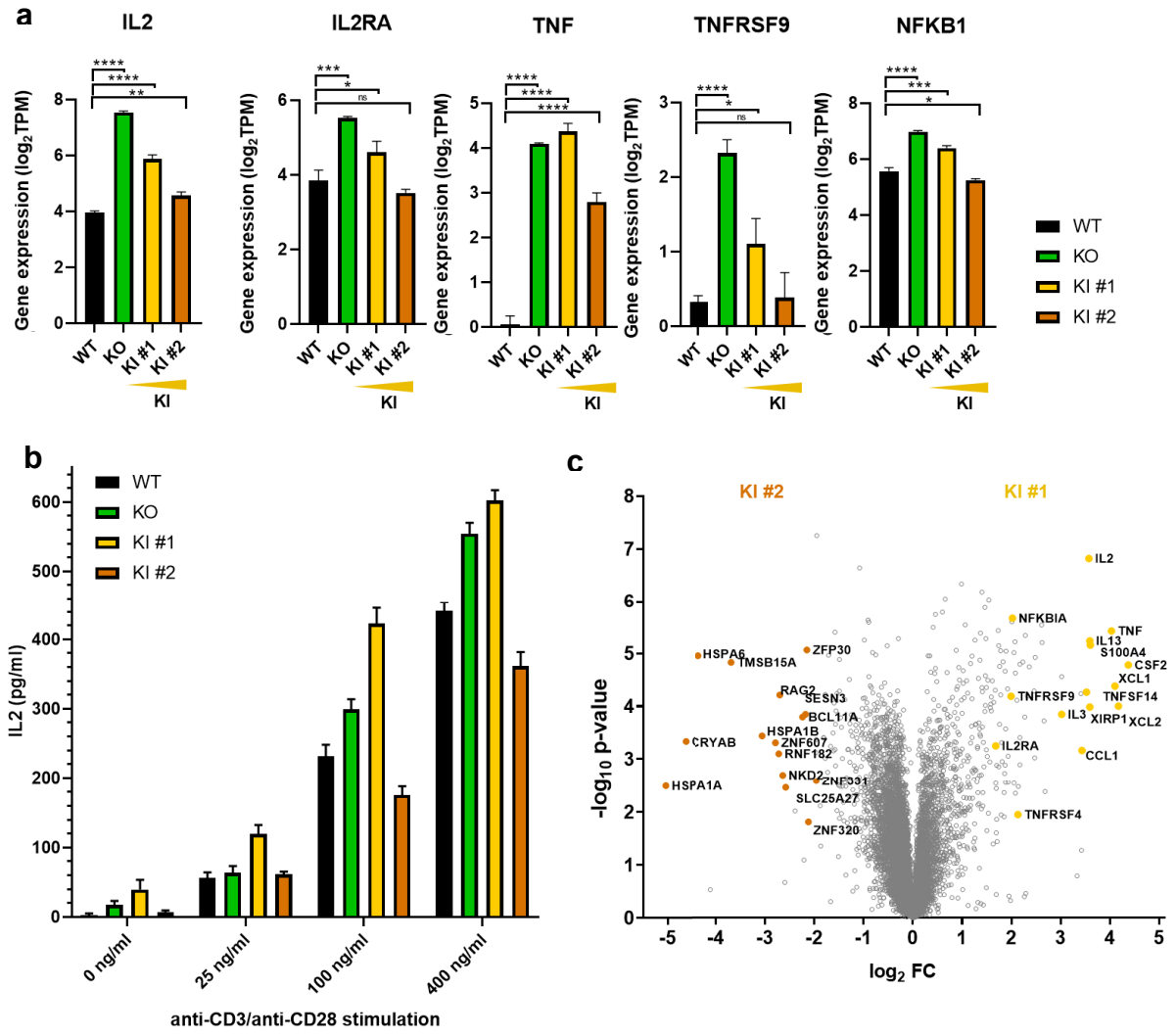

Figure 2.38. Comparison of effects of TNFAIP3 KO and KI (C103A) on TCR regulated gene expression and secretion of IL-2 in Jurkat cells

(a) Jurkat cells with TNFAIP3 KO or TNFAIP3 KI (C103A) clone #1 (KI#1) and clone #2 (KI#2) or wild type (WT) were stimulated with anti-CD3/CD28 for 3h. RNA-seq analysis was performed and gene expression analysis (log_2 TPM) of TCR induced genes in wild type (WT), TNFAIP3 KO (KO), and TNFAIP3 KI #1 and #2 cells displayed. KI #1 TNFAIP3 (C103A/-/-/-) cells show a similar phenotype as the KO cells whereby KI #2 (TNFAIP3 (C103A/C103A/-/-) does not, ; n = 3, Mean ± SD, unpaired t-test; * $p \leq 0.05$, ** $p \leq 0.01$, *** $p \leq 0.001$, **** $p \leq 0.0001$ (b) IL-2 secretion of cells described in a) after different anti-CD3/anti-CD28 stimulation (0,25,100 and 400 ng/ml) for 3 days (c) Vulcano plot from experiment described in a) displaying differentially expressed genes (DEGs) in TNFAIP3 KI clone #1 and clone #2 cells. Data analysis was performed by Dr. Helge Roider (Bayer Bioinformatics Department)

Thereby, similar to data described by Duwel et al., 2009 and Malewicz et al., 2003, the TNFAIP3 KO induced a significant upregulation of the expression of these genes in the Jurkat KO clone. In comparison, only the KI clone #1 with one mutated allele and the other three allele with TNFAIP3 KO, mimicked the gene expression effects observed in the homozygous KO clone. The clone with two mutated alleles (clone #2) showed a more similar expression profile as detected in the WT cells, implicating a rescue of enzyme function even though the expressed TNFAIP3 is deficient in its deubiquitinase function. Investigating the effects of KO and C103A KI on IL-2 secretion, (Figure 2.38b) confirmed this observation. To better understand the transcriptomic differences in the two KI clones the DEGs among both samples were analyzed in an RNA-seq experiment. The volcano plot in Figure 2.38c shows the top DEGs in the KI clone 1 and KI clone 2 cells. It depicts that genes known to be induced by TCR activation such as IL-2, TNF, TNFRSF9 and IL-2RA were upregulated exclusively in the KI clone #1 as found in the complete KO cells. However, the knockin of 2 copies of TNFAIP3 C103A in clone #2 rather induced the expression of heat shock genes, such as HSPA1A, HSPA1B, HSPA5, and CRYAB, not found to be induced in KI clone #1. By hierarchical sample and gene clustering based on the top 50 most variable genes, it could be confirmed that the KO and KI clone #1 sample clustered together and so the wild type and clone #2 belonged to one cluster (Figure 2.39).

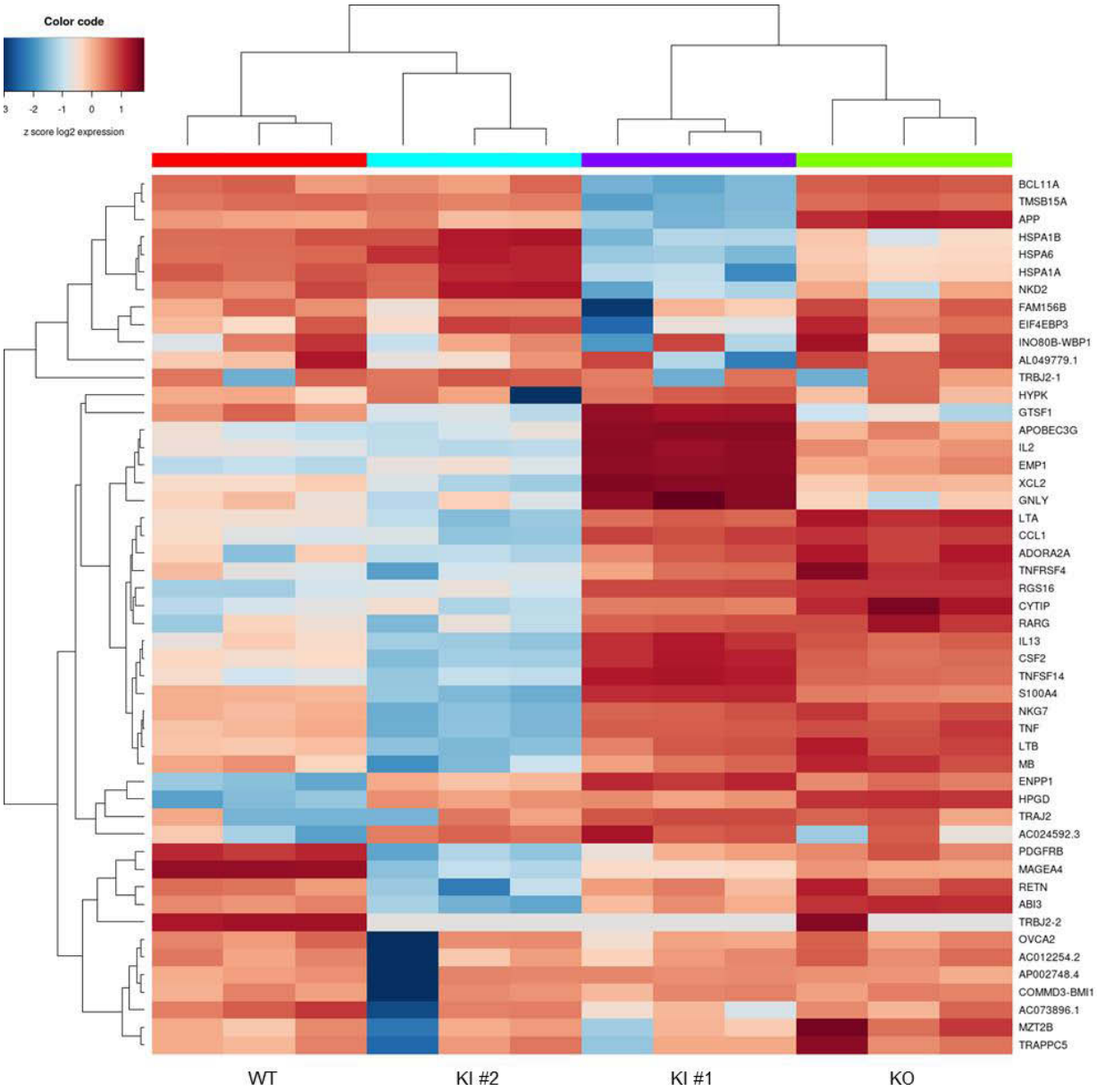

Figure 2.39. Gene clustering of WT, TNFAIP3 KO, TNFAIP3 KI clone #1 and clone #2 Jurkat cells
Wild type (WT), TNFAIP3 KO, TNFAIP3 KI (C103A) clone #1 and clone #2 Jurkat cells were stimulated for 3h with 400 ng/ml anti CD3/CD28. RNA-seq analysis was performed. Top 50 most variable genes (based on their variance) across all samples are shown and corresponding hierarchical clustering of both all samples and all the selected genes was performed. The color code represents the z score $\log_2$ expression. WT Jurkat cells and KI #2 cells cluster together and KO Jurkat cells and KI#1 cells. Data analysis was performed by Dr. Helge Roider (Bayer Bioinformatics Department)

Again, these results implicate that expression of enough TNFAIP3 C103A might rescue the proinflammatory phenotype induced by TNFAIP3 KO in Jurkat cells. This observed upregulation of heat shock genes belonging to the family of molecular chaperons points to a possible function of the TNFAIP3 deubiquitinase domain in protein maturation, re-folding and degradation which might affect the stability of TNFAIP3. These results further implicate that just inhibiting the deubiquitinase function will not be sufficient to induce the therapeutically relevant proinflammatory effect detected after a complete TNFAIP3 KO in these cells.

Overall, the effects of knocking out TNFAIP3 first detected in the THP-1 screen can be verified and cross validated in alternative cell models, most importantly in primary human monocytes. However, in the models used, the therapeutic potential of targeting specifically TNFAIP3's de-ubiquitinase activity could not be shown. Further research will be necessary to elucidate if there might be different means to target TNFAIP3's activity and still reaching a therapeutic window when addressing TNFAIP3.

3 Discussion

In recent years it became clear that reactivating the cancer patients' immune system to fight the tumor can be a very successful therapeutic approach. After bringing the first immune-oncological therapies into clinic about 10 years ago, with very impressive improvement of patient survival-rates, researchers and clinicians are now trying to understand why about 80 % of the patients do not respond or become resistant (Ott et al., 2017). There is a great interest in finding patient stratification markers and of course alternative therapeutic approaches to treat patients not amenable to these available treatments. Currently, the most widely used treatments are immune-checkpoint inhibitors targeting for instance molecules known to be expressed on tumor-infiltrating lymphocytes. These are cytotoxic T lymphocyte antigen 4 (CTLA-4) or programmed cell death-1 (PD-1) and its ligands (PD-L1 and PD-L2) (D. S. Chen & Mellman, 2017; Kyi & Postow, 2014; Sharma & Allison, 2015). They are mainly efficacious in "hot" tumor types, like melanoma or lung cancer, defined by a high tumor mutational burden, high expression of tumor-specific neoantigens and a high rate of tumor-infiltrating T cells (Popovic et al., 2018).

Many of the non-responsive tumors are often so-called immunologically "cold" tumors. Investigating the tumor microenvironment of these patients, it shows significant recruitment of immune-suppressive cell subsets, including regulatory T cells, myeloid-derived suppressor cells, and macrophages (Cheng & Ho, 2019). These immunosuppressive tumor associated macrophages (TAMs) are proposed to be key regulators of the tumor microenvironment (TME) and promote tumor growth and progression while resembling M2-like macrophages (Mantovani et al., 2017). Importantly, it has been shown in many types of solid tumors that the prevalence of TAMs correlates with poor patient survival (Belgiovine et al., 2016). Some progress has been made regarding combination therapy, where TAM-addressing therapeutic strategies are able to complement and synergize with chemo-, radio- and immunotherapy (antibody based or adoptive cell therapy) as well as small-molecule therapy (Engblom et al., 2016).

Despite progress in TAM-based anticancer therapy with anti-CSF-1R, CD40 antagonism, TLR agonists and HDAC inhibition, there is a lack of specific druggable proteins, especially for small molecules, inhibition of which would promote the proinflammatory M1 macrophage phenotype (Beatty et al., 2013; Evans et al., 2016; Wiehagen et al., 2017).

The present work describes a novel CRISPR/Cas9-based screening approach for the unbiased identification of those myeloid cell targets for potential immunotherapies.

3.1 *In vitro* CRISPR/Cas9 screen

This work establishes the feasibility of *in vitro* pooled CRISPR/Cas9-based screening to discover novel targets with a role in the immune-suppressive state of the TME.

Originally, human primary monocytes (HPMs) were intended to be used as the screening cell system. They are the progenitors of macrophages in the body and recapitulate best the immune cell biology, including key signaling pathways and effector functions. These might be de-regulated in immortalized cell lines.

Therefore, a protocol could be developed for the viral transduction of HPMs. However, it was only possible to transduce small constructs, such as sgRNA or shRNA harboring vectors. Yet, CRISPR/Cas9-based experiments require exogenous expression of Cas9. Viral packaging of the large Cas9 plasmid only yields very low viral titer, resulting in extremely low transduction efficiency not enough to detect Cas9 expression after viral transduction of HPMs.

A possible option to perform the CRISPR/Cas9 screen in HPMs became apparent with the publication of the method SLICE (sgRNA lentiviral infection with Cas9 protein electroporation). This method was established and used by Shifrut and colleagues to perform a genome wide CRISPR/Cas9 screen in human primary T cells (Shifrut et al., 2018). SLICE is a hybrid system introducing lentivirally packaged sgRNA followed by electroporation of Cas9 protein. However, after extensive testing it became obvious, that because of the number of HPMs required from the same source for the performance of a whole genome CRISPR/Cas9 screen, to obtain reliable and interpretable results, this was not an option to perform a genome-wide screen.

Another interesting approach has been utilized by Parnas et al. They used engineered Cas9-expressing mice to obtain Cas9 expressing screening cells and performed a CRISPR/Cas9 screen in mouse primary dendritic cells. Thus, bone marrow from these mice could be used and be differentiated into macrophages. Then, only a single transduction of the lentivirally packaged sgRNAs were required to carry out a CRISPR/Cas9 screen (Parnas et al., 2015). Although this system is limited to the mouse model, it opens the possibility to perform a CRISPR/Cas9 *in vivo* screen to find relevant targets for TAM polarization. This approach is planned as the next step and will allow identifying targets in a TME setup.

As an alternative to the HPMs, THP-1 cells were identified as feasible macrophage cell surrogates enabling pooled screening. These monocytic cells have been shown to be a suitable system to study macrophage polarization (Chanput et al., 2014; Daigneault et al., 2010). Most research on macrophage polarization has so far been conducted under *in vitro* culture conditions using primary or immortalized cells (Murray, 2017). Hereby, macrophages

are differentiated from monocytes and the derived macrophages are stimulated with M1 or M2 polarizing agents as IFN-γ and LPS, or IL-4 or IL-13, respectively. These conditions are designed to mimic the exposure of macrophages to polarized CD4+ T cells which produce distinct cytokine combinations. T_H1 cells produce IFN-γ and T_H2 cells IL-4 and IL-13 (Munder et al., 1998; Munder et al., 1999). Minimizing the variance in macrophage phenotype derived from *in vitro* conditions will help to better characterize the physiology of macrophage polarization. This can be achieved by standardizing protocols for *in vitro* polarization.

As described by others before, we could show that polarization of THP-1 macrophages induced a comparable expression pattern as observed by polarization of HPMs (Caras et al., 2011; Chanput et al., 2014; Genin et al., 2015; Z. Qin, 2012). Here, we used RNA-seq analysis to compare the effects of polarization on THP-1 cells vs. HPMs. We identified ~700 of 1,000 most highly expressed genes in any polarization condition (M0, M1 or M2) be shared between both cell systems. This was further supported by comparing the DEGs in THP-1 cell derived macrophages with MDMs showing expression changes in both cell systems for the same markers for M1 (CD38, CD80, CXCL8, CXCL9, CXCL10, IDO1, IL-1B, IL-6, IL-23A, CCL19 and TNFSF10) and M2 (ALOX15, CCL13, CCL26, CD209, F13A1 and FCER2). Based on these results, we considered the THP-1 cells as a sufficiently good cell system to study macrophage biology.

Surdziel and colleagues performed a similar screening approach in the search for candidate modulators of macrophage polarization. They also used human THP-1 cells, screening a pooled shRNA library (Surdziel et al., 2017) detecting expression changes of well-established markers for both M1 and M2 polarized cells using microarray technology. Surdziel et al. support our findings that polarization of THP-1 macrophages induced a comparable expression pattern as observed by polarization of HPMs. Though they had performed a similar screen to identify targets affecting macrophage polarization as planned in this project, our aim was not to merely repeat the work but relying on many studies showing the advantages of using CRISPR/Cas9 over RNAi to find truly novel results. RNAi-based screening, as Surdziel et al. used it, is a well-established method and shown to be a feasible approach for target identification. An impressive example is the shRNA screen by Zhou et al. finding novel targets involved in promoting T-cell activation *in vivo* (Zhou et al., 2014). However, CRISPR/Cas9 based approaches have been found to be even more efficient and accurate in comparison and show a greater specificity to its genomic target. This is mainly contributed to the induced complete gene KO rather than partial expression reduction as achieved by RNAi inducing stronger changes in phenotypes (Doench, 2018).

Also, in the present study a screening system was established allowing to target the entire genome. Surdziel et al. had focused on targeting 648 chromatin and signaling regulators. It wasn't possible to clarify, based on the publication, why they had restricted the screen to this subset as it most likely would have been possible to conduct a genome-wide RNAi screen also in the system they had established. Nevertheless, in the present study, to allow unbiased investigation of novel targets, an sgRNA library was used targeting the entire human genome.

Besides some known targets playing a role in macrophage polarization (BRD2, RELA, REL and MYD88) (Belkina et al., 2013; Fullard et al., 2012; Pittet et al., 2011; S. Shi et al., 2003), Surdziel et al. found O-linked β-N-acetylglucosamine transferase (OGT) as the top scoring target mediating M2 polarization and suppressing M1 polarization. OGT has been shown to be involved in macrophage biology before (Hwang et al., 2013; Li et al., 2017). Increased OGT expression in hyperglycemia skewed TAMs polarization to M2-like phenotype which drives cancer progression and immune evasion. When OGT was inhibited, the TAMs got repolarized to a proinflammatory and anti-tumoral phenotype (Mantuano et al., 2019). OGT has also been identified in the present study performing the CRISPR/Cas9 screen. It has been one of the top ranked targets (rank 3 (log_2 FC = 2.0) in the hitlist for M1 polarization conditions, rank 19 (log_2 FC = 1.6) in M2 polarizing conditions) confirming the validity of the described screening approaches. While the essential gene MYC was described by Surdziel et al. to serve as a suppressor of both M1 and M2 polarization it could not be identified in our screen due to the lethal effect of MYC KO on the screening cells. This demonstrates the incompleteness of protein depletion with knockdown (KD) in RNAi screening which should be considered when comparing results from RNAi KD screens with CRISPR/Cas9 KO screens.

The robustness of the screens performed by us was demonstrated by e.g. achieving high technical reproducibility. Also, comparison of the screening data with control sgRNAs targeting essential and non-essential genes resulted in a strong separation between these sgRNAs. This indicates the robust Cas9 activity, abundant cell sampling and the quality of sample processing and analysis after screening (Doench, 2018). As a result of this screening, a list of targets involved in the immunosuppressive phenotype of macrophages could be presented.

3.2 Validation of screening hits as potential immunosuppressive myeloid cell targets

To verify the role of the screening hits in macrophage polarization not to be restricted to THP-1 cells, an extensive protocol has been developed. Therefore, initially 20 out of the 170 hits were selected for validation experiments to allow performing this work in the scope of this thesis. These targets were selected based on their relevance in macrophage biology, putative druggability, and novelty. Among these 20 targets, TNFAIP3, KDM1A, OTX1 and GFI1 were verified to indeed not only show increased CD80 expression when inhibited but reprogramming the cells to a more M1-like phenotype.

KDM1A, also known as LSD1 (lysine-specific demethylase 1), is an H3K4 and H3K9 demethylase that has been implicated to be essential for myeloid cell differentiation (Kerenyi et al., 2013). Our data, showing that genetic knockout of LSD1 affects polarization of macrophages, is now being supported by work from Tan et al. published very recently (Tan et al., 2019). As we have seen in both, the THP-1 as well as the primary myeloid cells (data not shown), Tan and colleagues find that in mouse monocytic RAW264.7 cells, M1 polarization significantly decreases LSD1 expression. While they also see that inhibiting LSD1 activity significantly promotes M1 polarization *in vitro* and in a murine triple-negative breast cancer model, they could dissect the importance of the CoREST binding region of LSD1 in macrophage polarization. To do so, they used 2 different potent and specific chemical inhibitors of LSD1, phenelzine and GSK2879552. In contrast to GSK2879552, an inhibitor of the catalytic activity of LSD1 which only binds the FAD domain, phenelzine targets both, the flavin adenine dinucleotide (FAD) and CoREST binding domains of LSD1. Thereby, phenelzine induces structural changes in the CoREST binding region of LSD1 being important for stability and activity and thereby disrupting the LSD1/CoREST complex (Tan et al., 2019). In RAW264.7 cells, this is mimicking a similar response to M1 polarization by activating the epigenetic landscape of M1 selective gene signatures trough H3K4 and H3K9 methylation marks. Still further investigation in the molecular priming through LSD1's role in M1/M2 phenotypes is necessary.

Epigenetic reprogramming was shown before to be important for the regulation of macrophage polarization and can be addressed also with inhibitors against HDAC and BET (Belkina et al., 2013; X. Chen et al., 2012). So far, LSD1 inhibitors have found stimulating proinflammatory cytokine expression in monotherapy and combination with HDAC1 inhibitors (Janzer et al., 2012) indicating the importance of LSD1 inhibition in favoring antitumor immunity and showing direct connection with macrophages. Furthermore, treatment of BALB/c mice bearing orthotopic EMT6 tumors with the reversible LSD1 inhibitor HCI-2509 from XCessBio in

combination with a PD-1 monoclonal antibody displayed superior inhibitory effects against tumor progression and resulted in 70% reduction in tumor burden as compared to vehicle control group. Treatment with PD-1 antibody alone did not have any effects on EMT6 tumor growth (Y. Qin et al., 2019). Intriguingly, like phenelzine, HCI-2509 not only blocks the FAD-binding region of LSD1 (Sorna et al., 2013), but also abolished LSD1 protein–protein interactions e.g. with its complex partner CoREST (Fiskus et al., 2014; Macheleidt et al., 2018).

For the growth factor independent 1 transcriptional repressor (GFI1) and the transcription factor Orthodenticle Homeobox 1 (OTX1) no direct role in macrophage polarization has been described so far. Interestingly though, GFI1 has been implicated in regulating neutrophil differentiation, promoting proliferation of lymphoid cells, and being required for granulocyte development (van der Meer et al., 2010). OTX1 was shown, despite the essential role in brain development that it is also involved in hematopoiesis (Levantini et al., 2003). Further work will be required to elucidate their role in macrophage development. However, GFI1 and OTX1 are transcriptional regulators. Transcription factors are currently being generally considered as not easily pharmacologically targetable, meaning chemically intractable, as they are on one hand not very specific interacting within a large machinery of very similar transcriptional regulators. On the other hand, they commonly lack the specific binding pocket necessary for specific drug-binding (Dang et al., 2017). Though, there are examples of successfully targeting transcriptional regulators such as Rosiglitazone agonizing PPARγ activity or Nutlin-3 activating p53 (Kunkele et al., 2012; Sauer, 2015). Furthermore, new strategies of targeting the gene's DNA or RNA directly using for instance CRISPR/Cas9 are being in development like deletion of BCL11A to cure sickle cell disease (Khosravi et al., 2019).

However, these approaches are still very challenging. Therefore, verifying additional hits identified in the screen in parallel to not only find other novel targets but also broaden our understanding of macrophage polarization will be necessary.

3.2.1 TNFAIP3 validation

3.2.1.1 Function of TNFAIP3

Another interesting screening hit is TNFAIP3. Knockout of TNFAIP3 had been shown to induce the strongest effects on macrophage phenotype in both screens, the focused as well as the whole genome CRISPR/Cas9 screen and has also been postulated to be a mediator of M2 polarization elsewhere (L. Wang et al., 2012; Y. Wang et al., 2017).

TNFAIP3 is a (de)ubiquitinating enzyme and key player in the negative feedback regulation of NF-κB signaling which is essential for the priming phase and effector functions of immune cells

(Shembade and Harhaj, 2012; Verhelst, 2012). Inhibition of TNFAIP3 therefore might promote the inflammatory response which made it an attractive candidate hit to start the verification of the screening results. Although TNFAIP3 had already been implicated in macrophage biology, it was selected for further extensive exploration of the effects of inhibition on macrophage polarization and as a potential therapeutically relevant target. Thereby, also the validity of the screening approach could be examined and most importantly this work helped establishing the protocols for verifying the other screening hits.

The functions of TNFAIP3 in NF-κB regulation are most apparent in IL-1R, TLR and TNFR signaling pathways. TNFAIP3 mRNA is pre-dominantly expressed in lymphoid tissues-, and its expression is induced dramatically by TNF-α as well as by autoinduction (Das et al., 2018). It has two functional domains, an N-terminal de-ubiquitinase domain (DUB OTU domain) and C-terminal ubiquitin ligase domain (Zinc-finger motifs). In order to terminate NF-κB signaling, TNFAIP3 disassembles Lys63-linked polyubiquitin chains of proinflammatory proteins, such as RIP1, RIP2 and TRAF6, subsequently replacing them with Lys48-linked polyubiquitin. This leads to the degradation of the proteins and the inhibition of NF-κB signaling via a negative feedback loop (Verhelst et al, 2012).

We have presented a potential cellular mechanistic assay for possible compound screening by detecting the effects of TNFAIP3 KO on RIP1 and RIP2 protein stability in western blot analysis. As we described, TNFAIP3 knockout clearly prevents RIP1 and RIP2 protein degradation normally induced by LPS treatment (Wertz et al., 2004). Another possible approach to monitor compound-mediated effects on TNFAIP3 activity would be detecting deubiquitinylation/ ubiquitinylation of e.g RIP1.

The complete KO of TNFAIP3 in mice causes a severe inflammatory phenotype leading to multiple organ damage. These mice die within 2 weeks after birth (E. G. Lee et al., 2000).

Conditional TNFAIP3 KO mice are viable but develop various auto-immune diseases. Mice with TNFAIP3 deficient B cells developed systemic lupus erythematosus and show increased autoantibody production. They also displayed increased proinflammatory cytokine production and an expansion of effector T cells and myeloid cells (Chu et al., 2011; Hovelmeyer et al., 2011; Tavares et al., 2010). Similar phenotypes were observed in mice with TNFAIP3 deficient DCs also resulting in autoimmunity displayed by autoantibody production and nephritis (Kool et al., 2011). Furthermore, TNFAIP3 was shown to be crucial for TCR/CD28 mediated NF-κB activation and TCR-mediated survival (Duwel et al., 2009; Malewicz et al., 2003; L. Shi et al., 2013). Mice with TNFAIP3 deletion in mature T cells developed inflammatory lung and liver infiltrates. Also, the proportion of CD8+ T cells was increased. When these cells were

stimulated with anti-CD3/CD28 the cells produced more IL-2 and IFN-γ *in vitro*, also observed *in vivo* by increased IFN-γ and TNF-α in the serum (Giordano et al., 2014). These observations supported our findings, that TNFAIP3 KO Jurkat cells showed increased IL-2 secretion and increased TCR/CD28 mediated NF-κB activation.

To evaluate TNFAIP3s' role in myeloid cells, Matmati and colleagues have crossed $TNFAIP3^{fl/fl}$ with lysozyme M(LysM)-cre Tg mice generating $TNFAIP3^{LysM\text{-}KO}$ resulting in LysM-cre promoter being expressing in 95-99 % of macrophages. These mice developed enthesitis (De Wilde et al., 2017) and paw inflammation (Matmati et al., 2011). *Ex vivo* cultured $TNFAIP3^{LysM\text{-}KO}$ produced higher levels of proinflammatory cytokines compared to control macrophages (Matmati et al., 2011; Vande Walle et al., 2014). These observations confirm our data, that TNFAIP3 KO in *in vitro* cultured M1 and M2 macrophages from THP-1 or U937 cells as well as primary human monocytes have an increased expression of proinflammatory cytokines and chemokines. As TNFAIP3 knockout causes both, upregulation of M1 surface marker expression and downregulation of M2 markers, this could implicate a potential alternating effect in the tumor microenvironment that might inhibit tumor progression. Furthermore, we showed that IL-10 expression was diminished, which is known to play a crucial role in immune suppression but also suppression of all forms of inflammation. IL-10 is produced by different immune cell types, such as macrophages and is an essential anti-inflammatory factor. M2 macrophages produce much more IL-10 than M1 macrophages. IL-10 is further increasing the expression of IL-4R on the cell surface what makes macrophages more sensitive to IL-4 and IL-13. That again drives the macrophages more to the M2-like phenotype (Lang et al., 2002).

In line with this observation, we could further show that TNFAIP3 KO primary macrophages were able to stimulate T cells in coculture stronger than control macrophages. Not only increased T cell proliferation as well as IFN-γ expression was observed under M1 conditions but also under M2 tumor promoting conditions (IL-4) when TNFAIP3 was knocked out. To further investigate the role of TNFAIP3 in the TME experiments should be carried out in *in vivo* settings to analyze the effect of TNFAIP3s' KO on the macrophage phenotype, infiltration of immune cells and the tumor growth.

3.2.1.2 Therapeutical potential of targeting specifically TNFAIP3 de-ubiquitinase

There is conflicting evidence for the importance of the de-ubiquitination activity of TNFAIP3. On the one hand it was shown that mice with a bi-allelic knock-in (KI) of a C103A point mutation in the TNFAIP3 gene inducing a specific inactivation of the TNFAIP3 de-ubiquitinase activity did not show an inflammatory phenotype at all (De et al., 2014). They had normal proportions of B, T, DC and myeloid cells, responded normally to LPS and TNF and underwent normal NF-

kB activation. On the other hand, in a different mouse line TNFAIP3-C103A knockin caused an increased immune response. They showed increased immune cell populations, increased IL-6, and IL-1 production, and the mice developed colitis. However, the observed phenotype was much milder than the KO phenotype (Lu et al., 2013).

TNFAIP3's C103 based deubiquitinating enzyme (DUB) activity in the OTU (ovarian tumor) domain cleaves K48 and/or K63-linked ubiquitin chains from RIP1 and TRAF6. Furthermore, TNFAIP3 is thought to inhibit E2-E3 enzyme interactions with the C103 DUB motif and with this inhibits synthesis of ubiquitin chains (Shembade et al., 2010). The effect of TNFAIP3 KO in THP-1 cells was verified and cross validated in primary human monocytes, but the therapeutical potential of targeting specifically the TNFAIP3 de-ubiquitinase could not be confirmed in our hands. Jurkat cells harboring a bi-allelic KI of a point mutation C103A in the TNFAIP3 gene did not differ from cells with wild type TNFAIP3 in their response to TCR activation. This suggests that targeting the OTU domain by small molecules would not cause the therapeutically relevant inhibition of TNFAIP3's immunosuppressive function. It further implicates that a complete KO of the protein would be necessary to achieve a therapeutic effect. More research will be necessary to elucidate if there might be other options of targeting TNFAIP3. In a PROTAC approach (proteolysis targeting chimera) for instance highly specific TNFAIP3 binder would be coupled via a linker to an E3 ligase like a thalidomide analogue. Thereby, TNFAIP3 protein would be degraded via the proteasomal machinery (Winter et al., 2015).

Though in the course of this thesis we focused entirely on the function of TNFAIP3 on immune cell biology, there are data describing a role of TNFAIP3 in tumor cells. It has been described both, as a possible tumor suppressor in several subtypes of non-Hodgkin lymphomas (Honma et al., 2009) but also as an oncogene in glioblastoma (Guo et al., 2009; Hjelmeland et al., 2010). Here, TNFAIP3 is overexpressed in gliomas and KD of TNFAIP3 in these cells reduced proliferation and enhanced cell death. Also, the studies implicate that TNFAIP3 might be overexpressed in glioma stem cells (GSCs) on mRNA as well as on protein levels. Again, TNFAIP3 KD decreased GSCs growth, self-renewal and survival also in these cells. Furthermore, targeting TNFAIP3 further increases the survival of mice bearing human glioma xenografts. Using in silico analysis of glioma patient genomic database, Hjelmeland and colleagues further showed that overexpression of TNFAIP3 negatively correlates with patient survival. All in all, the finding of TNFAIP3's role as a tumor enhancer in glioma and tumor suppressor in lymphoma suggests that TNFAIP3's function in cancer may be tissue- and context-specific. This requires extensive investigation of possible anticancer therapies with TNFAIP3 inhibiting molecules, as these effects are likely to vary depending on the tumor. Also,

it should be taken into consideration that inhibiting TNFAIP3, as learned from studies with KO mice, can have fatal consequences on the immune homeostasis and induce autoimmunity. This is not only important in the context of TNFAIP3 but for all immunotherapies against cancer. The goal, for which further research is needed, is to prevent excessive inflammation and autoimmunity, which in addition to toxicity are possible side effects of anticancer immunotherapy, without attenuating the antitumor activity.

3.3 Conclusion and Outlook

Finding novel approaches for cancer therapy harnessing the immune system still holds great promises. The present study shows that new targets expressed in immune-suppressive TAMs can be identified, that might, when inhibited pharmacologically, potentially change the TME and lead to activation of the immune-system to attack the tumor. Using CRISPR/Cas9-based screening in a surrogate macrophage polarization model, about 170 genes were identified with a role in M2 macrophage polarization. Some were already known to be involved in immune-suppressive signaling pathways verifying the validity of the approach. More than half of the hits have never been described in this context. Thorough validation of first 20 hits has started, but more work needs to be done before starting a drug-development program. Mainly, the *in vitro* observed role in macrophage-polarization must be validated *in vivo*. Also, the translatability of this *in vitro* CRISPR/Cas9 screening approach as a technology to be done *in vivo* entirely might be very interesting and possibly yields to additional targets not to be found in the surrogate screening system.

Therefore, as next steps the identified genes will all be tested as potential drug targets for immunotherapy using the in this study established protocols and additionally in relevant mouse models. Furthermore, an *in vivo* screening approach is currently in development and a pilot screen using a small sgRNA library is planned to start in Q2/2020.

4 Material and methods

Further information about the materials and equipment used are listed in the supplementary S1 Materials.

4.1 Cell culture

4.1.1 *In vitro* culture of THP-1 and U937 cells

THP-1 (ATCC® TIB-202™) and U937 (ATCC® CRL-1593.2™) cells were cultured in RPMI 1640 GlutaMAX™ (Gibco) with 10 % heat inactivated Fetal Bovine Serum (FBS) (Sigma) and 1 % Penicillin-Streptomycin (Sigma). Additionally, 1 mM Sodium pyruvate (Gibco) and 0.055 mM beta mercapto-ethanol (Thermo) were added to the base medium of the THP-1 cells. The cells were cultured at 37 °C and 5 % CO_2. THP-1 and U937 cells were maintained in cell densities of $2x10^5$ – $1x10^6$ cells/ml.

4.1.2 Polarization and differentiation of THP-1 and U937 cells

THP-1 and U937 cells were seeded at concentration of $0.5x10^6$ cells/ml in cell culture plates and treated with 5 ng/ml PMA (Phorbol 12-myristate 13-acetate (Sigma)) for 48 h. Then, medium was refreshed with base medium. To obtain the M0 macrophage phenotype, 5 ng/ml PMA were added, 20 ng/ml IFN-γ (Sigma) and 20 ng/ml LPS (Sigma) added for M1 phenotype and for M2 phenotype cells were treated with 20 ng/ml IL4 (Sigma) for additionally 24 h.

4.1.3 Polarization and differentiation of primary human monocytes

Human peripheral blood CD14+ monocytes purchased from STEMCELL Technologies (70035) were polarized in RPMI 1640 GlutaMAX™ (Gibco) with 10 % heat inactivated FBS (Sigma) by adding 20 ng/ml GMCSF and 20 ng/ml MCSF for 7 days to obtain M0 macrophages. For differentiation and polarization to M1 macrophages the cells were treated with 20 ng/ml GMCSF for 6 days with 20 ng/ml IFN-γ (Sigma) and 20 ng/ml LPS (Sigma) for 24 h whereas M2 macrophages were generated with 20 ng/ml MCSF treatment for 6 days and additional 20 ng/ml IL4 (Sigma) treatment for 24 h.

4.1.4 *In vitro* culture of Jurkat cells

The Jurkat E6.1 (ATCC® TIB-152™) IL-2 promoter NLucP reporter cell line was generated by Axxam. To obtain the Jurkat IL-2 promoter NLucP reporter cell line the Jurkat E6.1 cells were stably transfected with the reporter vector pNL(NlucP/ Hygro) from Promega. The NanoLuc® luciferase (NLuc) has been stably introduced into the Jurkat cell's genome under the control of the IL-2 promoter. With the Nano-Glo® Luciferase Assay from Promega the NanoLuc® luciferase was detected.

The Jurkat cells were cultured in RPMI 1640 GlutaMAX™ (Gibco) with 10 % heat inactivated Fetal Bovine Serum (FBS) (Sigma), 1 % Penicillin-Streptomycin (Sigma) and 200 µg/ml hygromycin B (Invitrogen). The cells were cultured at 37 °C and 5 % CO_2. Jurkat cells were maintained in cell densities of $5x10^5$ – $2x10^6$ cells/ml.

4.1.5 Activation of Jurkat cells and primary T cells

Human Peripheral Blood Pan-T Cells from StemCELL Technologies (70024) were thawed in RPMI 1640 GlutaMAX™ (Gibco) and 10 % heat-inactivated FBS (Sigma). Primary T cells or Jurkat cells were stained with CellTrace™ CFSE Cell Proliferation Kit (Thermo) as described by the provider to monitor proliferation. Activation of the cells was achieved with anti-CD3/CD28 stimulation. 25 or 100 or 400 ng/ml anti-CD3 (BD Biosciences), 25 or 100 or 400 ng/ml anti-CD28 (BD Biosciences) and 100 or 400 or 1600 ng/ml Immunoglobulin G (IgG) (Thermo Fisher) were mixed before adding the mixture to the stained cells. The cells were cultured for 5 days until CFSE staining was monitored using FACS analysis. The supernatant was analyzed for IFN-γ secretion by ELISA.

4.1.6 Primary human monocytes and T cells obtained from STEMCELL Technologies

STEMCELL represents, warrants and covenants that STEMCELL provides only such human samples to Bayer

a) which have been collected in accordance with all laws, rules, regulations and guidelines applicable, including – without limitation – data protection legislations, such as the EU Data Protection Directive 95/46/EC and the Standards for Individually Identifiable Health Information (the "HIPPA Privacy Regulation") promulgated pursuant to the Health Insurance Portability and Accountability Act of 1996, ("Data Protection Legislation") all as updated from time to time,

b) which have been collected after all required approvals, including, without limitation, the approval by the competent Institutional Review Boards / Independent Ethics Committees were obtained and in compliance with all requirements of such bodies,

c) with respect to which the donors have been comprehensively informed and have provided their informed consent concerning

(1) the goals and purpose of the collection of the human samples, what kind of samples and data will be processed, and for which purpose they will be used, including, the performance of genetic analysis,

(2) the voluntariness of the donation of the human samples,

(3) the handling of the human samples,

(4) the transfer of the human samples, in – at least – coded form, to commercial/ pharmaceutical companies for the purpose of commercial pharmaceutical research and development,

(5) the donor's right to withdraw his/her consent at any time without consequence for his/her standard medical care and the consequences of such withdrawal.

d) with respect to which the donors have not withdrawn their informed consent.

4.2 Transduction of myeloid cells

4.2.1 Generation of THP-1 Cas9 clone

The Cas9 nuclease expression plasmid (Cellecta, SVC9-PS) (Figure 4.1), packaged into lenti-viral particles ($1x10^8$ TU/ml), was transduced into THP-1 parental cells. For this the cell concentration was adjusted to $1x10^6$ cells/ml and Hexadimethrine bromide (Polybrene) was added to the culture medium at a final concentration of 2 µg/ml. Virus was added with a multiplicity of infection (MOI) of 10 in a 96 well plate. After spinoculation for 90 min at 750 x g 150 µl fresh medium was added to each well to dilute the polybrene concentration. Three days post transduction the cells were washed to remove excess virus and medium was added containing hygromycin B (500 µg/ml) (Invitrogen) for selection. Clonal selection was conducted with single cell sorting using the BD FACSJazz™ cell sorter. Out of 360 single cells sorted, 12 clones grew out. The THP-1 Cas9 clone 8 showed high Cas9 expression and Cas9 activity (Figure 2.8) and was therefore selected as screening clone. The cells were maintained in medium supplemented with 200 µg/ml hygromycin B to ensure maintenance of the Cas9

expression vector. Cas9 expression was quantified by western blot analysis and Cas9 activity was assessed using the Cas9 activity test from Cellecta.

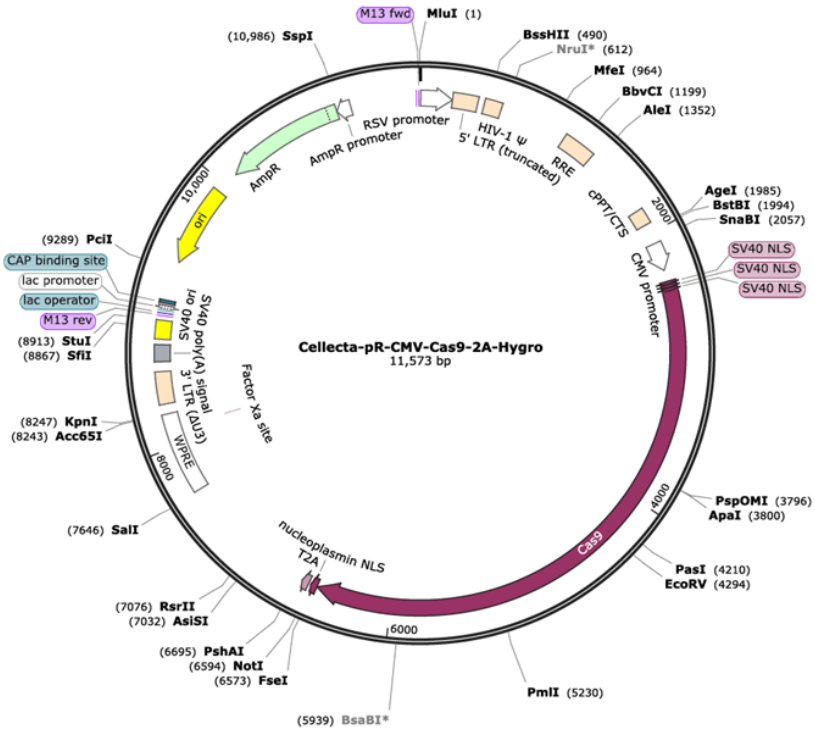

Figure 4.1. Vector map of the Cas9 nuclease expression vector

4.2.2 Cas9 activity test

Cellecta's CRISPRtest™ Functional Cas9 Activity Kit (CRISPRtest-GVO-CT) is used for measuring functional Cas9 activity in human cells. The assay is based on co-transduction of two lentiviral-packaged vectors with an sgRNA targeting the essential gene PCNA (Proliferating cell nuclear antigen), co-expressing GFP, and a non-targeting control gene co-expressing RFP in a specific limiting ratio. If there is Cas9 activity in the cell, cells transduced with the sgRNA targeting the essential gene will die and their GFP abundance will significantly reduce in comparison to the cell transduced with the RFP expressing non-toxic control sgRNA.

The manufacturer's protocol was followed and the FACS results were obtained with the BD FACSJazz™ and the software FlowJo™.

4.2.3 Determination of the optimal MOI for screening

In order to identify the optimal multiplicity of infection (MOI) to guarantee that in the screens only one sgRNA is transduced per cell, the MOI was determined.

Therefore, THP-1 Cas9 clone 8 cells were seeded into 12 well plates and different amounts of the whole genome library module 3 co-expressing RFP were added to achieve the following MOIs: 0, 0.1, 0.5, 1,5 and 10. Transduction was performed using the same conditions as described in chapter 4.2.1.

After incubation of three days and five times washing with 1x Phosphate buffered saline (PBS) the cells were FACS analyzed and RFP expression was determined.

4.2.4 Focused sgRNA library

The focused pooled lentiviral 2k sgRNA library is a custom library (CPLVSGL-P) obtained from Cellecta. 171 myeloid cell target genes are addressed each by 10 different sgRNAs. It also contains positive and negative control sgRNAs which sums up to 2000 sgRNA in the library. Cellecta's vector system was used to express the sgRNAs under a wild type U6 promoter. The human ubiquitin C promoter controls the expression of TagRFP and the puromycin resistance gene. The oligonucleotides which encode the sgRNA were designed by Cellecta based on the algorithm published by (Doench et al., 2016) and further optimized protocols by Cellecta in order to reduce target effects and exploit efficiency. The sgRNA expression cassettes are optimized for Illumina based NGS to detect the sgRNA inserted in the DNA in the desired cell.

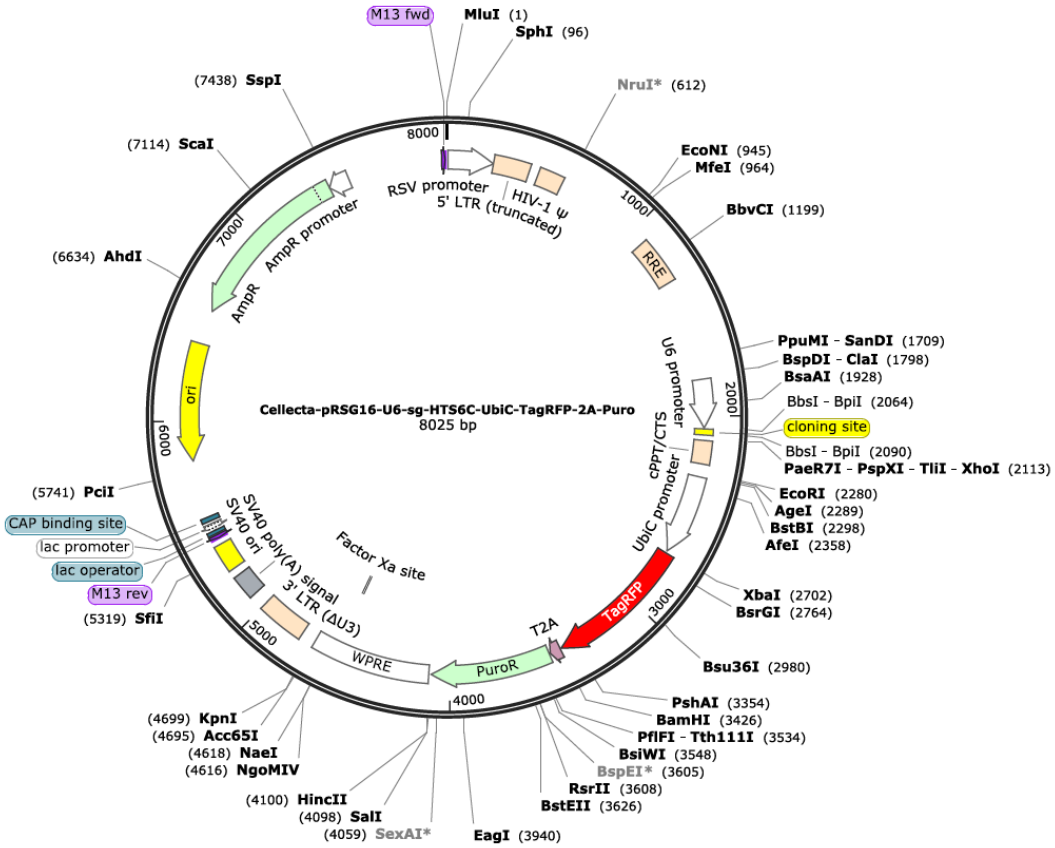

Figure 4.2. pRSG16-U6-sg-UbiC-TagRFP-2A-Puro vector system for sgRNAs library (Cellecta)
Vector system by Cellecta with HTS6 cassette for high-throughput sequencing UBIC (ubiquitin C) promoter controls puromycin and RFP co-expression who a linked by a T2A peptide. U6 promoter controls sgRNA expression.

4.2.5 Whole genome sgRNA library

The CRISPR Human Genome Knockout Library from Cellecta is designed in three modules (KOHGW-M1-V9, KOHGW-M2-V9, KOHGW-M3-V9) targeting each approximately 6,500 genes with 8 different sgRNAs per gene and the same negative and positive controls in total targeting up to 19,000 protein coding genes. The vector system is the same as described for the focused library and seen in Figure 4.2.

4.3 CD80 FACS staining for phenotypic sorting

4.3.1 Fluorescence staining

Differentiated and polarized THP-1 Cas9 clone 8 cells were detached using Accutase (STEMCELL Technologies) and the cells were washed once with 1x PBS. TruStain FcX™ (Fc Receptor Blocking Solution, Biolegend) was added to the samples as described by the provider. The cells were spun for 5 min at 400 g at 4 °C and then thoroughly resuspended in 1:50 diluted BV421 Mouse-Anti-Human CD80 antibody (BD Biosciences, Clone L307.4, 564160). The cells were stained for 1h at 4 °C in the dark and then washed three times with

1x PBS. To fix the cells, the Cytofix/Cytoperm™ solution (BD Biosciences) was used as recommended by the provider.

After washing the fixed cells two times with 1x PBS the pellet was resuspended in FACS buffer (filtered 1x PBS + 2 % FBS) and stored at 4 °C in the dark until sorting. The concentration of the cells was adjusted to 0.5 x10^6 cells/ml.

4.3.2 FACS sorting

The sorting was performed with the BD FACSJazz™ using the 100 µm nozzle. The sheet fluid was 1x PBS, pH 7.4 (flow cytometry grade – Thermo Fisher Scientific; A1286301). The two-tube holder was used as sorting device for the two-way sort in the 1.5 Drop Pure Sort Mode. The event rate while sorting was 5,000 – 8,000 events/sec.

To prevent clocking of the sorting system the cells were passed through a 30 µm large pre-separation filter (Miltenyi Biotec) just before sorting. The 15 ml collection tubes were precoated over night with 10 % FBS to minimize friction of the cell with the inside of the tube. One ml of FACS buffer was placed in the sorting tubes to prevent the cells of bursting when hitting the plastic surface.

The cells were gated on size, singularity and for RFP positivity. The lowest 10 % CD80 (BV421) expressing and 10 % highest CD80 expressing cells were gated and collected into the prepared collection tubes. While sorting the sample, the collected cells were cooled to 4 °C.

After sorting, the cells were re-analyzed by FACS assuring purity and cell yield. Therefore, the event rate was protocolled, as well as the PE/BV421 intensities. Also unsorted samples were collected as references. Analysis were performed with FlowJo V10.

4.4 Illumina library construction and sequencing

4.4.1 Genomic DNA Isolation of PFA-fixed cells

Genomic DNA isolation from PFA-fixed cells was performed with the GeneRead™ DNA FFPE Kit (Qiagen) according to manufacturer's instructions with some modifications. If the cell pellet contained more than 1x10^6 cells, double the amount of master mix was used. Accordingly, volumes used for subsequent steps including transferring the lysate to the elution columns had to be doubled.

The quality and concentration of the isolated DNA was measured with NanoDrop™ 8000 Spectrophotometer. Eluted DNA was stored at 4 °C until further analysis.

4.4.2 Two step PCR

With the two step PCR the sgRNA insert was amplified, Illumina adapters as well as indexing primers annealed, which are necessary for Illumina based sequencing. The primers are obtained from TIB Molbiol. Cellecta was providing the sequences. The primer P7-NFG16 was modified by reducing the primer's length. The P5-NFG16 primer was extended by 6 bases enabling the generation of distinguishable index primers. The index sequence was introduced directly after the Illumina P5 adapter sequence. Thus, no additional index primers were needed (supplementary S1 Materials).

4.4.2.1 1st PCR

To amplify the sgRNA of interest in the THP-1 Cas9 clone 8 screening cells, a PCR was performed with following conditions. One PCR reaction contained maximal 50 µg genomic DNA per 50 µl reaction mix. If more DNA had to be amplified, several PCR reactions were performed using up all the available DNA.

Table 4.1. 1st PCR components for amplification of genomic DNA

Component	Volume per reaction [µl]	Final concentration
Genomic DNA	XY	---
Deionized water	40 – XY	---
FwdU6-1 primer (10 µM)	1.5	0.6 µM
Rev-1 primer (10 µM)	1.5	0.6 µM
50x dNTP Mix (10 mM each)	1	1x
10x Titanium Taq Buffer	5	1x
50x Titanium Taq	1	1x
total	50	

Table 4.2. Thermocycler program for 1st PCR

Task	Temperature	Time	Cycle
Initialization	95 °C	2min	1x
Denaturing	95 °C	15s	x18
Primer annealing	63.5 °C	15s	
Elongation	72 °C	30s	
Final elongation	72 °C	1min	1x
Final hold	10 °C	end	∞

4.4.3 2nd PCR

The 1st PCR product was used in a 2nd PCR in which the Illumina adapters and specific index primers were annealed to the amplified sgRNA insert to enable Illumina based NGS. The PCR components and the Thermocycler program can be seen in Table 4.3 and Table 4.4.

Table 4.3. 2nd PCR components for amplification of genomic DNA and annealing of Illumina adapters and specific index primers

Component	Volume per reaction [µl]	Final concentration
1st PCR product	5	---
Deionized water	71	---
P7-NFG16 (10 µM)	5	1 µM
P5-NFG16-Ind (10 µM)	5	1 µM
50x dNTP Mix (10 mM each)	2	1x
10x Titanium Taq Buffer	10	1x
50x Titanium Taq	2	1x
total	100	

Table 4.4. Thermocycler program for 2nd PCR

Task	Temperature	Time	Cycle
Initialization	95 °C	2min	1x
Denaturing	95 °C	15s	x18
Primer annealing	62.5 °C	15s	
Elongation	72 °C	30s	
Final elongation	72 °C	1min	1x
Final hold	10 °C	end	∞

The size of 359 bp, quality and concentration of the 2nd PCR product were monitored by the Agilent 2100 bioanalyzer with the Agilent DNA 1000 Kit according to manufacturer's protocol.

4.4.4 DNA purification with magnetic beads

Purification of the PCR product before sequencing was performed with Agencourt AMPure XP (Beckman Coulter) magnetic beads. With this excess nucleotides, enzymes, salts, primers and other contaminants are removed for best quality PCR amplicons due to selectively binding of DNA fragments of 100 bp and larger to these magnetic beads. The PCR products were mixed with a ratio of 1:1 with the magnetic beads and after vortexing the mix was incubated for 15 min at room temperature. The mix was then transferred into 96 well round bottom plates and

placed onto a plate magnet. After incubation for 5 min the solution cleared and could be aspirated and discarded. 100 µl 80 % ethanol was added and discarded again after 30 seconds incubation time. This washing step was repeated twice and then the sample was dried for 15 min. The pellet was resuspended in 20 µl DNase-free water and thoroughly mixed. The plate was placed on the plate magnet and the eluent with the purified PCR amplicon transferred into a new DNase free tube, which was stored at 4 °C until sequencing.

4.4.5 DNA quantification with qPCR

The purified PCR products containing the Illumina libraries was quantified performing a quantitative polymerase chain reaction (qPCR) and using the PerfeCta NGS Library Quantification Kit – Illumina Low/ROX (Quantabio) according to manufacturer's instructions. The libraries were diluted 1:200,000 in Elution Buffer (Qiagen) with 0.1 % Tween20 (Sigma).

For sequencing, the libraries were diluted in Elution Buffer (Qiagen) with 0.1 % Tween20 (Sigma) to a 10 nM solution.

4.4.6 Illumina next generation sequencing of sgRNA insert

The sequencing was performed in Bayer's NGS laboratory.

The 10 nM libraries containing different index primers were pooled. Sequencing the samples of the focused screen, the MiSeq Reagent Kit v2 (Illumina) was used. The samples of the whole genome screen were sequenced using the HiSeq Rapid PE Cluster Kit v2 (Illumina).

For the sequencing with the MiSeq/*HiSeq* the library was diluted to 4 nM/*2 nM* with 10 mM Tris-Cl, ph-8.5 with 0.1 % Tween. Then the solution was mixed in a ratio of 1:1 with freshly diluted 0.2 N/*0.1 N* NaOH, vortexed and centrifuged for 1 min at 280 x g. After 5 min incubation, to allow the DNA (10 µl /*20 µl*) to denature, 990 µl/*980 µl* pre-chilled HT1 buffer (Illumina) was added to the tube. This resulted in a 20 pM denatured library in 1 mM NaOH. The libraries to be analyzed on the MiSeq were diluted to 10 pM with 300 µl of the 20 pM denatured DNA and 300 µl pre-chilled HT1 buffer. The libraries to be analyzed on the HiSeq were diluted to 10 pM with 210 µl of the 20 pM denatured DNA and 210 µl pre-chilled HT1 buffer. The PhiX Control v3 (Illumina) was prepared the same way and with the same concentrations as the DNA library of interest. The final concentration of the PhiX library for MiSeq was 12.5 pM and for HiSeq 12 pM. 60 µl of denatured 12.5 pM PhiX was spiked into 540 µl denatured 10 pM Library pool which results in 10 % of spiked in PhiX library for MiSeq. 4 µl of denatured 12 pM PhIX was

spiked into 416 µl denatured 10 pM Library pool, which resulted into 1 % spiked in PhiX library for HiSeq analysis.

10 % of the TruSeq HT library (Illumina) as well as 0.5 µM HP10 primer and 10 nM of the custom sequencing primer (Fseq-gRNA) was spiked in the denatured library.

Single-read dual indexing was performed on a paired-end flowcell on the HiSeq 2500 where only Read1 with the index i5 was used. The Q Scores for runs with the HiSeq were > 85 % and for MiSeq > 90 %. The cluster density in the HiSeq runs was 700-820 K/mm^2 and for the MiSeq runs 1000-1200 K/mm^2. 300-500 Mio reads were generated per HiSeq runs and 12-15 Mio reads per MiSeq run.

4.4.7 Analysis of NGS of sgRNA inserts

The aligning algorithm for obtaining the final raw sequencing reads was developed by our colleagues from the Bioinformatics Department. The sequencing reads were aligned to the custom library or whole genome library respectively which resulted in the information about the read count per sgRNA in each sample.

Finally, the read counts were normalized to the total number of read counts. The read counts of the CD80 low sorted sample were compared with the read counts from the CD80 high sorted sample and the fold change was calculated.

4.5 Performance of focused and whole genome CRISPR screen

The schematic workflow of the performed focused and whole genome screen can be seen in Figure 4.3.

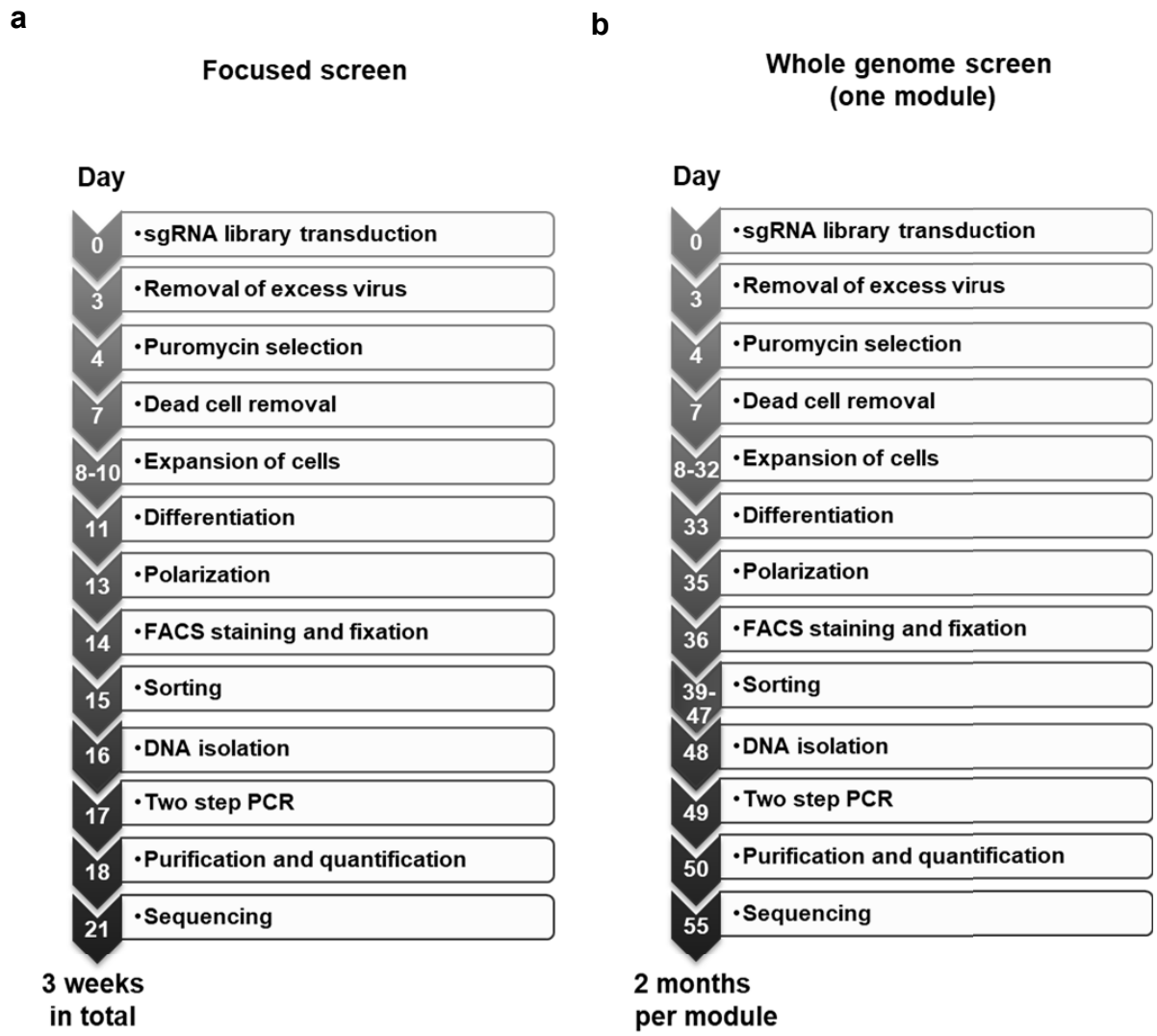

Figure 4.3. Workflow of performed focused and whole genome screen
Time lines for the performance of the pooled CRISPR screens in THP-1 Cas9 clone 8 cells is shown for the a) focused screen and for b) one module of the whole genome screen

THP-1 Cas9 clone 8 screening cells were transduced with an MOI of 1 (at least 500-fold representation of the sgRNAs required 8 x10^7 cells for the focused screen and 1.2 x10^8 cells for the whole genome screen) in 6 well plates with the focused sgRNA library and the whole genome sgRNA library which is divided into three modules. 2 µg/ml final polybrene were added to the cell culture plates. 1.2 x10^6 cells were used as control cells and were not transduced but treated with the same conditions as the transduced cells over the whole screening period. After adding the viral libraries to 2 x10^6 cells/ml/well, the plates were centrifuged for 1.5 h at 750 g. 3 ml of fresh medium was carefully added after centrifugation. Three days post transduction the cells were collected in falcons and washed five times to remove excess virus particles. Untransduced and transduced cells were analyzed with BD FACSJazz for their RFP expression of successfully transduced cells.

On day 4 post transduction the cells were resuspended in culture medium containing 2 µg/ml puromycin for selection and plated into T175 flasks. Three days post selection dead cells were removed by MACS microbeads with the dead cell removal kit from Miltenyi Biotec. After expansion, the cells were differentiated and polarized as described in 4.1.2. Therefore, the cell suspension was divided, one part for M1 polarization and the other for M2 polarization. Also, the untransduced cells were differentiated and polarized into M1 and M2 macrophages.

The cells were stained for CD80 and fixed as described in chapter 4.3.1 and sorted as outlined in chapter 4.3.2.

The sorted samples were further processed as described in chapter 4.4.

In Figure 4.4 the calculation of the required cell numbers for performing the whole genome screen with one module assuring the desired representation is shown.

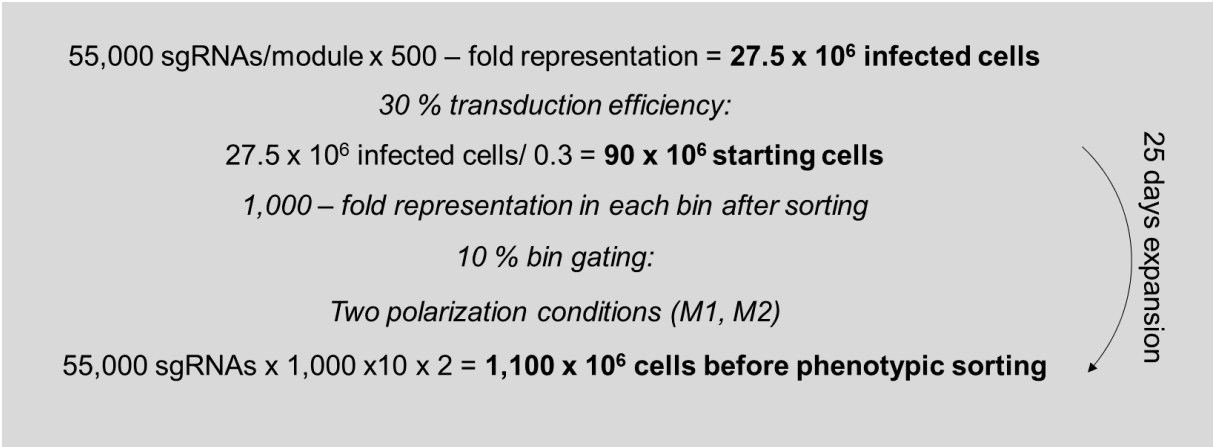

Figure 4.4. Calculation of cell numbers for one module of the whole genome CRISPR screen according to desired representation of library

4.6 Verification of screening hits

4.6.1 Electroporation of gRNA and RNPs

For validation of the top hits in THP-1, U937 cells and primary human monocytes gRNA (pre-complexed tracrRNA + crRNA) were used instead of viral sgRNAs. Therefore, cells were electroporated using the Amaxa 4D Nucleofector. Primary cells not expressing the Cas9 protein were electroporated with ribonucleoproteins (RNPs).

4.6.1.1 Hit verification in THP-1 Cas9 and U937 Cas9 cells

The synthetic tracrRNA was pre-complex with the crRNA of interest at a final concentration of 3 µM and incubated for 10 min at RT. The SG Cell Line 4D-Nucleofector™ X Kit L (Lonza) was used to electroporate $1x10^6$ cells per condition per crRNA. The procedure was carried out according to the protocol described by the manufacturer optimized for THP-1 cells. The pre-incubated 100 µl reaction mix of cells, nucleofector solution and gRNA were transferred into the Nucleocuvette™ and electroporated with the program FF-100 with the 4D-Nucleofector™ X unit. 400 µl prewarmed medium were added and the cells were incubated for 20 min at 37 °C. The cells were then transferred into 12-well plates. Four days post electroporation the cell concentration and viability were determined. The cells were differentiated and polarized to macrophages as described in chapter 4.1.2. mRNA analysis (chapter 4.6.2), cytokine expression analysis (chapter 4.6.3) and FACS analysis (chapter 4.3.1) were performed subsequently

4.6.1.2 Hit verification in primary monocytes

One day before electroporation, the human peripheral blood CD14+ monocytes purchased from STEMCELL Technologies (70035) were thawed in RPMI 1640 GlutaMAX™ (Gibco) with 10 % heat inactivated FBS (Sigma), supplemented with 20g/ml IL3, 50 ng/ml IL-6, 50 ng/ml SCF and 50 ng/ml TPO to boost cell proliferation and thereby increase electroporation efficiency.

The electroporation was conducted with the P3 Primary Cell 4D-Nucleofector™ X Kit S (Lonza) using the optimized protocol for primary monocytes by Lonza. The formation of the RNP complexes was conducted as followed: The synthetic tracrRNA was pre-complexed with the crRNA of interest at a final concentration of 3 µM and incubated for 10 min at RT. TrueCut Cas9 Protein (Thermo Fisher) was added to the gRNA at a final concentration of 1 µM and incubated for 20 min before it was mixed with the monocytes. The resulting 20 µl mix of cells and the RNPs were transferred into the Nucleocuvette™ and electroporated with the program EA100. 80 µl prewarmed medium were added and incubated for 20 min at 37 °C. After the incubation the cells were plated into 12-well plates for differentiation in culture medium containing 20 ng/ml MCSF or 20 ng/ml GMCSF according to the protocol described in 4.1.3.

4.6.2 mRNA expression analysis

4.6.2.1 RNA Isolation

Cells were lysed in 350 µl RLT buffer (Qiagen). RNA isolation was performed using the RNeasy® Mini Kit (Qiagen). The manufacturer's protocol was followed including one additional step of DNase I treatment with the Rnase-Free DNase Set (Qiagen) to get rid of genomic DNA. RNA quality and concentration were measured with the monochromator Tecan Infinite M1000 and the NanoQuant Plate and the RNA was stored at -80 °C until further processing.

4.6.2.2 cDNA synthesis

The reverse transcription of the isolated RNA was carried out with the Maxima First Strand cDNA Synthesis Kit for RT qPCR (Thermo Scientific). The manufacturer's instructions were followed performing 10 min incubation at 25 °C, followed by 30 min at 50 °C and 5 min at 85 °C. The resulting cDNA was stored at – 20 °C.

4.6.2.3 qRT PCR

To analyze gene expression a quantitative real-time polymerase chain reaction (qRT PCR) was performed. Therefore, the TaqMan Fast Universal PCR MasterMix (Applied Biosystems) and the ViiA™ 7 Real-Time PCR System (Applied Biosystems) were used to perform the amplification and the software Quantstudio ™ Real-Time PCR Software v1.1 for subsequent analysis. Following the manufacturer's instructions, the reactions were performed in MicroAmp Optical 384-Well reaction plates using technical triplicates. Data were analyzed by calculating the comparative ΔΔCt values. The used primer sequences can be found in the Supplements.

4.6.3 Cytokine expression analysis

The cell culture supernatant was collected and frozen at -20 °C until further processing. For detection of the cytokines of interest two methods were used – the ELISA BD OptEIA™ ELISA kits for detection of human IL-6, human IL-12p40, human IL-1β, human TNF, human IL-2 and human IFN-γ and the MSD ® 96 Well MULTI ARRAY ® and 7-SPOT ® Human Cytokine Assays (Mesoscale discovery) for the detection of proinflammatory cytokines: IL-6, IL-8, IL-10 IL-1β, IL-12p40, TNF and IFN-γ. Both assays were performed as recommended by the provider.

4.6.4 Western blotting

Radioimmunoprecipitation assay (RIPA) buffer (Millipore) supplemented with freshly added 1 × Halt™ Protease & Phosphatase Inhibitor Cocktail (Thermo Scientific) was used for cell lysis. Protein quantification was conducted with the Pierce™ BCA Protein Assay Kit (Thermo Fisher Scientific). The manufacturer's instructions were followed.

30 µg protein lysates per sample were loaded onto protein gels from NuPAGE™ (Novex™ 10 % Bis-Tris Protein Gels, 1.0 mm, 10 well).

NuPAGE LDS Sample Buffer (Life technologies) and NuPAGE Sample Reducing Agent (Life technologies) were used to adjust the sample to the final volume and concentration. The samples were denatured at 70 °C for 10 min and immediately kept on ice before loading. 5 µl of the marker (Chameleon Due Pre-Stained Protein Ladder, Licor) samples were loaded. NuPAGE® MOPS SDS Running Buffer (Invitrogen) was used. Blotting was performed with the iBlot® 2 Transfer Stacks, nitrocellulose, regular size (Novex by life technologies) with the iBlot® 2 gel transfer device using a dry blotting system. The preinstalled program 0 was used for the transfer: 20 V for 1 min, 23 V for 4 min and 25 V for 2 min. The membranes were then washed once with 1 × TBST (10 × Cell Signaling) and incubated in 5 % nonfat dried milk powder (AppliChem) dissolved in 1 × TBST for 1 h at room temperature while gently shaking. After blocking, the membranes were incubated with primary antibody diluted in 1 % milk overnight. The next morning the membranes were washed thrice with 1 × TBST for 5 min each while rocking. The housekeeping control antibody (GAPDH or HSP90) was incubated for 30 min at room temperature and the washing steps were repeated. The membranes were incubated with the fluorescence-labelled secondary antibody for 1 h. Again, the membranes were washed thrice with 1 × TBST. The detection of the fluorescence was conducted with the Odyssey Sa Infrared Imaging System (LI-COR). The used antibodies and their dilutions are shown in the chapter supplementary S1 Materials.

4.6.5 Coculture of macrophages with T cells

The primary monocytes were cultured as described in chapter 4.1.3. After polarization, the cells were washed once with 1 x PBS. Human Peripheral Blood Pan-T Cells from StemCELL Technologies (70024) were stained with CellTrace™ CFSE Cell Proliferation Kit (Thermo) as described by the provider to monitor proliferation. Activation of the T cells was achieved with anti-CD3/CD28 stimulation. 100 ng/ml anti-CD3 (BD Biosciences), 100 ng/ml anti-CD28 (BD Biosciences) and 400 ng/ml IgG (Thermo Fisher) were pre-incubated and added to the stained T cells. The T cells were plated on top of the polarized macrophages, spun down for 1 min at

200 x g and cocultured for five days until CFSE staining was monitored using FACS analysis and supernatant analyzed for IFN-γ secretion.

4.6.6 Generation of KO and KI cell lines

The TNFAIP3 KO or KI THP-1 and Jurkat cells were generated by Horizon Discovery. The genotypes of the clones are shown in Table 2.2.

KO cell lines

The THP-1 and Jurkat cells were transfected with the Cas9 nuclease and the gRNA targeting TNFAIP3. To generate clonal cell cultures, transfected cells were plated at 1 cell/384 well, and these taken forward for screening to identify those with insertions or deletions in at least one allele of the gene of interest. PCR and Sanger sequencing of selected clones was performed to identify KO clones.

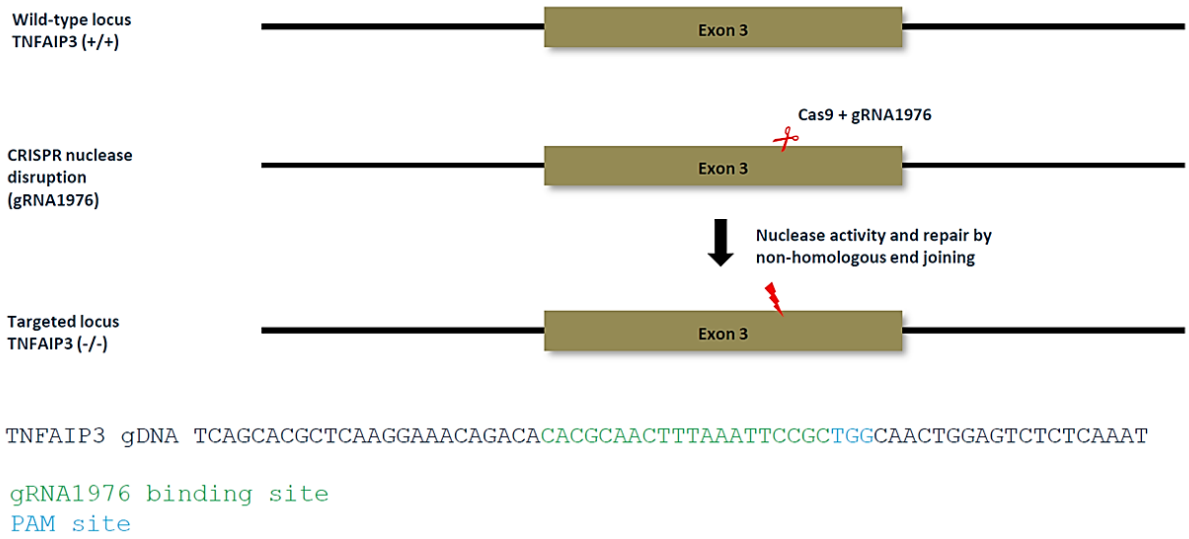

Figure 4.5 Vector design for TNFAIP3 KO generation in THP-1 and Jurkat cells
gRNA1976 binds to the complement of the green site in the sequence. Blue indicates the PAM site which is also required for cutting activity. The mechanism of repair of double strand breaks will result in insertions or deletions at the gRNA cut site. If such indels cause a frame shift, this will likely result in an early STOP codon and loss of expression at the protein level; (provided by Horizon Discovery)

Table 4.5 Genotype summary of KO THP-1 and Jurkat clones

Clone Name	Genotype	Allele	gDNA modification	Predicted impact on protein
THP-1 KO clone #1	TNFAIP3 (-/-/-)	1	19 bp deletion	Early STOP codon at position 209
		2	20 bp deletion	Early STOP codon at position 147
		3	159 bp deletion	Splicing of exon 3 Early STOP codon at position 102
THP-1 KO clone #2	TNFAIP3 (-/-/-)	1 and 2	19 bp deletion	Early STOP codon at position 209
		3	284 bp deletion	Splicing of exon 3 Early STOP codon at position 102
Jurkat KO clone	TNFAIP3 (+/-/-/-)	1	Wild type	Wild type protein
		2 and 3	6 bp deletion plus 7 bp insertion	Early STOP codon at position 154
		4	1 bp deletion plus 8 bp insertion	Early STOP codon at position 156

KI cell lines

The THP-1 and Jurkat cells were transfected with the Cas9 nuclease and the gRNA targeting TNFAIP3 as well as the plasmid donor.

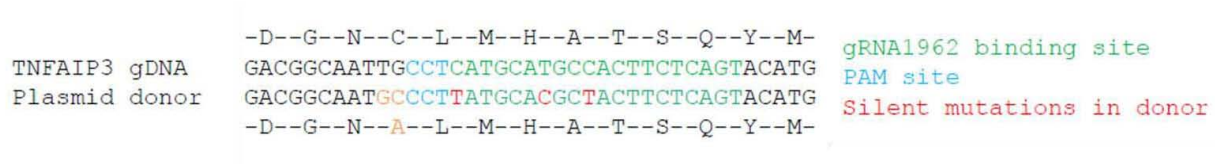

The detailed description of this procedure and the vector design for TNFAIP3 (C103A) KI point mutation in THP-1 and Jurkat cells is shown in Figure 2.37.

To generate clonal cell cultures, transfected cells were plated at 1 cell/384 well, and these taken forward for screening. PCR and Sanger sequencing of selected clones was performed to identify KI clones. The genotype of the obtained clones is depicted in Table 2.2.

4.6.7 RNA Sequencing

Parental THP-1 cells and homozygous TNFAIP3 KO THP-1 cells were differentiated and polarized as described in chapter 4.1.2.

Wild type primary human monocytes and TNFAIP3 KO primary human monocytes were differentiated and polarized as described in chapter 4.1.3.

TNFAIP3 KO Jurkat cells and TNFAIP3 KI (clone 1 and clone 2) Jurkat cells were stimulated with 25 ng/ml anti-CD3/CD28 or 400 ng/ml anti-CD3/CD28 for 3 h or 24 h.

Total RNA of each sample was extracted using the RNeasy® Mini Kit (Qiagen). Manufacturer's instructions were followed including one additional step of DNase I treatment with the RNase-Free DNase Set (Qiagen) to eliminate genomic DNA. 400 ng in 50 µl were used for subsequent library generation and sequencing.

The TruSeq RNA Sample Preparation Kit v2 (Illumina) was used to generate libraries for RNA sequencing. The library synthesis was conducted by Martina Runge from the Bayer NGS laboratory.

In summary, using oligo-dT attached magnetic beads the polyA containing mRNA molecules were purified, the RNA fragmented and primed for cDNA synthesis. The first strand synthesis with the reverse transcriptase and random primers was followed by the second strand cDNA synthesis with the DNA Polymerase I and RNase H. This results in blunt-ended cDNA. Adenylation of the 3' ends prior to indexing adapter ligation prevents these fragments from ligation to one another. In the last step of library preparation, the DNA fragments are enriched by selective PCR of fragments with adapter molecules on both ends.

The quality of the generated libraries was accessed with the Agilent DNA 1000 Chip Kit and DNA quantity was determined using PerfeCta NGS Library Quantification Kit – Illumina Low/ROX (Quanta Bioscience) as provided by the manufacturer. The libraries were pooled and the final concentration adjusted to 10 nM using Tris-Cl 10 mM, pH 8.5 with 0.1 % Tween 20. The average fragment size of 396 bp was used for calculation. Sequencing was performed according to standard protocols for the Illumina HiSeq® 2500. The pooled library was denatured with 0.1 M NaOH and diluted to 20 pM with pre-chilled HT1 buffer using the HiSeq SBS Reagent Kit v4 for cBot Clustering. The same was performed for the PhiX library (1 %). The sample library was mixed with a PhiX Library and applied to a HiSeq v4 flow cell (Illumina) which was subsequently clustered on a cBot (Illumina) using the HiSeq v4 PE cluster Kit (Illumina). Then all samples were sequenced in the HiSeq® 2500 system.

Mapping of reads and data analysis was performed by Dr. Helge Roider from the Bayer Bioinformatics department. Reads were mapped to human genome version hg38 with corresponding gencode version 28 gene annotations using the STAR aligner (version 2.4.2). Expression was subsequently quantified as transcripts per million (TPMs) using the RSEM algorithm (version 1.3.0). Statistical analysis was performed with the R statistical programming environment version 3.1.2. Fold changes and Benjamini-Hochberg corrected t-test p-values between samples and treatment conditions were calculated on TPM values. Gene and sample

clustering were performed via average based hierarchical clustering using distance metric Pearson correlation distances computed on TPM values.

4.7 Statistical analysis

The mean values, standard deviation (SD) values, standard error of the mean (SEM) values, log_2 fold change, and p-values were calculated and plotted with the GraphPad Prism 8 software. Two-tailed unpaired and paired t-test was performed to determine statistical significance between two groups or samples. P-Values < 0.05 were respected significantly different and are depicted in stars (* $p \leq 0.05$, ** $p \leq 0.01$, *** $p \leq 0.001$, **** $p \leq 0.0001$). Data is displayed as mean ± SEM or mean ± SD. Error bars in graphs represent SEM or SD.

5 References

Bao, Y. S., Ji, Y., Zhao, S. L., Ma, L. L., Xie, R. J., & Na, S. P. (2013). Serum levels and activity of indoleamine2,3-dioxygenase and tryptophanyl-tRNA synthetase and their association with disease severity in patients with chronic kidney disease. *Biomarkers, 18*(5), 379-385. doi: 10.3109/1354750X.2013.790074

Beatty, G. L., Torigian, D. A., Chiorean, E. G., Saboury, B., Brothers, A., Alavi, A., Troxel, A. B., Sun, W., Teitelbaum, U. R., Vonderheide, R. H., & O'Dwyer, P. J. (2013). A phase I study of an agonist CD40 monoclonal antibody (CP-870,893) in combination with gemcitabine in patients with advanced pancreatic ductal adenocarcinoma. *Clin Cancer Res, 19*(22), 6286-6295. doi: 10.1158/1078-0432.CCR-13-1320

Belgiovine, C., D'Incalci, M., Allavena, P., & Frapolli, R. (2016). Tumor-associated macrophages and anti-tumor therapies: complex links. *Cell Mol Life Sci, 73*(13), 2411-2424. doi: 10.1007/s00018-016-2166-5

Belkina, A. C., Nikolajczyk, B. S., & Denis, G. V. (2013). BET protein function is required for inflammation: Brd2 genetic disruption and BET inhibitor JQ1 impair mouse macrophage inflammatory responses. *J Immunol, 190*(7), 3670-3678. doi: 10.4049/jimmunol.1202838

Bingle, L., Brown, N. J., & Lewis, C. E. (2002). The role of tumour-associated macrophages in tumour progression: implications for new anticancer therapies. *J Pathol, 196*(3), 254-265. doi: 10.1002/path.1027

Bonapace, L., Coissieux, M. M., Wyckoff, J., Mertz, K. D., Varga, Z., Junt, T., & Bentires-Alj, M. (2014). Cessation of CCL2 inhibition accelerates breast cancer metastasis by promoting angiogenesis. *Nature, 515*(7525), 130-133. doi: 10.1038/nature13862

Burnet, M. (1957). Cancer; a biological approach. I. The processes of control. *Br Med J, 1*(5022), 779-786. doi: 10.1136/bmj.1.5022.779

Cao, X. (2016). Self-regulation and cross-regulation of pattern-recognition receptor signalling in health and disease. *Nat Rev Immunol, 16*(1), 35-50. doi: 10.1038/nri.2015.8

Caras, I., Tucureanu, C., Lerescu, L., Pitica, R., Melinceanu, L., Neagu, S., & Salageanu, A. (2011). Influence of tumor cell culture supernatants on macrophage functional polarization: in vitro models of macrophage-tumor environment interaction. *Tumori, 97*(5), 647-654. doi: 10.1700/989.10726

Chanput, W., Mes, J. J., & Wichers, H. J. (2014). THP-1 cell line: an in vitro cell model for immune modulation approach. *Int Immunopharmacol, 23*(1), 37-45. doi: 10.1016/j.intimp.2014.08.002

Chen, D. S., & Mellman, I. (2017). Elements of cancer immunity and the cancer-immune set point. *Nature, 541*(7637), 321-330. doi: 10.1038/nature21349

Chen, X., Barozzi, I., Termanini, A., Prosperini, E., Recchiuti, A., Dalli, J., Mietton, F., Matteoli, G., Hiebert, S., & Natoli, G. (2012). Requirement for the histone deacetylase Hdac3 for the inflammatory gene expression program in macrophages. *Proc Natl Acad Sci U S A, 109*(42), E2865-2874. doi: 10.1073/pnas.1121131109

Chen, Y., Song, Y., Du, W., Gong, L., Chang, H., & Zou, Z. (2019). Tumor-associated macrophages: an accomplice in solid tumor progression. *J Biomed Sci, 26*(1), 78. doi: 10.1186/s12929-019-0568-z

Cheng, W. C., & Ho, P. C. (2019). Firing Up Cold Tumors. *Trends Cancer, 5*(9), 528-530. doi: 10.1016/j.trecan.2019.06.005

Chu, Y., Vahl, J. C., Kumar, D., Heger, K., Bertossi, A., Wojtowicz, E., Soberon, V., Schenten, D., Mack, B., Reutelshofer, M., Beyaert, R., Amann, K., van Loo, G., & Schmidt-Supprian, M. (2011). B cells lacking the tumor suppressor TNFAIP3/A20 display impaired differentiation and hyperactivation and cause inflammation and autoimmunity in aged mice. *Blood, 117*(7), 2227-2236. doi: 10.1182/blood-2010-09-306019

Crowther, M. D., Dolton, G., Legut, M., Caillaud, M. E., Lloyd, A., Attaf, M., Galloway, S. A. E., Rius, C., Farrell, C. P., Szomolay, B., Ager, A., Parker, A. L., Fuller, A., Donia, M., McCluskey, J., Rossjohn, J., Svane, I. M., Phillips, J. D., & Sewell, A. K. (2020).

Genome-wide CRISPR-Cas9 screening reveals ubiquitous T cell cancer targeting via the monomorphic MHC class I-related protein MR1. *Nat Immunol, 21*(2), 178-185. doi: 10.1038/s41590-019-0578-8

Daigneault, M., Preston, J. A., Marriott, H. M., Whyte, M. K., & Dockrell, D. H. (2010). The identification of markers of macrophage differentiation in PMA-stimulated THP-1 cells and monocyte-derived macrophages. *PLoS One, 5*(1), e8668. doi: 10.1371/journal.pone.0008668

Dang, C. V., Reddy, E. P., Shokat, K. M., & Soucek, L. (2017). Drugging the 'undruggable' cancer targets. *Nat Rev Cancer, 17*(8), 502-508. doi: 10.1038/nrc.2017.36

Das, T., Chen, Z., Hendriks, R. W., & Kool, M. (2018). A20/Tumor Necrosis Factor alpha-Induced Protein 3 in Immune Cells Controls Development of Autoinflammation and Autoimmunity: Lessons from Mouse Models. *Front Immunol, 9*, 104. doi: 10.3389/fimmu.2018.00104

Davis, H. E., Morgan, J. R., & Yarmush, M. L. (2002). Polybrene increases retrovirus gene transfer efficiency by enhancing receptor-independent virus adsorption on target cell membranes. *Biophys Chem, 97*(2-3), 159-172. doi: 10.1016/s0301-4622(02)00057-1

De, A., Dainichi, T., Rathinam, C. V., & Ghosh, S. (2014). The deubiquitinase activity of A20 is dispensable for NF-kappaB signaling. *EMBO Rep, 15*(7), 775-783. doi: 10.15252/embr.201338305

De Wilde, K., Martens, A., Lambrecht, S., Jacques, P., Drennan, M. B., Debusschere, K., Govindarajan, S., Coudenys, J., Verheugen, E., Windels, F., Catrysse, L., Lories, R., McGonagle, D., Beyaert, R., van Loo, G., & Elewaut, D. (2017). A20 inhibition of STAT1 expression in myeloid cells: a novel endogenous regulatory mechanism preventing development of enthesitis. *Ann Rheum Dis, 76*(3), 585-592. doi: 10.1136/annrheumdis-2016-209454

Deltcheva, E., Chylinski, K., Sharma, C. M., Gonzales, K., Chao, Y., Pirzada, Z. A., Eckert, M. R., Vogel, J., & Charpentier, E. (2011). CRISPR RNA maturation by trans-encoded small RNA and host factor RNase III. *Nature, 471*(7340), 602-607. doi: 10.1038/nature09886

Doench, J. G. (2018). Am I ready for CRISPR? A user's guide to genetic screens. *Nat Rev Genet, 19*(2), 67-80. doi: 10.1038/nrg.2017.97

Doench, J. G., Fusi, N., Sullender, M., Hegde, M., Vaimberg, E. W., Donovan, K. F., Smith, I., Tothova, Z., Wilen, C., Orchard, R., Virgin, H. W., Listgarten, J., & Root, D. E. (2016). Optimized sgRNA design to maximize activity and minimize off-target effects of CRISPR-Cas9. *Nat Biotechnol, 34*(2), 184-191. doi: 10.1038/nbt.3437

Doench, J. G., Hartenian, E., Graham, D. B., Tothova, Z., Hegde, M., Smith, I., Sullender, M., Ebert, B. L., Xavier, R. J., & Root, D. E. (2014). Rational design of highly active sgRNAs for CRISPR-Cas9-mediated gene inactivation. *Nat Biotechnol, 32*(12), 1262-1267. doi: 10.1038/nbt.3026

Dunn, G. P., Bruce, A. T., Ikeda, H., Old, L. J., & Schreiber, R. D. (2002). Cancer immunoediting: from immunosurveillance to tumor escape. *Nat Immunol, 3*(11), 991-998. doi: 10.1038/ni1102-991

Duwel, M., Welteke, V., Oeckinghaus, A., Baens, M., Kloo, B., Ferch, U., Darnay, B. G., Ruland, J., Marynen, P., & Krappmann, D. (2009). A20 negatively regulates T cell receptor signaling to NF-kappaB by cleaving Malt1 ubiquitin chains. *J Immunol, 182*(12), 7718-7728. doi: 10.4049/jimmunol.0803313

Engblom, C., Pfirschke, C., & Pittet, M. J. (2016). The role of myeloid cells in cancer therapies. *Nat Rev Cancer, 16*(7), 447-462. doi: 10.1038/nrc.2016.54

Evans, C. A., Liu, T., Lescarbeau, A., Nair, S. J., Grenier, L., Pradeilles, J. A., Glenadel, Q., Tibbitts, T., Rowley, A. M., DiNitto, J. P., Brophy, E. E., O'Hearn, E. L., Ali, J. A., Winkler, D. G., Goldstein, S. I., O'Hearn, P., Martin, C. M., Hoyt, J. G., Soglia, J. R., Cheung, C., Pink, M. M., Proctor, J. L., Palombella, V. J., Tremblay, M. R., & Castro, A. C. (2016). Discovery of a Selective Phosphoinositide-3-Kinase (PI3K)-gamma Inhibitor (IPI-549) as an Immuno-Oncology Clinical Candidate. *ACS Med Chem Lett, 7*(9), 862-867. doi: 10.1021/acsmedchemlett.6b00238

Fiskus, W., Sharma, S., Shah, B., Portier, B. P., Devaraj, S. G., Liu, K., Iyer, S. P., Bearss, D., & Bhalla, K. N. (2014). Highly effective combination of LSD1 (KDM1A) antagonist and pan-histone deacetylase inhibitor against human AML cells. *Leukemia, 28*(11), 2155-2164. doi: 10.1038/leu.2014.119

Fullard, N., Wilson, C. L., & Oakley, F. (2012). Roles of c-Rel signalling in inflammation and disease. *Int J Biochem Cell Biol, 44*(6), 851-860. doi: 10.1016/j.biocel.2012.02.017

Gabrilovich, D. I., Ostrand-Rosenberg, S., & Bronte, V. (2012). Coordinated regulation of myeloid cells by tumours. *Nat Rev Immunol, 12*(4), 253-268. doi: 10.1038/nri3175

Genin, M., Clement, F., Fattaccioli, A., Raes, M., & Michiels, C. (2015). M1 and M2 macrophages derived from THP-1 cells differentially modulate the response of cancer cells to etoposide. *BMC Cancer, 15*, 577. doi: 10.1186/s12885-015-1546-9

Germano, G., Frapolli, R., Belgiovine, C., Anselmo, A., Pesce, S., Liguori, M., Erba, E., Uboldi, S., Zucchetti, M., Pasqualini, F., Nebuloni, M., van Rooijen, N., Mortarini, R., Beltrame, L., Marchini, S., Fuso Nerini, I., Sanfilippo, R., Casali, P. G., Pilotti, S., Galmarini, C. M., Anichini, A., Mantovani, A., D'Incalci, M., & Allavena, P. (2013). Role of macrophage targeting in the antitumor activity of trabectedin. *Cancer Cell, 23*(2), 249-262. doi: 10.1016/j.ccr.2013.01.008

Gilbert, L. A., Horlbeck, M. A., Adamson, B., Villalta, J. E., Chen, Y., Whitehead, E. H., Guimaraes, C., Panning, B., Ploegh, H. L., Bassik, M. C., Qi, L. S., Kampmann, M., & Weissman, J. S. (2014). Genome-Scale CRISPR-Mediated Control of Gene Repression and Activation. *Cell, 159*(3), 647-661. doi: 10.1016/j.cell.2014.09.029

Gilbert, L. A., Larson, M. H., Morsut, L., Liu, Z., Brar, G. A., Torres, S. E., Stern-Ginossar, N., Brandman, O., Whitehead, E. H., Doudna, J. A., Lim, W. A., Weissman, J. S., & Qi, L. S. (2013). CRISPR-mediated modular RNA-guided regulation of transcription in eukaryotes. *Cell, 154*(2), 442-451. doi: 10.1016/j.cell.2013.06.044

Ginhoux, F., & Guilliams, M. (2016). Tissue-Resident Macrophage Ontogeny and Homeostasis. *Immunity, 44*(3), 439-449. doi: 10.1016/j.immuni.2016.02.024

Giordano, M., Roncagalli, R., Bourdely, P., Chasson, L., Buferne, M., Yamasaki, S., Beyaert, R., van Loo, G., Auphan-Anezin, N., Schmitt-Verhulst, A. M., & Verdeil, G. (2014). The tumor necrosis factor alpha-induced protein 3 (TNFAIP3, A20) imposes a brake on antitumor activity of CD8 T cells. *Proc Natl Acad Sci U S A, 111*(30), 11115-11120. doi: 10.1073/pnas.1406259111

Gomez Perdiguero, E., Klapproth, K., Schulz, C., Busch, K., Azzoni, E., Crozet, L., Garner, H., Trouillet, C., de Bruijn, M. F., Geissmann, F., & Rodewald, H. R. (2015). Tissue-resident macrophages originate from yolk-sac-derived erythro-myeloid progenitors. *Nature, 518*(7540), 547-551. doi: 10.1038/nature13989

Gordon, S., & Taylor, P. R. (2005). Monocyte and macrophage heterogeneity. *Nat Rev Immunol, 5*(12), 953-964. doi: 10.1038/nri1733

Guerriero, J. L. (2018). Macrophages: The Road Less Traveled, Changing Anticancer Therapy. *Trends Mol Med, 24*(5), 472-489. doi: 10.1016/j.molmed.2018.03.006

Guerriero, J. L., Ditsworth, D., Catanzaro, J. M., Sabino, G., Furie, M. B., Kew, R. R., Crawford, H. C., & Zong, W. X. (2011). DNA alkylating therapy induces tumor regression through an HMGB1-mediated activation of innate immunity. *J Immunol, 186*(6), 3517-3526. doi: 10.4049/jimmunol.1003267

Guerriero, J. L., Sotayo, A., Ponichtera, H. E., Castrillon, J. A., Pourzia, A. L., Schad, S., Johnson, S. F., Carrasco, R. D., Lazo, S., Bronson, R. T., Davis, S. P., Lobera, M., Nolan, M. A., & Letai, A. (2017). Class IIa HDAC inhibition reduces breast tumours and metastases through anti-tumour macrophages. *Nature, 543*(7645), 428-432. doi: 10.1038/nature21409

Gul, N., Babes, L., Siegmund, K., Korthouwer, R., Bogels, M., Braster, R., Vidarsson, G., ten Hagen, T. L., Kubes, P., & van Egmond, M. (2014). Macrophages eliminate circulating tumor cells after monoclonal antibody therapy. *J Clin Invest, 124*(2), 812-823. doi: 10.1172/JCI66776

Guo, Q., Dong, H., Liu, X., Wang, C., Liu, N., Zhang, J., Li, B., Cao, W., Ding, T., Yang, Z., & Zhang, X. (2009). A20 is overexpressed in glioma cells and may serve as a potential

therapeutic target. *Expert Opin Ther Targets, 13*(7), 733-741. doi: 10.1517/14728220903045018

Hjelmeland, A. B., Wu, Q., Wickman, S., Eyler, C., Heddleston, J., Shi, Q., Lathia, J. D., Macswords, J., Lee, J., McLendon, R. E., & Rich, J. N. (2010). Targeting A20 decreases glioma stem cell survival and tumor growth. *PLoS Biol, 8*(2), e1000319. doi: 10.1371/journal.pbio.1000319

Honma, K., Tsuzuki, S., Nakagawa, M., Tagawa, H., Nakamura, S., Morishima, Y., & Seto, M. (2009). TNFAIP3/A20 functions as a novel tumor suppressor gene in several subtypes of non-Hodgkin lymphomas. *Blood, 114*(12), 2467-2475. doi: 10.1182/blood-2008-12-194852

Hovelmeyer, N., Reissig, S., Xuan, N. T., Adams-Quack, P., Lukas, D., Nikolaev, A., Schluter, D., & Waisman, A. (2011). A20 deficiency in B cells enhances B-cell proliferation and results in the development of autoantibodies. *Eur J Immunol, 41*(3), 595-601. doi: 10.1002/eji.201041313

Hume, D. A. (2006). The mononuclear phagocyte system. *Curr Opin Immunol, 18*(1), 49-53. doi: 10.1016/j.coi.2005.11.008

Hwang, S. Y., Hwang, J. S., Kim, S. Y., & Han, I. O. (2013). O-GlcNAc transferase inhibits LPS-mediated expression of inducible nitric oxide synthase through an increased interaction with mSin3A in RAW264.7 cells. *Am J Physiol Cell Physiol, 305*(6), C601-608. doi: 10.1152/ajpcell.00042.2013

Ino, Y., Yamazaki-Itoh, R., Shimada, K., Iwasaki, M., Kosuge, T., Kanai, Y., & Hiraoka, N. (2013). Immune cell infiltration as an indicator of the immune microenvironment of pancreatic cancer. *Br J Cancer, 108*(4), 914-923. doi: 10.1038/bjc.2013.32

Iwasaki, A., & Medzhitov, R. (2015). Control of adaptive immunity by the innate immune system. *Nat Immunol, 16*(4), 343-353. doi: 10.1038/ni.3123

Jahchan, N. S., Mujal, A. M., Pollack, J. L., Binnewies, M., Sriram, V., Reyno, L., & Krummel, M. F. (2019). Tuning the Tumor Myeloid Microenvironment to Fight Cancer. *Front Immunol, 10*, 1611. doi: 10.3389/fimmu.2019.01611

Janzer, A., Lim, S., Fronhoffs, F., Niazy, N., Buettner, R., & Kirfel, J. (2012). Lysine-specific demethylase 1 (LSD1) and histone deacetylase 1 (HDAC1) synergistically repress proinflammatory cytokines and classical complement pathway components. *Biochem Biophys Res Commun, 421*(4), 665-670. doi: 10.1016/j.bbrc.2012.04.057

Jinek, M., Chylinski, K., Fonfara, I., Hauer, M., Doudna, J. A., & Charpentier, E. (2012). A programmable dual-RNA-guided DNA endonuclease in adaptive bacterial immunity. *Science, 337*(6096), 816-821. doi: 10.1126/science.1225829

Jost, M., Chen, Y., Gilbert, L. A., Horlbeck, M. A., Krenning, L., Menchon, G., Rai, A., Cho, M. Y., Stern, J. J., Prota, A. E., Kampmann, M., Akhmanova, A., Steinmetz, M. O., Tanenbaum, M. E., & Weissman, J. S. (2017). Combined CRISPRi/a-Based Chemical Genetic Screens Reveal that Rigosertib Is a Microtubule-Destabilizing Agent. *Mol Cell, 68*(1), 210-223 e216. doi: 10.1016/j.molcel.2017.09.012

Joung, J., Konermann, S., Gootenberg, J. S., Abudayyeh, O. O., Platt, R. J., Brigham, M. D., Sanjana, N. E., & Zhang, F. (2017). Genome-scale CRISPR-Cas9 knockout and transcriptional activation screening. *Nat Protoc, 12*(4), 828-863. doi: 10.1038/nprot.2017.016

June, C. H., O'Connor, R. S., Kawalekar, O. U., Ghassemi, S., & Milone, M. C. (2018). CAR T cell immunotherapy for human cancer. *Science, 359*(6382), 1361-1365. doi: 10.1126/science.aar6711

Kather, J. N., Suarez-Carmona, M., Charoentong, P., Weis, C. A., Hirsch, D., Bankhead, P., Horning, M., Ferber, D., Kel, I., Herpel, E., Schott, S., Zornig, I., Utikal, J., Marx, A., Gaiser, T., Brenner, H., Chang-Claude, J., Hoffmeister, M., Jager, D., & Halama, N. (2018). Topography of cancer-associated immune cells in human solid tumors. *Elife, 7*. doi: 10.7554/eLife.36967

Kato, H., Takeuchi, O., Sato, S., Yoneyama, M., Yamamoto, M., Matsui, K., Uematsu, S., Jung, A., Kawai, T., Ishii, K. J., Yamaguchi, O., Otsu, K., Tsujimura, T., Koh, C. S., Reis e Sousa, C., Matsuura, Y., Fujita, T., & Akira, S. (2006). Differential roles of MDA5 and

RIG-I helicases in the recognition of RNA viruses. *Nature, 441*(7089), 101-105. doi: 10.1038/nature04734

Kelly, P. M., Davison, R. S., Bliss, E., & McGee, J. O. (1988). Macrophages in human breast disease: a quantitative immunohistochemical study. *Br J Cancer, 57*(2), 174-177. doi: 10.1038/bjc.1988.36

Kerenyi, M. A., Shao, Z., Hsu, Y. J., Guo, G., Luc, S., O'Brien, K., Fujiwara, Y., Peng, C., Nguyen, M., & Orkin, S. H. (2013). Histone demethylase Lsd1 represses hematopoietic stem and progenitor cell signatures during blood cell maturation. *Elife, 2*, e00633. doi: 10.7554/eLife.00633

Khosravi, M. A., Abbasalipour, M., Concordet, J. P., Berg, J. V., Zeinali, S., Arashkia, A., Azadmanesh, K., Buch, T., & Karimipoor, M. (2019). Targeted deletion of BCL11A gene by CRISPR-Cas9 system for fetal hemoglobin reactivation: A promising approach for gene therapy of beta thalassemia disease. *Eur J Pharmacol, 854*, 398-405. doi: 10.1016/j.ejphar.2019.04.042

Kitchens, R. L. (2000). Role of CD14 in cellular recognition of bacterial lipopolysaccharides. *Chem Immunol, 74*, 61-82. doi: 10.1159/000058750

Kool, M., van Loo, G., Waelput, W., De Prijck, S., Muskens, F., Sze, M., van Praet, J., Branco-Madeira, F., Janssens, S., Reizis, B., Elewaut, D., Beyaert, R., Hammad, H., & Lambrecht, B. N. (2011). The ubiquitin-editing protein A20 prevents dendritic cell activation, recognition of apoptotic cells, and systemic autoimmunity. *Immunity, 35*(1), 82-96. doi: 10.1016/j.immuni.2011.05.013

Kunkele, A., De Preter, K., Heukamp, L., Thor, T., Pajtler, K. W., Hartmann, W., Mittelbronn, M., Grotzer, M. A., Deubzer, H. E., Speleman, F., Schramm, A., Eggert, A., & Schulte, J. H. (2012). Pharmacological activation of the p53 pathway by nutlin-3 exerts anti-tumoral effects in medulloblastomas. *Neuro Oncol, 14*(7), 859-869. doi: 10.1093/neuonc/nos115

Kyi, C., & Postow, M. A. (2014). Checkpoint blocking antibodies in cancer immunotherapy. *FEBS Lett, 588*(2), 368-376. doi: 10.1016/j.febslet.2013.10.015

Lang, R., Patel, D., Morris, J. J., Rutschman, R. L., & Murray, P. J. (2002). Shaping gene expression in activated and resting primary macrophages by IL-10. *J Immunol, 169*(5), 2253-2263. doi: 10.4049/jimmunol.169.5.2253

Lee, E. G., Boone, D. L., Chai, S., Libby, S. L., Chien, M., Lodolce, J. P., & Ma, A. (2000). Failure to regulate TNF-induced NF-kappaB and cell death responses in A20-deficient mice. *Science, 289*(5488), 2350-2354. doi: 10.1126/science.289.5488.2350

Lee, S. H., Kim, S., & Hur, J. K. (2018). CRISPR and Target-Specific DNA Endonucleases for Efficient DNA Knock-in in Eukaryotic Genomes. *Mol Cells, 41*(11), 943-952. doi: 10.14348/molcells.2018.0408

Levantini, E., Giorgetti, A., Cerisoli, F., Traggiai, E., Guidi, A., Martin, R., Acampora, D., Aplan, P. D., Keller, G., Simeone, A., Iscove, N. N., Hoang, T., & Magli, M. C. (2003). Unsuspected role of the brain morphogenetic gene Otx1 in hematopoiesis. *Proc Natl Acad Sci U S A, 100*(18), 10299-10303. doi: 10.1073/pnas.1734071100

Li, X., Zhang, Z., Li, L., Gong, W., Lazenby, A. J., Swanson, B. J., Herring, L. E., Asara, J. M., Singer, J. D., & Wen, H. (2017). Myeloid-derived cullin 3 promotes STAT3 phosphorylation by inhibiting OGT expression and protects against intestinal inflammation. *J Exp Med, 214*(4), 1093-1109. doi: 10.1084/jem.20161105

Lobera, M., Madauss, K. P., Pohlhaus, D. T., Wright, Q. G., Trocha, M., Schmidt, D. R., Baloglu, E., Trump, R. P., Head, M. S., Hofmann, G. A., Murray-Thompson, M., Schwartz, B., Chakravorty, S., Wu, Z., Mander, P. K., Kruidenier, L., Reid, R. A., Burkhart, W., Turunen, B. J., Rong, J. X., Wagner, C., Moyer, M. B., Wells, C., Hong, X., Moore, J. T., Williams, J. D., Soler, D., Ghosh, S., & Nolan, M. A. (2013). Selective class IIa histone deacetylase inhibition via a nonchelating zinc-binding group. *Nat Chem Biol, 9*(5), 319-325. doi: 10.1038/nchembio.1223

Lu, T. T., Onizawa, M., Hammer, G. E., Turer, E. E., Yin, Q., Damko, E., Agelidis, A., Shifrin, N., Advincula, R., Barrera, J., Malynn, B. A., Wu, H., & Ma, A. (2013). Dimerization and

ubiquitin mediated recruitment of A20, a complex deubiquitinating enzyme. *Immunity, 38*(5), 896-905. doi: 10.1016/j.immuni.2013.03.008

Macheleidt, I. F., Dalvi, P. S., Lim, S. Y., Meemboor, S., Meder, L., Kasgen, O., Muller, M., Kleemann, K., Wang, L., Nurnberg, P., Russeler, V., Schafer, S. C., Mahabir, E., Buttner, R., & Odenthal, M. (2018). Preclinical studies reveal that LSD1 inhibition results in tumor growth arrest in lung adenocarcinoma independently of driver mutations. *Mol Oncol, 12*(11), 1965-1979. doi: 10.1002/1878-0261.12382

Malewicz, M., Zeller, N., Yilmaz, Z. B., & Weih, F. (2003). NF kappa B controls the balance between Fas and tumor necrosis factor cell death pathways during T cell receptor-induced apoptosis via the expression of its target gene A20. *J Biol Chem, 278*(35), 32825-32833. doi: 10.1074/jbc.M304000200

Mantovani, A., & Allavena, P. (2015). The interaction of anticancer therapies with tumor-associated macrophages. *J Exp Med, 212*(4), 435-445. doi: 10.1084/jem.20150295

Mantovani, A., Allavena, P., Sica, A., & Balkwill, F. (2008). Cancer-related inflammation. *Nature, 454*(7203), 436-444. doi: 10.1038/nature07205

Mantovani, A., Biswas, S. K., Galdiero, M. R., Sica, A., & Locati, M. (2013). Macrophage plasticity and polarization in tissue repair and remodelling. *J Pathol, 229*(2), 176-185. doi: 10.1002/path.4133

Mantovani, A., Marchesi, F., Malesci, A., Laghi, L., & Allavena, P. (2017). Tumour-associated macrophages as treatment targets in oncology. *Nat Rev Clin Oncol, 14*(7), 399-416. doi: 10.1038/nrclinonc.2016.217

Mantovani, A., & Sica, A. (2010). Macrophages, innate immunity and cancer: balance, tolerance, and diversity. *Curr Opin Immunol, 22*(2), 231-237. doi: 10.1016/j.coi.2010.01.009

Mantovani, A., Sozzani, S., Locati, M., Allavena, P., & Sica, A. (2002). Macrophage polarization: tumor-associated macrophages as a paradigm for polarized M2 mononuclear phagocytes. *Trends Immunol, 23*(11), 549-555. doi: 10.1016/s1471-4906(02)02302-5

Martinez, F. O., Sica, A., Mantovani, A., & Locati, M. (2008). Macrophage activation and polarization. *Front Biosci, 13*, 453-461. doi: 10.2741/2692

Matmati, M., Jacques, P., Maelfait, J., Verheugen, E., Kool, M., Sze, M., Geboes, L., Louagie, E., Mc Guire, C., Vereecke, L., Chu, Y., Boon, L., Staelens, S., Matthys, P., Lambrecht, B. N., Schmidt-Supprian, M., Pasparakis, M., Elewaut, D., Beyaert, R., & van Loo, G. (2011). A20 (TNFAIP3) deficiency in myeloid cells triggers erosive polyarthritis resembling rheumatoid arthritis. *Nat Genet, 43*(9), 908-912. doi: 10.1038/ng.874

Munder, M., Eichmann, K., & Modolell, M. (1998). Alternative metabolic states in murine macrophages reflected by the nitric oxide synthase/arginase balance: competitive regulation by CD4+ T cells correlates with Th1/Th2 phenotype. *J Immunol, 160*(11), 5347-5354.

Munder, M., Eichmann, K., Moran, J. M., Centeno, F., Soler, G., & Modolell, M. (1999). Th1/Th2-regulated expression of arginase isoforms in murine macrophages and dendritic cells. *J Immunol, 163*(7), 3771-3777.

Murphy, K., Travers, P., Walport, M., & Janeway, C. (2012). Janeway's immunobiology. xix, 868 p.

Murray, P. J. (2017). Macrophage Polarization. *Annu Rev Physiol, 79*, 541-566. doi: 10.1146/annurev-physiol-022516-034339

Murray, P. J., Allen, J. E., Biswas, S. K., Fisher, E. A., Gilroy, D. W., Goerdt, S., Gordon, S., Hamilton, J. A., Ivashkiv, L. B., Lawrence, T., Locati, M., Mantovani, A., Martinez, F. O., Mege, J. L., Mosser, D. M., Natoli, G., Saeij, J. P., Schultze, J. L., Shirey, K. A., Sica, A., Suttles, J., Udalova, I., van Ginderachter, J. A., Vogel, S. N., & Wynn, T. A. (2014). Macrophage activation and polarization: nomenclature and experimental guidelines. *Immunity, 41*(1), 14-20. doi: 10.1016/j.immuni.2014.06.008

Neggers, J. E., Kwanten, B., Dierckx, T., Noguchi, H., Voet, A., Bral, L., Minner, K., Massant, B., Kint, N., Delforge, M., Vercruysse, T., Baloglu, E., Senapedis, W., Jacquemyn, M., & Daelemans, D. (2018). Target identification of small molecules using large-scale

CRISPR-Cas mutagenesis scanning of essential genes. *Nat Commun, 9*(1), 502. doi: 10.1038/s41467-017-02349-8

Noman, M. Z., Desantis, G., Janji, B., Hasmim, M., Karray, S., Dessen, P., Bronte, V., & Chouaib, S. (2014). PD-L1 is a novel direct target of HIF-1alpha, and its blockade under hypoxia enhanced MDSC-mediated T cell activation. *J Exp Med, 211*(5), 781-790. doi: 10.1084/jem.20131916

O'Neill, L. A., Golenbock, D., & Bowie, A. G. (2013). The history of Toll-like receptors - redefining innate immunity. *Nat Rev Immunol, 13*(6), 453-460. doi: 10.1038/nri3446

Ott, P. A., Hodi, F. S., Kaufman, H. L., Wigginton, J. M., & Wolchok, J. D. (2017). Combination immunotherapy: a road map. *J Immunother Cancer, 5*, 16. doi: 10.1186/s40425-017-0218-5

Parnas, O., Jovanovic, M., Eisenhaure, T. M., Herbst, R. H., Dixit, A., Ye, C. J., Przybylski, D., Platt, R. J., Tirosh, I., Sanjana, N. E., Shalem, O., Satija, R., Raychowdhury, R., Mertins, P., Carr, S. A., Zhang, F., Hacohen, N., & Regev, A. (2015). A Genome-wide CRISPR Screen in Primary Immune Cells to Dissect Regulatory Networks. *Cell, 162*(3), 675-686. doi: 10.1016/j.cell.2015.06.059

Philpott, D. J., Sorbara, M. T., Robertson, S. J., Croitoru, K., & Girardin, S. E. (2014). NOD proteins: regulators of inflammation in health and disease. *Nat Rev Immunol, 14*(1), 9-23. doi: 10.1038/nri3565

Pittet, L. A., Quinton, L. J., Yamamoto, K., Robson, B. E., Ferrari, J. D., Algul, H., Schmid, R. M., & Mizgerd, J. P. (2011). Earliest innate immune responses require macrophage RelA during pneumococcal pneumonia. *Am J Respir Cell Mol Biol, 45*(3), 573-581. doi: 10.1165/rcmb.2010-0210OC

Pollard, J. W. (2004). Tumour-educated macrophages promote tumour progression and metastasis. *Nat Rev Cancer, 4*(1), 71-78. doi: 10.1038/nrc1256

Popovic, A., Jaffee, E. M., & Zaidi, N. (2018). Emerging strategies for combination checkpoint modulators in cancer immunotherapy. *J Clin Invest, 128*(8), 3209-3218. doi: 10.1172/JCI120775

Qin, Y., Vasilatos, S. N., Chen, L., Wu, H., Cao, Z., Fu, Y., Huang, M., Vlad, A. M., Lu, B., Oesterreich, S., Davidson, N. E., & Huang, Y. (2019). Inhibition of histone lysine-specific demethylase 1 elicits breast tumor immunity and enhances antitumor efficacy of immune checkpoint blockade. *Oncogene, 38*(3), 390-405. doi: 10.1038/s41388-018-0451-5

Qin, Z. (2012). The use of THP-1 cells as a model for mimicking the function and regulation of monocytes and macrophages in the vasculature. *Atherosclerosis, 221*(1), 2-11. doi: 10.1016/j.atherosclerosis.2011.09.003

Re, F., & Strominger, J. L. (2002). Monomeric recombinant MD-2 binds toll-like receptor 4 tightly and confers lipopolysaccharide responsiveness. *J Biol Chem, 277*(26), 23427-23432. doi: 10.1074/jbc.M202554200

Rostam, H. M., Reynolds, P. M., Alexander, M. R., Gadegaard, N., & Ghaemmaghami, A. M. (2017). Image based Machine Learning for identification of macrophage subsets. *Sci Rep, 7*(1), 3521. doi: 10.1038/s41598-017-03780-z

Sanson, K. R., Hanna, R. E., Hegde, M., Donovan, K. F., Strand, C., Sullender, M. E., Vaimberg, E. W., Goodale, A., Root, D. E., Piccioni, F., & Doench, J. G. (2018). Optimized libraries for CRISPR-Cas9 genetic screens with multiple modalities. *Nat Commun, 9*(1), 5416. doi: 10.1038/s41467-018-07901-8

Sauer, S. (2015). Ligands for the Nuclear Peroxisome Proliferator-Activated Receptor Gamma. *Trends Pharmacol Sci, 36*(10), 688-704. doi: 10.1016/j.tips.2015.06.010

Scholl, S. M., Pallud, C., Beuvon, F., Hacene, K., Stanley, E. R., Rohrschneider, L., Tang, R., Pouillart, P., & Lidereau, R. (1994). Anti-colony-stimulating factor-1 antibody staining in primary breast adenocarcinomas correlates with marked inflammatory cell infiltrates and prognosis. *J Natl Cancer Inst, 86*(2), 120-126. doi: 10.1093/jnci/86.2.120

Schreiber, R. D., Old, L. J., & Smyth, M. J. (2011). Cancer immunoediting: integrating immunity's roles in cancer suppression and promotion. *Science, 331*(6024), 1565-1570. doi: 10.1126/science.1203486

Schuster, A., Erasimus, H., Fritah, S., Nazarov, P. V., van Dyck, E., Niclou, S. P., & Golebiewska, A. (2019). RNAi/CRISPR Screens: from a Pool to a Valid Hit. *Trends Biotechnol, 37*(1), 38-55. doi: 10.1016/j.tibtech.2018.08.002

Shah, S. A., Erdmann, S., Mojica, F. J., & Garrett, R. A. (2013). Protospacer recognition motifs: mixed identities and functional diversity. *RNA Biol, 10*(5), 891-899. doi: 10.4161/rna.23764

Sharma, P., & Allison, J. P. (2015). Immune checkpoint targeting in cancer therapy: toward combination strategies with curative potential. *Cell, 161*(2), 205-214. doi: 10.1016/j.cell.2015.03.030

Sharma, P., Hu-Lieskovan, S., Wargo, J. A., & Ribas, A. (2017). Primary, Adaptive, and Acquired Resistance to Cancer Immunotherapy. *Cell, 168*(4), 707-723. doi: 10.1016/j.cell.2017.01.017

Shembade, N., & Harhaj, E. W. (2012). Regulation of NF-kappaB signaling by the A20 deubiquitinase. *Cell Mol Immunol, 9*(2), 123-130. doi: 10.1038/cmi.2011.59

Shembade, N., Ma, A., & Harhaj, E. W. (2010). Inhibition of NF-kappaB signaling by A20 through disruption of ubiquitin enzyme complexes. *Science, 327*(5969), 1135-1139. doi: 10.1126/science.1182364

Shi, L., Chen, S., Lu, Y., Wang, X., Xu, L., Zhang, F., Yang, L., Wu, X., Li, B., & Li, Y. (2013). Changes in the MALT1-A20-NF-kappaB expression pattern may be related to T cell dysfunction in AML. *Cancer Cell Int, 13*(1), 37. doi: 10.1186/1475-2867-13-37

Shi, S., Nathan, C., Schnappinger, D., Drenkow, J., Fuortes, M., Block, E., Ding, A., Gingeras, T. R., Schoolnik, G., Akira, S., Takeda, K., & Ehrt, S. (2003). MyD88 primes macrophages for full-scale activation by interferon-gamma yet mediates few responses to Mycobacterium tuberculosis. *J Exp Med, 198*(7), 987-997. doi: 10.1084/jem.20030603

Shifrut, E., Carnevale, J., Tobin, V., Roth, T. L., Woo, J. M., Bui, C. T., Li, P. J., Diolaiti, M. E., Ashworth, A., & Marson, A. (2018). Genome-wide CRISPR Screens in Primary Human T Cells Reveal Key Regulators of Immune Function. *Cell, 175*(7), 1958-1971 e1915. doi: 10.1016/j.cell.2018.10.024

Shiratori, H., Feinweber, C., Luckhardt, S., Linke, B., Resch, E., Geisslinger, G., Weigert, A., & Parnham, M. J. (2017). THP-1 and human peripheral blood mononuclear cell-derived macrophages differ in their capacity to polarize in vitro. *Mol Immunol, 88*, 58-68. doi: 10.1016/j.molimm.2017.05.027

Sorna, V., Theisen, E. R., Stephens, B., Warner, S. L., Bearss, D. J., Vankayalapati, H., & Sharma, S. (2013). High-throughput virtual screening identifies novel N'-(1-phenylethylidene)-benzohydrazides as potent, specific, and reversible LSD1 inhibitors. *J Med Chem, 56*(23), 9496-9508. doi: 10.1021/jm400870h

Strezoska, Z., Licon, A., Haimes, J., Spayd, K. J., Patel, K. M., Sullivan, K., Jastrzebski, K., Simpson, K. J., Leake, D., van Brabant Smith, A., & Vermeulen, A. (2012). Optimized PCR conditions and increased shRNA fold representation improve reproducibility of pooled shRNA screens. *PLoS One, 7*(8), e42341. doi: 10.1371/journal.pone.0042341

Surdziel, E., Clay, I., Nigsch, F., Thiemeyer, A., Allard, C., Hoffman, G., Reece-Hoyes, J. S., Phadke, T., Gambert, R., Keller, C. G., Ludwig, M. G., Baumgarten, B., Frederiksen, M., Schubeler, D., Seuwen, K., Bouwmeester, T., & Fodor, B. D. (2017). Multidimensional pooled shRNA screens in human THP-1 cells identify candidate modulators of macrophage polarization. *PLoS One, 12*(8), e0183679. doi: 10.1371/journal.pone.0183679

Tan, A. H. Y., Tu, W., McCuaig, R., Hardy, K., Donovan, T., Tsimbalyuk, S., Forwood, J. K., & Rao, S. (2019). Lysine-Specific Histone Demethylase 1A Regulates Macrophage Polarization and Checkpoint Molecules in the Tumor Microenvironment of Triple-Negative Breast Cancer. *Front Immunol, 10*, 1351. doi: 10.3389/fimmu.2019.01351

Tapping, R. I., & Tobias, P. S. (2000). Soluble CD14-mediated cellular responses to lipopolysaccharide. *Chem Immunol, 74*, 108-121. doi: 10.1159/000058751

Tavares, R. M., Turer, E. E., Liu, C. L., Advincula, R., Scapini, P., Rhee, L., Barrera, J., Lowell, C. A., Utz, P. J., Malynn, B. A., & Ma, A. (2010). The ubiquitin modifying enzyme A20

restricts B cell survival and prevents autoimmunity. *Immunity, 33*(2), 181-191. doi: 10.1016/j.immuni.2010.07.017

Tedesco, S., Bolego, C., Toniolo, A., Nassi, A., Fadini, G. P., Locati, M., & Cignarella, A. (2015). Phenotypic activation and pharmacological outcomes of spontaneously differentiated human monocyte-derived macrophages. *Immunobiology, 220*(5), 545-554. doi: 10.1016/j.imbio.2014.12.008

Tedesco, S., De Majo, F., Kim, J., Trenti, A., Trevisi, L., Fadini, G. P., Bolego, C., Zandstra, P. W., Cignarella, A., & Vitiello, L. (2018). Convenience versus Biological Significance: Are PMA-Differentiated THP-1 Cells a Reliable Substitute for Blood-Derived Macrophages When Studying in Vitro Polarization? *Front Pharmacol, 9*, 71. doi: 10.3389/fphar.2018.00071

Thomas, L. (1982). On immunosurveillance in human cancer. *Yale J Biol Med, 55*(3-4), 329-333.

Tu, E., Chia, P. Z., & Chen, W. (2014). TGFbeta in T cell biology and tumor immunity: Angel or devil? *Cytokine Growth Factor Rev, 25*(4), 423-435. doi: 10.1016/j.cytogfr.2014.07.014

van de Laar, L., Saelens, W., De Prijck, S., Martens, L., Scott, C. L., Van Isterdael, G., Hoffmann, E., Beyaert, R., Saeys, Y., Lambrecht, B. N., & Guilliams, M. (2016). Yolk Sac Macrophages, Fetal Liver, and Adult Monocytes Can Colonize an Empty Niche and Develop into Functional Tissue-Resident Macrophages. *Immunity, 44*(4), 755-768. doi: 10.1016/j.immuni.2016.02.017

van der Meer, L. T., Jansen, J. H., & van der Reijden, B. A. (2010). Gfi1 and Gfi1b: key regulators of hematopoiesis. *Leukemia, 24*(11), 1834-1843. doi: 10.1038/leu.2010.195

Vande Walle, L., Van Opdenbosch, N., Jacques, P., Fossoul, A., Verheugen, E., Vogel, P., Beyaert, R., Elewaut, D., Kanneganti, T. D., van Loo, G., & Lamkanfi, M. (2014). Negative regulation of the NLRP3 inflammasome by A20 protects against arthritis. *Nature, 512*(7512), 69-73. doi: 10.1038/nature13322

Verhelst, K., Carpentier, I., Kreike, M., Meloni, L., Verstrepen, L., Kensche, T., Dikic, I., & Beyaert, R. (2012). A20 inhibits LUBAC-mediated NF-kappaB activation by binding linear polyubiquitin chains via its zinc finger 7. *EMBO J, 31*(19), 3845-3855. doi: 10.1038/emboj.2012.240

Wang, L., Hong, B., Jiang, X., Jones, L., Chen, S. Y., & Huang, X. F. (2012). A20 controls macrophage to elicit potent cytotoxic CD4(+) T cell response. *PLoS One, 7*(11), e48930. doi: 10.1371/journal.pone.0048930

Wang, T., Birsoy, K., Hughes, N. W., Krupczak, K. M., Post, Y., Wei, J. J., Lander, E. S., & Sabatini, D. M. (2015). Identification and characterization of essential genes in the human genome. *Science, 350*(6264), 1096-1101. doi: 10.1126/science.aac7041

Wang, Y., Song, Z., Bi, J., Liu, J., Tong, L., Song, Y., Bai, C., & Zhu, X. (2017). A20 protein regulates lipopolysaccharide-induced acute lung injury by downregulation of NF-kappaB and macrophage polarization in rats. *Mol Med Rep, 16*(4), 4964-4972. doi: 10.3892/mmr.2017.7184

Wargo, J. A., Reddy, S. M., Reuben, A., & Sharma, P. (2016). Monitoring immune responses in the tumor microenvironment. *Curr Opin Immunol, 41*, 23-31. doi: 10.1016/j.coi.2016.05.006

Wertz, I. E., O'Rourke, K. M., Zhou, H., Eby, M., Aravind, L., Seshagiri, S., Wu, P., Wiesmann, C., Baker, R., Boone, D. L., Ma, A., Koonin, E. V., & Dixit, V. M. (2004). De-ubiquitination and ubiquitin ligase domains of A20 downregulate NF-kappaB signalling. *Nature, 430*(7000), 694-699. doi: 10.1038/nature02794

Wiehagen, K. R., Girgis, N. M., Yamada, D. H., Smith, A. A., Chan, S. R., Grewal, I. S., Quigley, M., & Verona, R. I. (2017). Combination of CD40 Agonism and CSF-1R Blockade Reconditions Tumor-Associated Macrophages and Drives Potent Antitumor Immunity. *Cancer Immunol Res, 5*(12), 1109-1121. doi: 10.1158/2326-6066.CIR-17-0258

Winter, G. E., Buckley, D. L., Paulk, J., Roberts, J. M., Souza, A., Dhe-Paganon, S., & Bradner, J. E. (2015). DRUG DEVELOPMENT. Phthalimide conjugation as a strategy for in vivo

target protein degradation. *Science, 348*(6241), 1376-1381. doi: 10.1126/science.aab1433

Wolchok, J. D., Chiarion-Sileni, V., Gonzalez, R., Rutkowski, P., Grob, J. J., Cowey, C. L., Lao, C. D., Wagstaff, J., Schadendorf, D., Ferrucci, P. F., Smylie, M., Dummer, R., Hill, A., Hogg, D., Haanen, J., Carlino, M. S., Bechter, O., Maio, M., Marquez-Rodas, I., Guidoboni, M., McArthur, G., Lebbe, C., Ascierto, P. A., Long, G. V., Cebon, J., Sosman, J., Postow, M. A., Callahan, M. K., Walker, D., Rollin, L., Bhore, R., Hodi, F. S., & Larkin, J. (2017). Overall Survival with Combined Nivolumab and Ipilimumab in Advanced Melanoma. *N Engl J Med, 377*(14), 1345-1356. doi: 10.1056/NEJMoa1709684

Wynn, T. A. (2013). Myeloid-cell differentiation redefined in cancer. *Nat Immunol, 14*(3), 197-199. doi: 10.1038/ni.2539

Yu, X., Abe, R., & Hodes, R. J. (1998). The role of B7-CD28 co-stimulation in tumor rejection. *Int Immunol, 10*(6), 791-797. doi: 10.1093/intimm/10.6.791

Zeisberger, S. M., Odermatt, B., Marty, C., Zehnder-Fjallman, A. H., Ballmer-Hofer, K., & Schwendener, R. A. (2006). Clodronate-liposome-mediated depletion of tumour-associated macrophages: a new and highly effective antiangiogenic therapy approach. *Br J Cancer, 95*(3), 272-281. doi: 10.1038/sj.bjc.6603240

Zhou, P., Shaffer, D. R., Alvarez Arias, D. A., Nakazaki, Y., Pos, W., Torres, A. J., Cremasco, V., Dougan, S. K., Cowley, G. S., Elpek, K., Brogdon, J., Lamb, J., Turley, S. J., Ploegh, H. L., Root, D. E., Love, J. C., Dranoff, G., Hacohen, N., Cantor, H., & Wucherpfennig, K. W. (2014). In vivo discovery of immunotherapy targets in the tumour microenvironment. *Nature, 506*(7486), 52-57. doi: 10.1038/nature12988

Zhu, Y., Knolhoff, B. L., Meyer, M. A., Nywening, T. M., West, B. L., Luo, J., Wang-Gillam, A., Goedegebuure, S. P., Linehan, D. C., & DeNardo, D. G. (2014). CSF1/CSF1R blockade reprograms tumor-infiltrating macrophages and improves response to T-cell checkpoint immunotherapy in pancreatic cancer models. *Cancer Res, 74*(18), 5057-5069. doi: 10.1158/0008-5472.CAN-13-3723

Natália Rodrigues Mantuano, Michal A. Stanczak, Isadora de Araújo Oliveira, Nicole Kirchhammer, Alessandra Filardy, Gianni Monaco, Ronan Christian Santos, Agatha Carlos Fonseca, Miguel Fontes, César de Souza Bastos Jr, Wagner B. Dias, Alfred Zippelius, Adriane R. Todeschini, View ORCID ProfileHeinz Läubli. Hyperglycemia enhances cancer immune evasion by inducing alternative macrophage polarization through increased O-GlcNAcylation. Doi: https://doi.org/10.1101/831610 (preprint)

6 Supplementary

S1 Materials

Table 6.1. Chemicals and consumables

Product	Manufacturer	Catalog Number
10 × NuPAGE Sample Reducing Agent	GIBCO by life technologies	NP009
10 × RIPA Lysis Buffer	Millipore	20-188
10 × TBST	Cell Signaling	9997S
1 × PBS	Thermo Fisher Scientific	10010023
1 × PBS (flow cytometry grade)	Thermo Fisher Scientific	A1286301
20 × NuPAGE® MOPS SDS Running Buffer	Invitrogen	NP0001
Pre-separation filter (30 µm)	Miltenyi Biotec	130-041-407
4 × NuPAGE LDS Sample Buffer	GIBCO by life technologies	NP0007
96 well cell culture plate	TPP	92096
Accutase	Stem Cell Technologies	7920
Agencourt AMPure XP	Beckman Coulter	A63881
Agilent DNA 1000 Kit	Agilent Technologies	5067-1504
Amaxa® Cell Line Nucleofector ® Kit V	Lonza	VCA-1003
Anti-CAS9 monoclonal antibody	Cell Signaling Technologies	14697
Anti-GAPDH antibody [6C5] – Loading Control	Abcam	ab8245
Anti-HSP90 Monoclonal Antibody	BD Biosciences	610419
APC anti-human CD163 Antibody	BD Biosciences	333610
APC anti-Human CD209 Antibody	BD Biosciences	551545
Beta Mercapto-ethanol	Thermo Fisher Scientific	31350-010
Brilliant Violet 421™ anti-human HLA-DR Antibody	BD Biosciences	307636
Brilliant Violet 421™ Anti-Human CD80 antibody (Clone L307.4)	BD Biosciences	564160
Cas9 nuclease expression plasmid	Cellecta	SVC9-PS
CRISPRtest™ Functional Cas9 Activity Kit	Cellecta	CRISPRtest-GVO-CT
CellTrace™ CFSE Cell Proliferation Kit	Thermo Fisher Scientific	C34554
Chameleon Due Pre-stained Protein Ladder	Licor	928-60000
Custom sgRNA library	Cellecta	CPLVSGL-P
Cytofix/Cytoperm™ solution	BD Biosciences	554714
Dead Cell Removal Kit	Miltenyi Biotec	130-090-101
DMSO	Sigma Aldrich	D2650
Dnase/ Rnase free water	GIBCO by life technologies	10977-035
dNTP, 50x	GE Healthcare LifeScience	28-4065-64
Elution Buffer	Qiagen	19086
Ethanol absolute	AppliChem	A1613
Falcon® 12 Well Clear Flat Bottom TC-Treated Multiwell Cell Culture Plate	Corning	353043
GeneRead™ DNA FFPE Kit	Qiagen	180134
Gigasept Instru AF	Schülke	107411
Goat anti-Mouse IgG (H+L)	Thermo Fisher Scientific	31160

Granulocyte-Macrophage Colony-Stimulating Factor human	Sigma Aldrich	G5035
Halt™ Protease & Phosphatase Inhibitor Cocktail	Thermo Fisher Scientific	1861281
Heat inactivated FBS	Sigma Aldrich	F4135
Hexadimethrine bromide	Sigma Aldrich	H9268
HiSeq SBS Kit v4 (50 Cycle Kit)	Illumina	FC-401-4002
HiSeq SR Cluster Kit v4	Illumina	GD-401-4001
HT1 buffer	Illumina	20015892
Human IFN-γ ELISA Set	BD Biosciences	555142
Human IL-12 ELISA Set	BD Biosciences	555171
Human IL-1β ELISA Set	BD Biosciences	557953
Human IL-2 ELISA Set	BD Biosciences	555190
Human recombinant IL-6	Thermo Fisher Scientific	PHC0065
Human IL-6 ELISA Set	BD Biosciences	555220
Human TNF ELISA Set	BD Biosciences	555212
Hygromycin B	Invitrogen	10687010
iBlot® 2 Transfer Stacks, nitrocellulose, regular size	Novex by life technologies	IB23001
Interferon-γ human	Sigma Aldrich	I3265
Interleukin-4 human	Sigma/ Merck	I4269
Lipopolysaccharide E. coli	Sigma Aldrich	L4391
Macrophage Colony-Stimulating Factor human	Sigma Aldrich	M6518
Maxima First Strand cDNA Synthesis Kit for RT-qPCR	Thermo Scientific	K1642
MicroAmp Optical 384-Well reaction plates	Thermo Fisher Scientific	4326270
MSD ® 96 Well MULTI ARRAY ® and 7-SPOT ® Human Cytokine Assays	Mesoscale discovery	K15008b-4
NaOH 1M	Sigma Aldrich	71463
Nonfat dried milk powder	AppliChem	A0830
Novex™ 10 % Bis-Tris Protein Gels, 1.0 mm	Thermo Fisher Scientific	NP0301BOX
NuPAGE™ (Novex™ 10 % Bis-Tris Protein Gels, 1.0 mm, 10 well).	Thermo Fisher Scientific	NP0301BOX
P3 Primary Cell 4D-NucleofectorTM X Kit S	Lonza	V4XP-3032
Penicillin-Streptomycin	Sigma Aldrich	P4333
PerfeCta NGS Library Quantification Kit – Illumina Low/ROX	Quanta Bioscience	95156-500
Perkin Elmer 384 well plates with a clear bottom	Perkin Elmer	6007550
PhiX Control v3	Illumina	15017666
Phorbol 12-myristate 13-acetate (PMA)	Sigma Aldrich	P1585
Pierce™ BCA Protein Assay Kit	Thermo Fisher Scientific	23225
Purified NA/LE Mouse Anti-Human CD28	Sigma Aldrich	555725
Purified NA/LE Mouse Anti-Human CD3	Sigma Aldrich	555329
Puromycin Dihydrochloride	GIBCO by life technologies	A1113802
QIAamp DNA Mini Kit	Qiagen	51304
Recombinant Human IL-3 Protein	Thermo Fisher Scientific	PHC0031
Recombinant Human SCF Protein	R&D	255-SC-200
Recombinant Human Thrombopoietin (TPO)	Thermo Fisher Scientific	PHC9511
RLT buffer	Qiagen	79216
Rnase-Free Dnase Set	Qiagen	79254

RNeasy® Mini Kit	Qiagen	74106
RPMI 1640 GlutaMax	GIBCO by life technologies	61870-010
SG Cell Line 4D-NucleofectorTM X Kit L	Lonza	V4XC-3024
Sodium pyruvate	Thermo Fisher Scientific	11360-070
T175 culture flasks	Sigma Aldrich	CLS431080
TaqMan Fast Universal PCR	Applied Biosystems	4352042
Titanium® Taq DNA Polymerase	Clontech-Takara	639242
TrueCut Cas9 Protein	Thermo Fisher Scientific	A36499
TruSeq HT library	Illumina	RS-122-2103
TruSeq RNA Sample Preparation Kit v2	Illumina	RS-122-2001
TruStain FcX™ (Fc Receptor Blocking Solution)	Biolegend	422302
Tween 20	Sigma Aldrich	20P7949
Ultrapure water	Fisher Scientific	11357090
Whole genome sgRNA library (Module 1-3)	Cellecta	KOHGW-M1-V9 KOHGW-M2-V9 KOHGW-M3-V9

Table 6.2. Devices

Product	Manufacturer
4D Nucleofector core unit and X-unit	Lonza
Automated cell counter (Countess II)	Thermo Fisher Scientific
Bioanalyzer 2001	Agilent Technologies
Cell sorter BD FACS JAZZ™	BD Biosciences
HiSeq 2500 System	Illumina
iBlot 2 gel transfer device	Novex by life technologies
IncuCyte® Live Cell Analysis System	Essen BioScience
Magnetic Stand-96	Ambion
Mastercycler nexus gradient	Eppendorf
MiSeq System	Illumina
Monochromator Infinite M1000	Tecan
NanoDrop™ 8000 Spectrophotometer	Thermo Fisher Scientific
NanoQuant Plate	Tecan
Odyssey Sa Infrared Imaging System	LI-COR
QIAcube	Qiagen
ViiA™ 7 Real-Time PCR System	Applied Biosystems

Primers for 1st and 2nd PCR

1st PCR

Reverse Primer

Rev-1

5’ CGACAACAACGCAGAAATTTTGAAT 3’

Forward Primer

FwdU6-1

5’ CAAGGCTGTTAGAGAGATAATTGG 3’

2nd PCR

Reverse Primer

P7-NFG16

CAAGCAGAAGACGGCATACGAGATGCATGTATGTCTGTTGCTATTATGTCTACT

Forward Primer

Bases which are marked in red represent the index sequences.

P5-NFG16-IndA

AATGATACGGCGACCACCGAGATCTACACTACGACATGGACTATCATATGCTTACCGTAACTTGAA

P5-NFG16-IndB

AATGATACGGCGACCACCGAGATCTACACCTGATGATGGACTATCATATGCTTACCGTAACTTGAA

P5-NFG16-IndC

AATGATACGGCGACCACCGAGATCTACACGCATCAATGGACTATCATATGCTTACCGTAACTTGAA

P5-NFG16-IndD

AATGATACGGCGACCACCGAGATCTACACAGTCGTATGGACTATCATATGCTTACCGTAACTTGAA

P5-NFG16-IndE

AATGATACGGCGACCACCGAGATCTACACTCGCATATGGACTATCATATGCTTACCGTAACTTGAA

P5-NFG16-IndF

AATGATACGGCGACCACCGAGATCTACACCATAGCATGGACTATCATATGCTTACCGTAACTTGAA

P5-NFG16-IndG

AATGATACGGCGACCACCGAGATCTACACAGCGTAATGGACTATCATATGCTTACCGTAACTTGAA

P5-NFG16-IndH

AATGATACGGCGACCACCGAGATCTACACGTATCGATGGACTATCATATGCTTACCGTAACTTGAA

P5-NFG16-IndP

AATGATACGGCGACCACCGAGATCTACACATCAGCATGGACTATCATATGCTTACCGTAACTTGAA

Sequencing Primer

Fseq-gRNA

GGCTTTATATATCTTGTGGAAAGGACGAAACACCG

171 Genes targeted by focused sgRNA library

ABL2	CD86	FGL2	MKNK1	SCAF1
ACOD1	CFB	FGR	MLKL	SCYL2
ACVRL1	CLEC10A	FLT4	MMP19	SERPINA1
ADA2	CLEC11A	FPR1	MMP9	SERPINB2
ADAMDEC1	CLEC12A	FPR2	MPEG1	SERPING1
ADORA2A	CLEC12B	FPR3	MRC1	SIGLEC1
ALK	CLEC1A	GRK3	MSR1	SLA
ALOX15	CLEC4A	HCK	NAMPT	SLAMF7
ALOX5	CLEC4C	ICAM1	NEK6	SLC11A1
APOBEC3A	CLEC4D	IDO1	NPL	SLC15A3
BCKDK	CLEC4E	IL10RA	PAK2	SLC6A12
BCL2A1	CLEC4M	IL12B	PARP14	SOCS1
BIRC3	CLEC5A	IL1B	PARP9	SRC
BMP2K	CLEC6A	IL2RA	PCSK1	STAT1
BTK	CLEC7A	IL4I1	PDE4B	STK10
C3AR1	CPM	IL4R	PIK3CA	STK40
C5AR1	CPVL	IL6	PIK3CD	SYK
CAMK1	CSF1R	IRAK2	PIK3CG	TAP1
CASP1	CSF2RA	IRAK3	PIK3R5	TBK1
CCL14	CSF2RB	ITGAL	PIK3R6	TEX14
CCL2	CSK	ITGB2	PIM1	TGFBR1
CCL7	CSTA	JAK2	PIM3	TLR2
CCR1	CTSB	KMO	PLAUR	TLR4
CCR5	CTSS	KYNU	PLK3	TLR8
CCR7	CTSZ	LIMK1	PRKCD	TNFAIP3
CCRL2	CXCL1	LIMK2	PTGER2	TNFRSF1B
CD14	CXCL2	LY96	PTGER4	TNFSF10
CD163	CXCR2	LYN	PTGS1	TREM1
CD209	DAPK1	MAF	PTGS2	TYMP
CD33	F13A1	MAP2K3	PTPN6	VRK2
CD38	FABP4	MAP3K11	PTPRE	WARS
CD40	FCER1A	MAP3K8	RIPK2	
CD52	FCGR1A	MAPKAPK3	RIPK3	
CD74	FCGR2A	MARCO	RPS6KA1	
CD80	FES	MERTK	RPS6KA4	

S2 Hit list

Table 6.3. Hit list with top 100 targets from both M1 and M2 polarization

Rank	Gene	M1 pol (log_2 FC)	Rank	Gene	M2 pol (log_2 FC)
1	SHOC2	2.4507	1	GFI1	4.0099
2	SCRIB	2.0449	2	KDM1A	2.7692
3	OGT	2.0056	3	OTX1	2.7430
4	MAPK1	1.7399	4	MEN1	2.2294
5	HIVEP3	1.6209	5	NCAPD2	2.1371
6	FBXO11	1.5556	6	KAT6A	2.0024
7	LDB1	1.3427	7	BRPF1	1.9594
8	NCAPD2	1.2636	8	DOT1L	1.9178
9	GOLGA7	1.2522	9	PLAC8	1.8873
10	CEBPB	1.2261	10	DRAP1	1.8245
11	MED13L	1.2099	11	NANS	1.7264
12	ELP5	1.1757	12	SETD2	1.6667
13	ZCRB1	1.1647	13	DR1	1.6624
14	FOSL1	1.1636	14	TKT	1.6602
15	TNFAIP3	1.1504	15	VPS39	1.6414
16	NUP188	1.1268	16	MYB	1.6272
17	RREB1	1.1219	17	PAICS	1.5841
18	RFC5	1.1201	18	WIPI2	1.5801
19	GFI1	1.1109	19	OGT	1.5674
20	PLAC8	1.0930	20	C9orf41	1.4875
21	KAT6A	1.0720	21	INTS2	1.4673
22	IL1R1	1.0658	22	NDUFAF5	1.4360
23	TCEB3	1.0469	23	PRPF38B	1.4288
24	PTPRC	1.0446	24	CDK2	1.3553
25	IRF2BP2	1.0431	25	DENND4B	1.3135
26	GSE1	1.0075	26	ZDHHC13	1.3029
27	LMO2	1.0024	27	MED25	1.2616
28	FNTA	0.9910	28	GSE1	1.2549
29	UBA2	0.9741	29	ATIC	1.2508
30	ZC3H10	0.9624	30	HIF1A	1.2368
31	IL1RAP	0.9582	31	TUT1	1.2345
32	RFC4	0.9556	32	GAL	1.2320
33	SPTY2D1	0.9148	33	CUL2	1.2277
34	ELP6	0.9123	34	FAM49B	1.2179
35	AHCTF1	0.9091	35	TSC1	1.2091
36	ARNT	0.9068	36	CYLD	1.2069
37	KDM1A	0.8700	37	CAPRIN1	1.2022
38	PTPN2	0.8671	38	EDC4	1.1931
39	PHIP	0.8557	39	CNOT1	1.1797
40	TMEM199	0.8553	40	MED24	1.1774
41	CASC5	0.8525	41	ARNT	1.1758
42	TARDBP	0.8437	42	AHCTF1	1.1737
43	DPH3	0.8199	43	COQ2	1.1713
44	RASGRP3	0.8128	44	NDUFS1	1.1572
45	ZDHHC13	0.8089	45	IGF2R	1.1554
46	USPL1	0.8081	46	MED27	1.1523
47	ASUN	0.8079	47	PHIP	1.1519
48	POGZ	0.8048	48	RAB1A	1.1366
49	SERBP1	0.8038	49	TANGO6	1.1123

50	IRF2	0.7988
51	CHAMP1	0.7976
52	NR2C2AP	0.7974
53	SENP2	0.7953
54	FBXL17	0.7915
55	API5	0.7912
56	DYNLL1	0.7871
57	ELP3	0.7844
58	CAPRIN1	0.7790
59	SRSF3	0.7744
60	AIP	0.7730
61	DAZAP1	0.7620
62	ARID4B	0.7585
63	BRPF1	0.7510
64	LYL1	0.7489
65	G3BP1	0.7476
66	ELP4	0.7430
67	TBK1	0.7286
68	SLC11A1	0.7203
69	BMP8B	0.7201
70	UTY	0.7098
71	ACTR5	0.7067
72	ZC3HC1	0.6969
73	OR2T1	0.6963
74	IRF1	0.6934
75	MIB2	0.6889
76	GNAS	0.6875
77	CCDC30	0.6853
78	RELA	0.6840
79	ZC3H13	0.6825
80	SYNCRIP	0.6726
81	IFIT2	0.6705
82	TPR	0.6633
83	AHR	0.6617
84	USP7	0.6611
85	TMEM131	0.6589
86	SNRPA	0.6562
87	IKBKAP	0.6551
88	MYB	0.6520
89	C1orf50	0.6473
90	KTI12	0.6463
91	ETV5	0.6455
92	ELP2	0.6449
93	HYI	0.6447
94	ELL	0.6441
95	PHF6	0.6434
96	TMEM189	0.6430
97	TCEA1	0.6409
98	ATG12	0.6407
99	NUP43	0.6358
100	STUB1	0.6350

50	SLC11A1	1.1111
51	NDUFB10	1.1003
52	PPOX	1.0814
53	NDUFA1	1.0790
54	TTC1	1.0735
55	FBXL5	1.0554
56	KIF14	1.0539
57	PELO	1.0536
58	ZSWIM8	1.0505
59	RABIF	1.0407
60	TAF1	1.0392
61	LDB1	1.0322
62	DAZAP1	1.0307
63	MED10	1.0306
64	INS-IGF2	1.0295
65	RABGGTB	1.0256
66	CDK7	1.0246
67	ERAL1	1.0244
68	CHTF8	1.0170
69	MED7	1.0087
70	SPTY2D1	1.0085
71	NDUFAF7	1.0054
72	NUP188	1.0045
73	SLFNL1	1.0010
74	RELA	0.9956
75	COQ4	0.9926
76	C7orf26	0.9865
77	RQCD1	0.9832
78	TMEM189	0.9802
79	MORC3	0.9801
80	CTC1	0.9706
81	TCEB1	0.9600
82	BTAF1	0.9582
83	RABGAP1L	0.9572
84	NPRL2	0.9496
85	SMG6	0.9468
86	CCDC132	0.9462
87	MED6	0.9428
88	MXI1	0.9389
89	TRUB2	0.9357
90	PHF6	0.9086
91	TNFAIP3	0.9051
92	USP7	0.8747
93	ELL	0.8743
94	SERBP1	0.7963
95	FBXL17	0.7956
96	ZC3H10	0.7838
97	MIB2	0.7801
98	CBFB	0.7638
99	LMO2	0.7528
100	ATG7	0.7271

Abbreviations

A

ADORA3	Adenosine A3 receptor
ALOX15	Arachidonate 15-Lipoxygenase
APC	Allophycocyanin
APCs	Antigen presenting cells
ARNT	Aryl hydrocarbon receptor nuclear translocator

B

BCA	Bicinchoninic acid
BCL11A	B-cell lymphoma/leukemia 11A
BET	Bromodomain and Extra-Terminal motif
BRD2	Bromodomain-containing protein 2
BRPF1	Bromodomain and PHD finger-containing protein 1
BV421	Brilliant Violet 421

C

CAR	Chimeric antigen receptor
Cas9	CRISPR-associated protein 9
CBFB	Core-binding factor subunit beta
CCL	Chemokine (C-C motif) ligand
CD	Cluster of differentiation
CDC16	Cell division cycle protein 16 homolog
CEBPB	CCAAT/enhancer-binding protein beta
CFSE	Carboxyfluorescein succinimidyl ester
CoREST	Repressor element-1 silencing transcription factor corepressor 1
CRISPR	Clustered regularly interspaced short palindromic repeats
CRISPRa	Clustered regularly interspaced short palindromic repeats activation
CRISPRi	Clustered regularly interspaced short palindromic repeats interference
CRISPRko	Clustered regularly interspaced short palindromic repeats knock out
crRNA	CRISPR RNA
CRYAB	Alpha-crystallin B chain
CSF	Colony stimulating factor
CSF-1R	Colony stimulating factor 1 receptor
Ct	Cycle threshold
CTLA-4	Cytotoxic T-lymphocyte-associated antigen-4
CXCL	Chemokine (C-X-C motif) ligand

D

DAMP	Damage-associated molecular pattern
DC	Dendritic cell
dCas9	Nuclease-deficient Cas9
DEG	Differentially expressed gene
DENND4B	DENN Domain Containing Protein 4B
DKFZ	Deutsches Krebsforschungszentrum

DMSO	Dimethyl sulfoxide
DNA	Deoxyribonucleic acid
DNase	Deoxyribonuclease
DSB	Double strand break
DUB	Deubiquitinating enzyme

E

e.g.	exempli gratia
ELISA	Enzyme-linked immunosorbent assay
et al.	et alia/alii/aliae

F

F13A1	Coagulation factor XIII A
FACS	Fluorescence activated cell sorting
FBS	Fetal bovine serum
FC	Fold change
FCER2	Fc epsilon receptor 2
FSC	Foward Scatter

G

GAPDH	Glyceraldehyde 3-phosphate dehydrogenase
gDNA	Genomic DNA
GFI1	Growth Factor Independent 1 Transcriptional Repressor
GFP	Green fluorescent protein
GMCSF	Granulocyte-macrophage colony-stimulating factor
gRNA	Guide ribonucleic acid
GSC	Glioma stem cell
GTF2B	General transcription factor II B

H

H3K4	Histone H3 Lysine 4
H3K9	Histone H3 Lysine 9
HCA	High-content-analysis
HDAC	Histone deacetylase
HIF1A	Hypoxia-inducible factor 1-alpha
HLA	Human leukocyte antigen
HLA-DRA	HLA class II histocompatibility antigen, DR alpha chain
HPM	Human primary monocyte
HSC	Hematopoietic stem cell
HSP90	Heat shock protein 90
HSPA1A	Heat shock protein family A (Hsp70) member 1A
HSPA1B	Heat shock 70 kDa protein 1B
HSPA5	Heat shock 70 kDa protein 5
HSPA9	Heat shock protein family A (Hsp70) member 9
HTS	High-throughput screening

I

i.e.	id est
IDO	Indoleamine-pyrrole 2,3-dioxygenase
IFN	Interferon
IgG	Immunglobulin G
IKBKAP	Inhibitor of kappa light polypeptide gene enhancer in B-cells, kinase complex-associated protein
IL	Interleukin
IL-1R	Interleukin-1 receptor
IL-1Ra	Interleukin-1 receptor antagonist
Indel	Insertion/deletion
IRF	Interferon regulated factor
IRF2BP2	Interferon regulatory factor 2 binding protein 2

K

KD	Knockdown
kDa	Kilodalton
KDM1A	Lysine-specific histone demethylase 1A
KO	Knockout

L

LDS	Lithium dodecyl sulfate
LPS	Lipopolysaccharide
LSD1	Lysine-specific demethylase 1
LY96	Lymphocyte antigen 96
Lys	Lysine

M

M1	Classically activated macrophages
M2	Alternatively activated macrophages
MAPK	Mitogen-activated protein kinase
MCSF	Macrophage colony-stimulating factor
MDM	Monocyte derived macrophage
MDSC	Myeloid derived suppressor cell
MFI	Mean fluorescence intensity
MHC	Major histocompatibility complex
Mio	Million
Mod	Module
MOI	Multiplicity of infection
MOPS	3-(N-morpholino)propanesulfonic acid
MR1	Major histocompatibility complex class I
MRC1	Mannose receptor C-type 1
mRNA	Messenger ribonucleic acid
MYC	MYC proto-oncogene
MYD88	Myeloid differentiation primary response 88

N

NFKB1	Nuclear Factor Kappa B Subunit 1
NF-κB	Nuclear Factor kappa-light-chain-enhancer of activated B cells
NGS	Next generation sequencing
NHEJ	Non-homologous end joining
NK cell	Natural killer cell
NLR	Nucleotide-binding oligomerization domain-like receptor
NO	Nitric oxide
NT.CTRL or NTC	Non-targeting control

O

OGT	O-linked β-N-acetylglucosamine transferase
oligo-dT	a short sequence of deoxy-thymidine nucleotides
OTU	Ovarian tumor
OTX1	Orthodenticle Homeobox 1

P

PAFAH1B1	Platelet-activating factor acetylhydrolase, isoform 1b, subunit 1
PAM	Protospacer Adjacent Motif
PAMP	Pathogen-associated molecular patterns
PBS	Phosphate buffered saline
PC	Principal component
PCA	Principal component analysis
PCNA	Proliferating cell nuclear antigen
PCR	Polymerase chain reaction
PD-1	Programmed cell death protein 1
PD-L1	Programmed-death ligand 1
PFA	Paraformaldehyde
pH	Negative of the logarithm to base 10 of the activity of the hydrogen ion
PI3K	Phosphoinositide 3-kinase
PLAC8	Placenta-specific 8
PLK1	Polo-like kinase 1
PMA	Phorbol 12-myristate 13-acetate
POLR2L	DNA-directed RNA polymerases I, II, and III subunit
polyA	polyadenylic acid
PROTAC	Proteolysis targeting chimera
PRR	Pattern-recognition receptor
PTPRC	Protein tyrosine phosphatase, receptor type, C

Q

qRT PCR	Quantitative real time Polymerase chain reaction

R

R^2	Correlation coefficient
RASGRP3	RAS Guanyl Releasing Protein 3

REL	V-rel avian reticuloendotheliosis viral oncogene homolog
RELA	V-rel avian reticuloendotheliosis viral oncogene homolog A
RFP	Red fluorescent protein
RIP	Receptor-interacting serine/threonine-protein kinase
RIPA	Radioimmunoprecipitation assay
RISC	RNA-induced silencing complex
RLR	Retinoic acid-inducible gene-I-like receptor
RNA	Ribonucleic acid
RNAi	RNA Interference
RNase	Ribonuclease
RNA-seq	RNA sequencing
RNP	Ribonucleoprotein
ROS	Reactive oxygen species
RPL9	60S ribosomal protein L9
RPM	Reads per million
RT	Room temperature

S

SCF	Stem cell factor
SCRIB	Scribbled Homolog
SD	Standard deviation
SEM	Standard error of the mean
SF3A3	Splicing factor 3A subunit 3
SF3B3	Splicing factor 3B subunit 3
sgRNA	Single guide ribonucleic acid
SHOC2	Leucine Rich Repeat Scaffold Protein
shRNA	Short hairpin ribonucleic acid
siRNA	Small interfering ribonucleic acid
SLICE	sgRNA lentiviral infection with Cas9 protein electroporation
SSC	Side Scatter
STAT1	Signal transducer and activator of transcription 1

T

TAM	Tumor-associated macrophage
TBST	Tris-buffered saline and Tween 20
TCR	T cell receptor
TGF-β	Transforming growth factor beta
T_H	T helper cell
TLR	Toll-like receptor
TME	Tumor-microenvironment
TNF	Tumor necrosis factor
TNFAIP3	Tumor necrosis factor, alpha-induced protein 3
TNFR	Tumor necrosis factor receptor
TNFRSF9	Tumor necrosis factor receptor Superfamily Member 9
TNFSF10	Tumor necrosis factor ligand superfamily member 10
TPM	Transcripts Per Million

TPO	Thrombopoetin
tracrRNA	Transactivating crRNA
TRAF6	TNF receptor-associated factor 6
T_{reg}	Regulatory T cell
TU / ml	Transducing units per milliliter

U

UBIC	Ubiquitin C

W

WARS	Tryptophanyl-tRNA synthetase, cytoplasmic
WG	Whole genome
WT	Wild type